



Earth Observation for Sustainable Development



Urban Development Project

EO4SD-Urban Project: Lima City Report

ESA Ref: AO/1-8346/15/I-NB
Doc. No.: City Operations Report
Issue/Rev.: 1.1
Date: 19.11.2019

Consortium Partners

No.	Name	Short Name	Country
1	GAF AG	GAF	Germany
2	Système d'Information à Référence Spatiale SAS	SIRS	France
3	GISAT S.R.O.	GISAT	Czech Republic
4	Egis SA	EGIS	France
5	Deutsche Luft- und Raumfahrt e. V	DLR	Germany
6	Netherlands Geomatics & Earth Observation B.V.	NEO	The Netherlands
7	JOANNEUM Research Forschungsgesellschaft mbH	JR	Austria
8	GISBOX SRL	GISBOX	Romania

Disclaimer:

The contents of this document are the copyright of GAF AG and Partners. It is released by GAF AG on the condition that it will not be copied in whole, in section or otherwise reproduced (whether by photographic, reprographic or any other method) and that the contents thereof shall not be divulged to any other person other than of the addressed (save to the other authorised officers of their organisation having a need to know such contents, for the purpose of which disclosure is made by GAF AG) without prior consent of GAF AG.

Summary

This document contains information related to the provision of geo-spatial products over Lima city, Peru, from the European Space Agency (ESA) supported project “Earth Observation for Sustainable Development - Urban Applications” (EO4SD-Urban) to the Inter-American Development Bank (IADB) funded program called “Emerging and Sustainable Cities Initiative” (ESCI).

	Affiliation/Function	Name	Date
Prepared	SIRS NEO GISBOX JR	S. Delbour, D. Fretin F. Fang R. Ocoliseanu M. Hirschmugl	26/04/2019
Reviewed	SIRS	C. Sannier	29/04/2019
Approved	GAF AG, Project Coordinator	T. Haeusler	30/04/2019

The document is accepted under the assumption that all verification activities were carried out correctly and any discrepancies are documented properly.

Distribution

Affiliation	Name	Copies
ESA	Z. Bartalis	electronic copy
IADB	Avelina Ruiz	electronic copy

Document Status Sheet

Issue	Date	Details
1.0	30/04/2019	First Document Issue
1.1	19/11/2019	Addition of section 4.4 Sustainable Development Goal 11 Indicators

Document Change Record

#	Date	Request	Location	Details
1	30/04/2019			Initial version

This page is intentionally left blank!

Executive Summary

The European Space Agency (ESA) has been working closely together with the International Finance Institutes (IFIs) and their client countries to demonstrate the benefits of Earth Observation (EO) in the IFI development programmes. Earth Observation for Sustainable Development (EO4SD) is a new ESA initiative, which aims to achieve an increase in the uptake of satellite-based information in the regional and global IFI programmes. The overall aim of the EO4SD Urban project is to integrate the application of satellite data for urban development programmes being implemented by the IFIs or Multi-Lateral Development Banks (MDBs) with the developing countries. The overall goal will be achieved via implementation of the following main objectives:

- To provide a service portfolio of Baseline and Derived urban-related geo-spatial products
- To provide the geo-spatial products and services on a geographical regional basis
- To ensure that the products and services are user-driven

This Report describes the generation and the provision of EO-based information products to the Inter-American Development Bank (IADB) for supporting it in the implementation of “**Emerging and Sustainable Cities Initiative**” (ESCI) funded program linked to the GEF funded project called “Global Platform for Sustainable Cities” (GPSC) and the Peruvian Ministry of Environment as main stakeholder. The Report provides a Service Description by referring to the user driven service requirements and the associated product list with the detailed product specifications. The following products were requested:

- Urban Extent
- Percentage Impervious Surface
- Urban Land Use / Land Cover (LU/LC) & Changes
- Urban Green Areas & Changes
- Building Footprints & Changes
- Flood Risk & Assessment

The current Version of this Report contains the description of the generation and delivery of each requested product. The Land Use / Land Cover (LU/LC), Urban Green Areas and Building Footprints products have been generated for two reference dates (current status and historical one) and thus include also the changes occurred during this period.

This City Operations Report for Lima systematically reviews the main production steps involved and importantly highlights the Quality Control (QC) mechanisms involved; the steps of QC and the assessment of quality is provided in related QC forms in the Annexe of this Report. There is also the provision of standard analytical work undertaken with the products which can be further included as inputs into further urban development assessments, modelling and reports.

This page is intentionally left blank!

Table of Contents

1	GENERAL BACKGROUND OF EO4SD-URBAN	1
2	SERVICE DESCRIPTION.....	1
2.1	STAKEHOLDERS AND REQUIREMENTS.....	1
2.2	SERVICE AREA SPECIFICATION	2
2.3	PRODUCT LIST AND PRODUCT SPECIFICATIONS.....	3
2.4	LAND USE/LAND COVER NOMENCLATURE.....	4
2.5	WORLD SETTLEMENT EXTENT	7
2.6	PERCENTAGE IMPERVIOUS SURFACE	8
2.7	URBAN GREEN AREAS NOMENCLATURE	8
2.8	BUILDING FOOTPRINTS NOMENCLATURE	9
2.9	TERMS OF ACCESS	9
3	SERVICE OPERATIONS.....	10
3.1	SOURCE DATA	10
3.2	PROCESSING METHODS	11
3.3	ACCURACY ASSESSMENT OF MAP PRODUCTS	11
3.3.1	Accuracy Assessment of LU/LC Product.....	12
3.3.2	Accuracy Assessment of World Settlement Extent Product.....	16
3.3.3	Accuracy Assessment of the Percentage Impervious Surface Product.....	18
3.3.4	Accuracy Assessment of Urban Green Areas Product	20
3.3.5	Accuracy Assessment of Building Footprints Product.....	20
3.4	QUALITY CONTROL/ASSURANCE	22
3.5	METADATA	23
4	ANALYSIS OF MAPPING RESULTS	24
4.1	LAND USE / LAND COVER FOR 2007/2009 AND 2016.....	24
4.1.1	LU/LC Mapping for AOI 1	24
4.1.2	Spatial Distribution of Main LU/LC Change Categories for AOI 1.....	27
4.1.3	LU/LC Mapping for AOI 2	29
4.1.4	Spatial Distribution of Main LU/LC Change Categories for AOI 2.....	32
4.2	URBAN GREEN AREAS.....	35
4.2.1	Urban Green Areas for AOI 1	35
4.2.2	Urban Green Areas for AOI 2	37
4.3	BUILDING FOOTPRINTS.....	39
4.3.1	Mapping Results for 2016.....	39
4.3.2	Mapping Results for 2007	40

4.3.3	Change Mapping Results	42
4.4	SUSTAINABLE DEVELOPMENT GOAL 11 INDICATORS.....	44
4.4.1	SDG 11 Indicator 11.2.1	45
4.4.2	SDG 11 Indicator 11.3.1	46
4.5	CONCLUDING POINTS	48
5	FLOOD HAZARD AND RISK ASSESSMENT.....	49
5.1	GENERAL CHARACTERISTICS OF THE STUDY AREA.....	49
5.2	EO DATA USED	55
5.3	SHORT DESCRIPTION OF METHODOLOGICAL APPROACH.....	56
5.4	PRODUCT DESCRIPTION.....	60
5.4.1	Tsunami Inundations	60
5.4.2	River Floods and Flash Floods.....	66
5.5	ACCURACY ASSESSMENT	78
5.6	ANALYSIS OF MAPPING RESULTS.....	80
6	REFERENCES	84

Annexes

Annex 1: Processing Methods for EO4SD-Urban Products

Annex 2: Filled Quality Control Sheets

List of Figures

Figure 1: Illustration of the Areas of Mapping for Lima.....	3
Figure 2: Mapping result over AOI 1 and 2 of the year 2016 overlaid with randomly distributed sample points used for accuracy assessment.	14
Figure 3: Subset of building footprints randomly distributed per stratum used for accuracy assessment.	21
Figure 4: Quality Control process for EO4SD-Urban product generation. At each intermediate processing step output properties are compared against pre-defined requirements.	22
Figure 5: AOI 1 - Detailed Land Use Land Cover 2016 over Lima.....	24
Figure 6: AOI 1 - Detailed Land Use Land Cover 2009 structure presented as Overall in % (left) and km ² (right).	25
Figure 7: AOI 1 - Detailed Land Use Land Cover 2016 structure presented as Overall in % (left) and km ² (right).	25
Figure 8: AOI 1 - Land Use Land Cover change types and spatial distribution.	27
Figure 9: AOI 1 - Land Use Land Cover Change Types 2009-2016 presented in % (left) and km ² (right).....	28
Figure 10: AOI 2 - Detailed Land Use Land Cover 2016 over Lima.....	29
Figure 11: AOI 2 - Insight on the detailed Land Use Land Cover 2016 within the city centre.	29
Figure 12: AOI 2 - Detailed Land Use Land Cover 2007 structure presented as Overall in % (left) and km ² (right).	30
Figure 13: AOI 2 - Detailed Land Use Land Cover 2016 structure presented as Overall in % (left) and km ² (right).	30
Figure 14: AOI 2 - Land Use Land Cover change types and spatial distribution.	33
Figure 15: AOI 2 - Land Use Land Cover Change Types 2007-2016 presented in % (left) and km ² (right).....	34
Figure 16: AOI 1 - Urban Green Areas changes and spatial distribution.....	35
Figure 17: AOI 1 - Status and change of urban green areas in-between 2009 and 2016 expressed in %.	36
Figure 18: AOI 1 - Status and change of urban green areas in-between 2009 and 2016 expressed in area.	36
Figure 19: AOI 2 - Urban Green Areas changes and spatial distribution.....	37
Figure 20: AOI 2 - Status and change of urban green areas in-between 2007 and 2016 expressed in %.	38
Figure 21: AOI 2 - Status and change of urban green areas in-between 2009 and 2016 expressed in area.	38
Figure 22: Mapping of Building Footprints in the heart of Lima in 2016.....	39
Figure 23: Number and type of buildings in the heart of Lima in 2016.....	40
Figure 24: Mapping of Building Footprints in the heart of Lima in 2007.....	41
Figure 25: Number and type of buildings in the heart of Lima in 2007.....	41
Figure 26: Building Footprints changes in the heart of Lima between 2007 and 2016.....	42
Figure 27: Relative proportion and area of changes related to building footprints-between 2007 and 2016.....	43
Figure 28: Example of significant change between 2007 and 2016.....	43
Figure 29: Proportion of population with convenient access to public transport.	45
Figure 30: Ratio of land consumption rate to population growth rate between 2005 and 2015.....	46
Figure 31: Percentage change of population and land consumption between 2005 and 2015.	47

Figure 32: Lima, Peru – Service Area (Image: DigitalGlobe 22/02/2017, 13/05/2016; DHM: ALOS World 3D – 30m, version 2.1 - ©JAXA)	50
Figure 33: Spatial distribution of the total annual precipitation (isohyets) in the catchment area of the Rímac River in the period 1964 - 2009 (Ministerio De Agricultura 2010)	51
Figure 34: Monthly distribution of average total precipitation in the Rímac River basin – based on the method of Thiessen polygons for the Chosica weather station (Ministerio De Agricultura 2010).	52
Figure 35: The catchment areas of the Rivers Chillón, Rímac and Lurín on the western slopes of the Central Andes (Drenkhan 2010).....	53
Figure 36: Adaptation of AOI in the northern part of Metropolitan area of Lima aiming at covering both sides of flood prone lower course of Chillan River	54
Figure 37: VHR DSM mosaic based on aerial drone survey (acquisition date 07/04/2015 and 20/01/2017, Source: Cenepred, Sistema de Información para la Gestión del Riesgo de Desastres - SIGRID) Background Image: Sentinel 2 – acquired 20/02/2017.....	56
Figure 38: Metropolitan area of Lima covered by EOWORLD LULC classification (full AOI – pink) and area of EO4SD-Urban LULC classification (green) (Background: Hillshade ALOS World 3D – 30m (AW3D30), version 2.1).....	58
Figure 39: Tsunami Flood Hazard Map for Metropolitan area of Lima. Yellow line: limits of Area of Interest (Background: Hillshade ALOS World 3D – 30m (AW3D30), version 2.1)	61
Figure 40: Inundation map published by DHN for the La Punta district and Callao Port: pinkish: inundation zones generated by a seismic event of 8.5 Mw; red: additional inundation zones generated by a seismic event of 9.0 Mw; black arrows: evacuation routes.	62
Figure 41: left: Tsunami Inundation Hazard Map for the Callao – La Punta area based on the maximum inundation from 12 scenarios (Mas et al. 2014); right: Comparison with result of DHN modelling: red: most probable inundation scenario, orange: scenario according to the 1746 event.	63
Figure 42: Aerial sight of Callao - La Punta which obviously is the most vulnerable area of metropolitan Lima in case of a Tsunami (Source: Arvo Corporación)	64
Figure 43: Crowded beaches of the Costa Verde on a summer day (Source: http://www.peru4you.de/tsunami.html#).....	65
Figure 44: Visualization of a possible tsunami at the Costa Verde of Lima (Bahia de Miraflores) where high cliffs protect the built up area (Source: MINAM Ministerio del Ambiente / Ministry of Environment).....	65
Figure 45: Rímac River in sector of San Antonio de Carapongo (District of Lurigancho) – pre-event situation on 3rd of March 2017 (Image © DigitalGlobe).....	69
Figure 46: Rímac River in sector of San Antonio de Carapongo (District of Lurigancho) – post-event situation on 21st of March 2017 (Image © DigitalGlobe)	69
Figure 47: Quebrada Yanacoto, Lurigancho District (Eastern Lima): pre-event situation on 3rd of March 2017 (Image © DigitalGlobe)	70
Figure 48: Quebrada Yanacoto, Lurigancho District (Eastern Lima): post-event situation on 17th of April 2017 (Image © DigitalGlobe)	70
Figure 49: Chillon River in sector of Puente Piedra (District of Comas) – pre-event situation on 11th of March 2017 (Image © DigitalGlobe).....	71
Figure 50: Chillon River in sector of Puente Piedra (District of Comas) – post-event situation on 21st of March 2017 (Image © DigitalGlobe).....	71
Figure 51: Subset of flood extent map showing the flood extent in Carapongo/Santa María de Huachipa and Cajamarquilla (Lima). Visual interpretation of WorldView-2 Images acquired on 18th and 21st of March 2017. Background Image: Sentinel 2 – acquired 20/02/2017.	72
Figure 52: River and Flash Flood Hazard Map for Metropolitan area of Lima. Green line: limits of Area of Interest (Background: Hillshade ALOS World 3D – 30m (AW3D30), version 2.1).....	73

Figure 53: Hydrograph of the Rimác River at the Chosica water gauge, dated 22nd of January 2018 (SENAMHI - National Meteorology and Hydrology Service of Peru): the different alarm levels (yellow: 50 m³/s, orange: 70 m³/s, red: 95 m³/s) are shown as well as the hydrograph for 2016/2017 (dotted blue line) with its maximum in March 2017..... 74

Figure 54: Flood Hazard Classification in Metropolitan Lima merged for Tsunami Hazard and River and Flash Flood Hazard. Green line: limits of Area of Interest (Background: Hillshade ALOS World 3D – 30m (AW3D30), version 2.1)..... 75

Figure 55: Flood Hazard Classification displaying proportions of areas prone to flooding in area of EO4SD-Urban LULC classification only (cf. Figure 35)..... 76

Figure 56: Flood Hazard Classification displaying proportions of areas prone to flooding in Metropolitan Lima area – shown separately for Tsunami Hazard and River and Flash Flood Hazard. 76

Figure 57: Susceptibility Map for Mass Movements in the Rímac Valley in eastern Lima (District of Lurigancho and Chaclacayo) (Source: INGEMMET 2015)..... 77

Figure 58: Mapping result of the Flood Extent of March 2017 event overlaid with randomly distributed sample points used for accuracy assessment. 79

Figure 59: Flood Risk Map for Metropolitan Lima considering Tsunamis, River and Flash Floods (Background: Hillshade ALOS World 3D – 30m (AW3D30), version 2.1) 80

Figure 60: Subset of Flood Risk Map for Callao – La Punta and Central Lima considering Tsunamis and flooding from River Rímac (Background Image: Sentinel2A 20170220)..... 81

Figure 61: Proportion of Residential and Public Urban Fabric in Flood Risk Zones in Lima Central Area covered by EO4SD-Urban LULC classification (cf. Figure 35) 82

Figure 62: Map of Residential and Public Urban Fabric based on classification of 2016 VHR imagery combined with Flood Risk Zoning in Callao – La Punta and Central Lima (Background Image: Sentinel2A 20170220)..... 82

Figure 63: Map of Residential and Public Urban Fabric based on EOWORLD 2013 classification combined with Flood Risk Zoning in Eastern Lima - Districts of Lurigancho and Chaclacayo, Chosica (Background Image: Sentinel2A 20170220; Pink Line: limits of AOI)..... 83

List of Tables

Table 1: LU/LC Nomenclature for historic and recent year..... 5

Table 2: Nomenclature used for the mapping and identification of Urban Green Areas. 8

Table 3: Nomenclature used for the classification of Building Footprints..... 9

Table 4: Number of sampling points for the EO4SD-Urban mapping classes after applied sampling design with information on overall land cover by class. 13

Table 5: Accuracies exhibited by the WSF2015 according to the three considered agreement criteria for different definitions of settlement..... 17

Table 6: Acquisition dates and size of the WV2 images available for the 5 test sites analysed in the validation exercise along with the number of corresponding 30x30m validation samples. 19

Table 7: Number of sampling units per stratum for the Building Footprints product. 20

Table 8: AOI 1 - Detailed information on area and percentage of total area for each class for 2009 and 2016 as well as the changes..... 26

Table 9: AOI 1 - Overall Main LU/LC Changes Statistics. 28

Table 10: AOI 2 - Detailed information on area and percentage of total area for each class for 2007 and 2016 as well as the changes. 31

Table 11: AOI 2 - Overall Main LU/LC Changes Statistics. 34

Table 12: SDG 11 indicators measurable with the support of EO4SD-Urban products. 44

Table 13: Land use classes and reclassification to pre-defined damage levels 59

Table 14: Flood Hazard and Risk classification..... 59

List of Abbreviations

AOI	Area of Interest
CDS	City Development Strategy
CS	Client States
DEM	Digital Elevation Model
DLR	German Space Agency
EEA	European Environmental Agency
EGIS	Consulting Company for Environmental Impact Assessment and Urban Planning, France
EO	Earth Observation
ESA	European Space Agency
ESCI	Emerging and Sustainable Cities Initiative
EU	European Union
GAF	GAF AG, Geospatial Service Provider, Germany
GIS	Geographic Information System
GISAT	Geospatial Service Provider, Czech Republic
GISBOX	Romanian company with activities of Photogrammetry and GIS
GPSC	Global Platform for Sustainable Cities
HR	High Resolution
HRL	High Resolution Layer
IADB	Inter-American Development Bank
IFI	International Financing Institute
INSPIRE	Infrastructure for Spatial Information in the European Community
ISO/TC 211	Standardization of Digital Geographic Information
JR	JOANNEUM Research, Austria
LULC	Land Use / Land Cover
LULCC	Land Use and Land Cover Change
MMU	Minimum Mapping Unit
NDVI	Normalized Difference Vegetation Index
NEO	Geospatial Service Provider, The Netherlands
PIS	Percentage Impervious Surface
QA	Quality Assurance
QC	Quality Control
QM	Quality Management
SIRS	Geospatial Service Provider, France
SP	Service Provider
VHR	Very High Resolution
WB	World Bank
WSF	World Settlement Footprint

This page is intentionally left blank!

1 General Background of EO4SD-Urban

Since 2008 the European Space Agency (ESA) has worked closely together with the International Finance Institutes (IFIs) and their client countries to harness the benefits of Earth Observation (EO) in their operations and resources management. Earth Observation for Sustainable Development (EO4SD) is a new ESA initiative, which aims to achieve an increase in the uptake of satellite-based information in the regional and global IFI programmes. The EO4SD-Urban project initiated in May 2016 (with a duration of 3 years) has the overall aim to integrate the application of satellite data for urban development programmes being implemented by the IFIs with the developing countries. The overall goal will be achieved via implementation of the following main objectives:

- To provide the services on a regional basis (i.e. large geographical areas); in the context of the current proposal with a focus on S. Asia, SE Asia and Africa, for at least 35-40 cities.
- To ensure that the products and services are user-driven; i.e. priority products and services to be agreed on with the MDBs in relation to their regional programs and furthermore to implement the project with a strong stakeholder engagement especially in context with the validation of the products/services on their utility.
- To provide a service portfolio of Baseline and Derived urban-related geo-spatial products that have clear technical specifications and are produced on an operational manner that are stringently quality controlled and validated by the user community.
- To provide a technology transfer component in the project via capacity building exercises in the different regions in close co-operation with the MDB programmes.

This Report supports the fulfilment of the third objective which requires the provision of geo-spatial Baseline and Derived geo-spatial products to various stakeholders in the IFIs and counterpart City authorities. The Report provides a Service Description, and then in Chapter 3 systematically reviews the main production steps involved and importantly highlights whenever there are Quality control (QC) mechanisms involved with the related QC forms in the Annexe of this Report. The description of the processes is kept intentionally at a top level and avoiding technical details as the Report is considered mainly for non-technical IFI staff and experts and City authorities. Finally, Chapter 4 presents the standard analytical work undertaken with the products which can be inputs into further urban development assessments, modelling and reports.

2 Service Description

The following Section summarises the service as it has been performed for the city of Lima, Peru, within the EO4SD-Urban Project and as it has been delivered to Avelina Ruiz, Climate Change Consultant at IADB, and Javier Eduardo Lazarte Remisio, Urban Development Coordinator at the Peruvian Ministry of Environment.

2.1 Stakeholders and Requirements

The EO4SD-Urban products described in this Report has been provided for Lima, Peru, upon request of the Inter-American Development Bank (IADB) for supporting its funding project called “Emerging and Sustainable Cities Initiative” (ESCI). This is linked to the GEF funded project called “Global Platform for Sustainable Cities” (GPSC).

The main stakeholder is therefore the Peruvian Ministry of Environment who is in charge of urban development policies. Otherwise, many companies have been contracted by the Bank to develop urban studies in Peru (and elsewhere) and could be called upon for studies in which the EO4SD-Urban products may prove to be useful.

The ESCI project aims at providing useful tools to the Ministry and city authorities for supporting the decision making and development of the urban code. There are four main components in this project, which involves four different districts in Lima:

- Urban vulnerability to various risks, such as floods, coastal erosion and earthquakes. The intent is to obtain a mapping of the risks linked to the modelling of hydrology (local rivers);
- Software development on hydrology modelling, focusing on the watershed areas, and highlighting both the flood risks and the water scarcity. This modelling is made in cooperation with the National Agency of Water;
- Indicators for biodiversity assessment knowing that one pilot project for a district is ongoing;
- Improvement of the design of the metro stations in Lima.

The Peruvian Ministry of Environment has a GIS division, which processes already Land Use / Land Cover and other thematic data for environmentally sensitive areas. However, the Ministry encounters some difficulties to acquire images especially due to heavy cloud cover over Lima and to gather new information; geospatial data are often outdated, too coarse or only partial with very little topographic information for example. On the other hand, the Municipality of Lima has only a small department dedicated to urban planning. Therefore, the Ministry is responsible for these activities and thus expects a significant support of EO4SD-Urban products to alleviate the difficulties and to provide new geo-information relevant for the main components defined within ESCI project. He is especially involved in the definition of a large public ecological park in the north of Lima (Antonio Raimondi National Park), wants to improve the public transportation network access and operation, and needs a better assessment of flood risks over the metropolitan area.

The Ministry is also interested in capacity building programs that focus on the integration of data around an existing “Global City Platform” decision-support system – and the equivalent platform that runs in the IADB, in such a way that the data can be either shared or compared for issues relevant to biodiversity, water and hydrology, and urban development themes.

In addition, the geospatial products from EO4SD-Urban can be useful for the IADB regarding internal analytics improving the level of urban information to counterparts and the Bank itself, knowledge of utilities, better and cheaper techniques, homogeneous data and rather difficult to obtain, and quick assessment of the land use evolution over time.

2.2 Service Area Specification

The Areas of Interest (AOI) for the service implementation which has finally been agreed with the stakeholders are the following:

- AOI 1 - Ancon District (266 km²) because a large public ecological park is under development
- AOI 2 - Core Urban Area (304 km²) because there is high interest for urban development and growth assessment
- AOI 3 – Metropolitan Area (1,153 km²) defined for implementing the vulnerability assessment to the flood risk

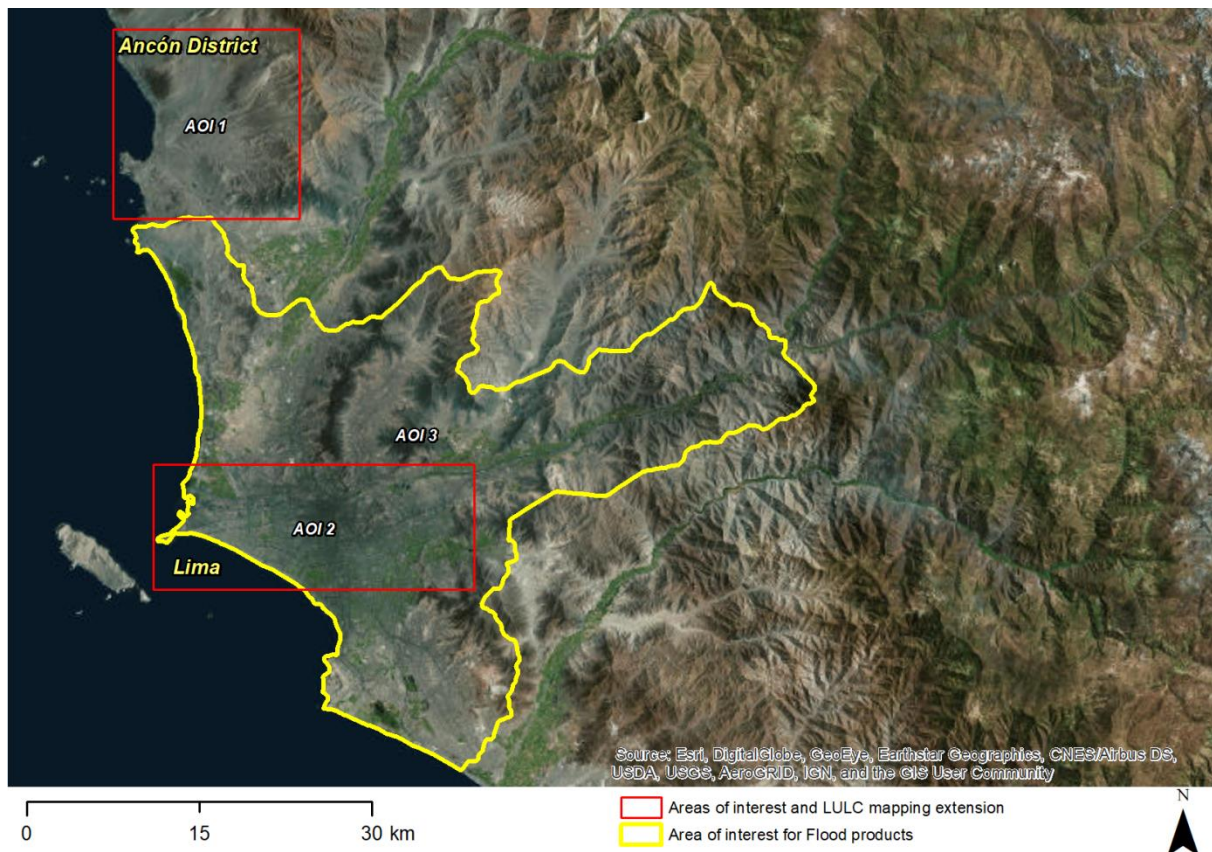


Figure 1: Illustration of the Areas of Mapping for Lima

2.3 Product List and Product Specifications

Given the requirements and discussions with the stakeholders, the final list of products is as follows:

- Settlement Extent & Change (producer: DLR)
- Percentage Impervious Surface & Change (producer: DLR)
- Urban Land Use / Land Cover (LU/LC) & Change (producer: SIRS)
- Urban Green Areas & Change (producer: NEO)
- Building Footprints & Change (producer: GISBOX)
- Flood Hazard & Risk Assessment (producer: JR)

The first two products have been generated by the German Aerospace Agency (DLR) over the full metropolitan area for six reference years: 1990 - 1995 - 2000 - 2005 - 2010 - 2015.

For each of the other products two time slots were used to provide historic and recent information. In detail, LU/LC and Urban Green Areas products have been generated over AOI 1 for 2009 and 2016 and over AOI 2 for 2007 and 2016 depending on the EO data availability. Building Footprints product has been generated only over a subset of AOI 2 defined alongside the metro line 2 crossing the city from west to east and an irrigation canal, because this is a costly product firstly aiming in this case at providing insight on building density and types and the proportion of population served by public transport.

Finally, the flood risk and assessment have been conducted over AOI 3 considering all EO and ancillary data made available considering all significant events occurred over time.

2.4 Land Use/Land Cover Nomenclature

A pre-cursor to starting production was the establishment with the stakeholders on the relevant Land Use/Land Cover (LU/LC) nomenclature as well as class definitions. The approach taken was to use a standard remote sensing based LU/LC nomenclature i.e. the European Urban Atlas Nomenclature (European Union, 2011) and adapt it to the User's LU requirements. Thus, the remote-sensing based LU/LC classes in the urban context can be grouped into five Level 1 classes, which are Artificial Surfaces, Natural/ Semi Natural Areas, Agricultural Areas, Wetlands, and Water. These classes can then be sub-divided into several different more detailed classes such that the dis-aggregation can be down to Level 2-4. This hierarchical classification system is often used in operational Urban mapping programmes and is the basis for example of the European Commission's Urban Atlas programme which provides pan-European comparable LU/LC data with regular updates. A depiction of the way the levels and classes in the Urban Atlas programme are structured is presented as follows:

Level I Artificial surfaces

- Level II: Urban Fabric

Level III

- Continuous Urban Fabric (Sealing Layer-S.L. > 80%)
- Discontinuous Urban Fabric (S.L. 10% - 80%)

Level IV

- Discontinuous Dense Urban Fabric (S.L. 50% - 80%)
- Discontinuous Medium Density Urban Fabric (S.L. 30% - 50%)
- Discontinuous Low Density Urban Fabric (S.L. 10% - 30%)
- Discontinuous Very Low Density Urban Fabric (S.L. < 10%)

- Level II: Industrial, Commercial, Public, Military, Private Units and Transport

Level III

- Industrial, Commercial, Public, Military and Private Units
- Transport Infrastructure

Level IV

- Fast Transit Roads
- Other Roads
- Railway
- Port and associated land
- Airport and associated land

- Level II: Mine, Dump and Construction Sites

Level III

- Mineral Extraction and Dump Sites
- Construction Sites
- Land Without Current Use

- Level II: Artificial Non-Agricultural Vegetated Areas

Level III

- Green Urban Areas
- Sports and Leisure Facilities

(Reference: European Union, 2011)

The different Levels, classes and sub-classes from the remote sensing based Urban classification, were adapted to the User requirements based on existing Master Plans for cities and/or direct advise from the User on critical classes required. The final LU/LC nomenclature had to be endorsed by the user before production started.

Table 1: LU/LC Nomenclature for historic and recent year

LU/LC classification				
Level I	Level II	Level III	Level IV	
1000 Artificial Surfaces	1100 Residential	1110 Very Low Density		
		1120 Low Density		
		1130 Medium Density		
		1140 High Density		
		1150 Very High Density		
	1200 Industrial, Commercial, Public, Military, Private and Transport Units		1210 Industrial, Commercial, Public, Military and Private Units	1211 Commercial
				1212 Industry
				1213 University
				1214 Schools
				1215 Government
				1216 Military
				1217 Hospitals
				1218 Public Buildings
				1219 Non-Residential Urban Fabric
			1220 Roads	1221 Arterial
				1222 Collector
				1223 Local Road
			1230 Railway	
			1240 Airport	
	1250 Port			
	1300 Mine, Dump and Construction Sites		1310 Mineral Extraction and Dump Sites	
			1320 Construction Sites	
			1330 Land without Current Use	
	1400 Urban Open Spaces		1410 Urban Parks	
1420 Recreation Facilities (Sport Facilities, Stadiums, Golf				

		Courses, etc.)	
		1430 Cemeteries	
2000 Agricultural Area			
3000 Natural and Semi-Natural Areas	3100 Forest and Shrub Lands		
	3200 Natural Areas (Savannah, Grassland)		
	3300 Bare Soil		
4000 Wetlands			
5000 Water	5100 Inland Water		
	5200 Marine Water		

It is important to note that the possibility to classify at Level IV was highly dependent on the availability of reliable reference datasets from the City or sources such as Google Earth. This aspect is further discussed in Chapter 3.

Especially regarding the road hierarchy used in the classification at Level IV, the international road classification standards have been followed; this is for example defined by the European Commission (https://ec.europa.eu/transport/road_safety/specialist/knowledge/road/designing_for_road_function/road_classification_en).

Roads are divided into three groups: arterial or through traffic flow routes (in our case **Arterial Roads**), distributor roads (in our case **Collector Roads**), and access roads (or **Local Roads**). The three road types are defined as follows:

Arterial Roads:

Roads with a flow function allow efficient throughput of (long distance) motorized traffic. All motorways and express roads as well as some urban ring roads have a flow function. The number of access and exit points is limited. (https://ec.europa.eu/transport/road_safety/specialist/knowledge/road/designing_for_road_function/road_classification_en)

Collector Roads:

Roads with an area distributor function allow entering and leaving residential areas, recreational areas, industrial zones, and rural settlements with scattered destinations. Junctions are for traffic exchange (allowing changes in direction etc.); road sections between junctions should facilitate traffic in flowing. (https://ec.europa.eu/transport/road_safety/specialist/knowledge/road/designing_for_road_function/road_classification_en)

Local Roads:

Roads with an access function allow actual access to properties alongside a road or street. Both junctions and the road sections between them are for traffic exchange. (https://ec.europa.eu/transport/road_safety/specialist/knowledge/road/designing_for_road_function/road_classification_en).

2.5 World Settlement Extent

Reliably outlining settlements is of high importance since an accurate characterization of their extent is fundamental for accurately estimating, among others, the population distribution, the use of resources (e.g. soil, energy, water, and materials), infrastructure and transport needs, socioeconomic development, human health and food security. Moreover, monitoring the change in the extent of settlements over time is of great support for properly modelling the temporal evolution of urbanization and thus, better estimating future trends and implementing suitable planning strategies.

At present, no standard exists for defining settlements and worldwide almost each country applies its own definition either based on population, administrative or geometrical criteria. The German Space Agency (DLR) were responsible for the provision of the “Settlement Extent” product; when generating the settlement extent maps from HR imagery, pixels are labelled as **settlement** if they *intersect any building, lot or – just within urbanized areas – roads and paved surface* where we define:

- **building** as any structure having a roof supported by columns or walls and intended for the shelter, housing, or enclosure of any individual, animal, process, equipment, goods, or materials of any kind;
- **lot** as the area contained within an enclosure (wall, fence, hedge) surrounding a building or a group of buildings. In cases where there are many concentric enclosures around a building, the lot is considered to stop at the inner most enclosure;
- **road** as any long, narrow stretch with a smoothed or paved surface, made for traveling by motor vehicle, carriage, etc., between two or more points;
- **paved surface** as any level horizontal surface covered with paving material (i.e., asphalt, concrete, concrete pavers, or bricks but excluding gravel, crushed rock, and similar materials).

Instead, pixels not satisfying this condition are marked as **non-settlement**.

The settlement extent product is a binary mask outlining - in the given Area of Interest (AOI) – settlements in contrast to all other land-cover classes merged together into a single information class. The settlement class and the non-settlement class are associated with values “255” and “0”, respectively.

2.6 Percentage Impervious Surface

Settlement growth is associated not only to the construction of new buildings, but – more in general – to a consistent increase of all the impervious surfaces (hence also including roads, parking lots, squares, pavement, etc.), which do not allow water to penetrate, forcing it to run off. To effectively map the percentage impervious surface (PIS) is then of high importance being it related to the risk of urban floods, the urban heat island phenomenon as well as the reduction of ecological productivity. Moreover, monitoring the change in the PIS over time is of great support for understanding, together with information about the spatiotemporal settlement extent evolution, also more details about the type of urbanization occurred (e.g. if areas with sparse buildings have been replaced by highly impervious densely built-up areas or vice-versa).

In the framework of the EO4SD-Urban project, one pixel in the generated PIS maps is associated with the estimated percentage of the corresponding surface at the ground covered by buildings or paved surfaces, are defined as:

- **building** as any structure having a roof supported by columns or walls and intended for the shelter, housing, or enclosure of any individual, animal, process, equipment, goods, or materials of any kind;
- **paved surface** as any level horizontal surface covered with paving material (i.e. asphalt, concrete, concrete pavers, or bricks but excluding gravel, crushed rock, and similar materials).

The product provides for each pixel in the considered AOI the estimated PIS. Specifically, values are integer and range from 0 (no impervious surface in the given pixel) to 100 (completely impervious surface in the given pixel) with step 5.

2.7 Urban Green Areas Nomenclature

Developing cities in a sustainable way implies to preserve and promote green areas also and especially within the urban extent. Green areas refer to any surfaces covered by vegetation (grass, bushes, trees).

Table 2: Nomenclature used for the mapping and identification of Urban Green Areas.

Single date	
Code 0	Non-green area
Code 1	Urban green area
Code 255	Non-urban areas. All areas that do not fall in “Artificial Surfaces” Level 1 class of the Land Use Land Cover product (See Table 1).
Change product	
Code 0	Non-green area. No vegetated surfaces occurring on “Artificial Surfaces”, Level I, at both points in time.
Code 1	Permanent urban green area. Vegetated surfaces in historic and recent year.
Code 2	Loss of urban green area. Vegetated areas in historic year, which changed to non-vegetated areas in recent year.
Code 3	New urban green area. Non-vegetated surfaces in historic year with vegetation cover in recent year.
Code 255	Non-Urban Areas. All areas that do not fall in “Artificial Surfaces” Level 1 class of the Land Use Land Cover product.

2.8 Building Footprints Nomenclature

The product provides information on the spatial distribution, number and size of building footprints which are defined as the contour of houses and other manmade buildings as they are commonly represented in cadastral systems. Each digitised footprint can be further attributed with user required information to specify the type of building. Within the scope of EO4SD-Urban service, the use/function of buildings was especially derived from the LU/LC product at level IV of the ‘1000 – Artificial Surfaces’ Level I class.

Table 3 provides the full nomenclature used for the classification of building footprints. Building facility with residential use is defined as a group of contiguous residential buildings which are too difficult to distinguish and extract separately from VHR optical satellite imagery. This additional class is introduced because of the high building density which characterizes the city centre of many cities.

Table 3: Nomenclature used for the classification of Building Footprints.

Building Footprints - Nomenclature		
1100 - Residential	1215 - Government	1230 - Transportation (Railway Station)
1170 - Building Facility / Residential	1216 - Military	1310 - Mineral Extraction and Dump Site
1211 - Commercial	1217 - Hospital	1320 - Construction Building
1212 - Industry	1218 - Public Building	1410 - Building inside Urban Park
1213 - University	1219 - Non-Residential Urban Fabric	1420 - Recreation Facility
1214 - School		1430 - Cemetery

Information about the spatial location and type of buildings in urban and peri-urban areas is a valuable baseline information for many purposes. Topological analyses can be performed to distinguish different types of building blocks and generate different classes of housing density. Furthermore, with the integration of 3D information, models related to volume and estimated space for living can be designed. In case of natural disasters like floods, landslides, wind storms, the extent and level of damages can be immediately assessed and rescue organised.

2.9 Terms of Access

The Dissemination of the digital data and the Report was undertaken via FTP.

3 Service Operations

The following Sections present all steps of the service operations including the necessary input data, the processing methods, the accuracy assessment and the Quality Control procedures. Methods are presented in a top-level and standardised manner for all the EO4SD-Urban City Reports.

The service operations related to Flood Hazard & Risk Assessment are presented with the mapping results separately in the dedicated Section 5 of this report due to the technical specifications and high level of complexity of such a study.

3.1 Source Data

This Section presents a summary of the remote sensing and ancillary datasets that were used. Different types of data from several data providers have been acquired. A complete list of source data as well as a quality assessment is provided in Annex 2.

High Resolution Optical EO Data

The main source data for the generation of Settlement Extent and PIS products were archive images from Landsat and Sentinel-2 satellite sensors which were accessible and downloadable free of charge from open web platforms.

Very High Resolution Optical EO Data

The VHR optical images required for the generation of LU/LC, Urban Green Areas and Building Footprints products had to be acquired and purchased through commercial EO Data Providers such as Airbus Defence & Space and European Space Imaging. It has to be noted that under the current collaboration project the VHR EO data had to be purchased under **mono-license agreements** between GAF AG and the EO Data Providers. If EO data would have to be distributed to other stakeholders, then further licences for multiple users would have to be purchased.

The following VHR sensor data have been acquired to cover the defined Areas of Interest:

- **Pléiades-1A/B:**
 - 2 scenes acquired in 2016 for covering AOI 1
 - 4 scenes acquired in 2016 for covering AOI 2
- **Quickbird-2:**
 - 2 scenes acquired in 2009 for covering AOI 1
 - 3 scenes acquired in 2007 for covering AOI 2

Ancillary Data

- Land Use / Land Cover product over Lima for the reference year 2013 generated as part of the **eoworld2** initiative (Urban Service) resulting from the partnership between ESA and the World Bank. This product was used as a basis for generating the LU/LC required within the frame of EO4SD-Urban service.
- Open Street Map (OSM) data: OSM data is freely available and generated by volunteers across the globe. The so-called crowd sourced data is not always complete but has for the most parts of the world valuable spatial information. Data was downloaded to complement the transport network to be extracted in the LU/LC product.

Detailed lists of the used EO and ancillary data as well as their quality is documented in the attached Quality Control Sheets in Annex 2.

3.2 Processing Methods

Data processing starts at an initial stage with quality checks and verification of all incoming data. This assessment is performed in order to guarantee the correctness of data before geometric or radiometric pre-processing is continued. These checks follow defined procedures in order to detect anomalies, artefacts and inconsistencies. Furthermore, all image and statistical data were visualised and interpreted by operators.

The main techniques and standards used for data analysis, processing and modelling for each product are described in Annex 1.

3.3 Accuracy Assessment of Map Products

Data and maps derived from remote sensing contain - like any other map - uncertainties which can be caused by many factors. The components, which might have an influence on the quality of the maps derived from EO include quality and suitability of satellite data, interoperability of different sensors, radiometric and geometric processing, cartographic and thematic standards, and image interpretation procedures, post-processing of the map products and finally the availability and quality of reference data. However, the accuracy of map products has a major impact on secondary products and its utility and therefore an accuracy assessment was considered as a critical component of the entire production and products delivery process. The main goal of the thematic accuracy assessment was to guarantee the quality of the mapping products with reference to the accuracy thresholds set by the user requirements.

The applied accuracy assessments were based on the use of reference data and applying statistical sampling to deduce estimates of error in the classifications. In order to provide an efficient, reliable and robust method to implement an accuracy assessment, there are three major components that had to be defined: the **sampling design**, which determines the spatial location of the reference data, the **response design** that describes how the reference data is obtained and an **analysis design** that defines the accuracy estimates. These steps were undertaken in a harmonised manner for the validation of all the geo-spatial products.

3.3.1 Accuracy Assessment of LU/LC Product

Sampling Design

The sampling design specifies the sample size, sample allocation and the reference assessment units (i.e. pixels or image blocks). Generally, different sampling schemes can be used in collecting accuracy assessment data including: simple random sampling, systematic sampling, stratified random sampling, cluster sampling, and stratified systematic unaligned sampling. In the current project a **single stage stratified random sampling** based on the method described by Olofson et al (2013¹) was applied which used the map product as the basis for stratification. This ensured that all classes even very minor ones were included in the sample.

However, in complex LU/LC products with many classes, this usually results in a large number of strata (one stratum per LU/LC class), of which some classes cover only very small areas (e.g. sport fields, cemeteries) and not being adequately represented in the sampling. In order to achieve a representative sampling for the statistical analyses of the mapping accuracy it was decided to extend the single stage stratified random sampling. At the first stage the number of required samples was allocated within each of the Level I strata. In the second stage all Level III classes that were not covered by the first sampling, were grouped into one new stratum. Within that stratum the same number of samples was randomly allocated as the Level I strata received. To avoid a clustering of point samples within classes and to minimise the effect of spatial autocorrelation a minimum distance in between the sample points was set to be 150 m. The final sample size for each class can be considered as close as possible to the proportion of the area covered by each stratum considering that the target was to determine the overall accuracy of the entire map.

The total sample size per stratum was determined by the expected standard error and the estimated error rate based on the following formula which assumes a simple random sampling (i.e. the stratification is not considered):

$$n = \frac{P*q}{\left(\frac{E}{Z}\right)^2}$$

n = number of samples per strata / map class

p = expected accuracy

$q = 1 - p$

E = Level of acceptable (allowable) sample error

Z = z-value (the given level of significance)

Hence, with an expected accuracy of $p = 0.85$, a 95% confidence level and an acceptable sampling error of 5%, the minimum sample size is 196. A 10% oversampling was applied to compensate for stratification inefficiencies and potentially inadequate samples (e.g. in case of cloudy or shady reference data). For each Level I strata 215 samples have been randomly allocated. Afterwards, within all classes of Level III that did not received samples in the first run, additionally 215 samples were randomly drawn across all these classes.

¹ Olofsson, P., Foody, G. M., Stehman, S. V., & Woodcock, C. E. (2013). Making better use of accuracy data in land change studies: Estimating accuracy and area and quantifying uncertainty using stratified estimation. *Remote Sensing of Environment*, 129, 122–131. doi:10.1016/j.rse.2012.10.031

Table 4: Number of sampling points for the EO4SD-Urban mapping classes after applied sampling design with information on overall land cover by class.

Class Name	Class ID	No. of Sampling Points	Area coverage (km ²)
Residential	1100	362	105.44
Industrial, Commercial, Public, Military and Private Units	1210	163	51.13
Roads	1220	163	51.05
Railway	1230	1	0.28
Airport	1240	9	2.56
Port	1250	3	1.22
Mineral Extraction and Dump Sites	1310	10	2.49
Construction Sites	1320	18	4.48
Vacant Land not obviously being prepared for construction	1330	3	0.7
Urban Parks	1410	44	11.54
Recreation Facilities (Sport Facilities, Stadiums, Golf Courses, etc.)	1420	27	8.05
Cemeteries	1430	4	0.92
Agricultural Area	2000	11	6.18
Natural Areas (Savannah, Grassland)	3200	1	1.27
Bare Soil	3300	102	221.26
Wetlands	4000	5	0.56
Inland Water	5100	3	1.84
Marine Water	5200	71	97.77
Total	--	1000	569.02 km²

Response Design

The response design determines the reference information for comparing the map labels to the reference labels. Collecting reference data on the ground by means of intensive fieldwork is both costly, time consuming and, in most projects, not feasible. The most cost-effective reference data sources are VHR satellite data with 0.5 m to 1 m spatial resolution. Czaplewski (2003)² indicated that visual interpretation of EO data is acceptable if the spatial resolution of EO data is sufficiently better compared to the thematic classification system. However, if there are no EO data with better spatial resolution available, the assessment results need to be checked against the imagery used in the production process.

The calculated number of necessary sampling points for each mapping category was randomly distributed among the strata and overlaid to the VHR data of each epoch. Figure 2 is showing the mapping result with the overlaid sample points.

² Czaplewski, R. L. (2003). Chapter 5: accuracy assessment of maps of forest condition: statistical design and methodological considerations, pp. 115–140. In Michael A. Wulder, & Steven E. Franklin (Eds.), Remote sensing of forest environments: concepts and case studies. Boston: Kluwer Academic Publishers (515 pp.).

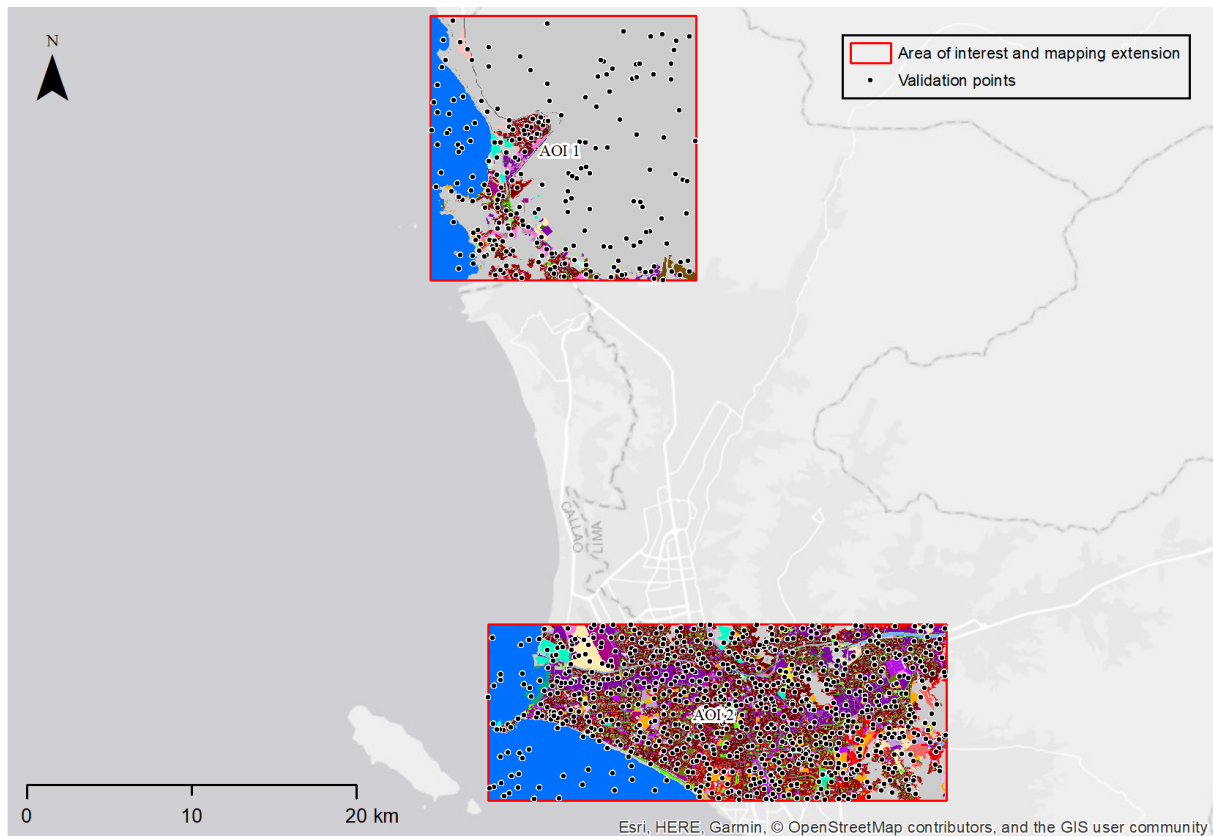


Figure 2: Mapping result over AOI 1 and 2 of the year 2016 overlaid with randomly distributed sample points used for accuracy assessment.

In this way a reference information could be extracted for each sample point by visual interpretation of the VHR data for all mapped classes. The size of the area to be observed had to be related to the Minimum Mapping Unit (MMU) of the map product to be assessed. The reference information of each sampling point was compared with the mapping results and the numbers of correctly and not-correctly classified observations were recorded for each class. From this information the specific error matrices and statistics were computed (see next Section).

Analysis

Each class usually has errors of both omission and commission, and in most situations, these errors for a class are not equal. In order to calculate these errors as well as the uncertainties (confidence intervals) for the area of each class a statistically sound accuracy assessment was implemented.

The confusion matrix is a common and effective way to represent quantitative errors in a categorical map, especially for maps derived from remote sensing data. The matrices for each assessment epoch were generated by comparing the “reference” information of the samples with their corresponding classes on the map. The *Reference* represented the “truth”, while the *Map* provided the data obtained from the map result. Thematic accuracy for each class and overall accuracy is then presented in error matrices (see Annex 2). Unequal sampling intensity resulting from the random sampling approach was accounted for by applying a weight factor (p) to each sample unit based on the ratio between the number of samples and the size of the stratum considered³:

³ Selkowitz, D. J., & Stehman, S. V. (2011). Thematic accuracy of the National Land Cover Database (NLCD) 2001 land cover for Alaska. *Remote Sensing of Environment*, 115(6), 1401–1407. doi:10.1016/j.rse.2011.01.020.

$$\hat{p}_{ij} = \left(\frac{1}{M}\right) \sum_{x \in (i,j)} \frac{1}{\pi_{uh}^*}$$

Where i and j are the columns and rows in the matrix, M is the total number of possible units (population) and π is the sampling intensity for a given sample unit u in stratum h .

Overall accuracy and User and producer accuracy were computed for all thematic classes and 95% confidence intervals were calculated for each accuracy metric.

The standard error of the error rate was calculated as follows: $\sigma_h = \sqrt{\frac{p_h(1-p_h)}{n_h}}$ where n_h is the sample size for stratum h and p_h is the expected error rate. The standard error was calculated for each stratum and an overall standard error was calculated based on the following formula:

$$\sigma = \sqrt{\sum w_h^2 \cdot \sigma_h^2}$$

In which w_h^2 is the proportion of the total area covered by each stratum. The 95% Confidence Interval (CI) is $\pm 1.96 \cdot \sigma$.

Results

The confusion matrices are provided within the Annex 2 and showing the mapping error for each relevant class. For each class the number of samples which are correctly and not correctly classified are listed, which allows the calculation of the user and producer accuracies for each class as well as the confidence interval at 95% confidence levels based on the formulae above.

The Land Use / Land Cover product covering AOI 1 & 2 within Lima for 2016 has an overall mapping accuracy of 96.39% with a CI ranging from 95.23 % to 97.54% at a 95% CI. The specific class accuracies are given in Annex 2.

3.3.2 Accuracy Assessment of World Settlement Extent Product

In the following, the strategy designed for validating the World Settlement Extent (WSE) or World Settlement Footprint (WSF) 2015, i.e. a global settlement extent layer obtained as a mosaic of ~18.000 tiles of 1x1 degree size where the same technique employed in the EO4SD-Urban project is presented. In particular, specific details are given for all protocols adopted for each of the accuracy assessment components, namely response design, sampling design, and analysis; final results are discussed afterwards. In the light of the quality and amount of validation points considered, it can be reasonably assumed that the corresponding quality assessment figures are also representative for any settlement extent map generated in the framework of EO4SD-Urban.

Response Design

The response design encompasses all steps of the protocol that lead to a decision regarding agreement of the reference and map classifications. The four major features of the response design are the source of information used to determine the source of reference data, the spatial unit, the labelling protocol for the reference classification, and a definition of agreement.

- **Source of Reference Data:** Google Earth (GE) satellite/aerial VHR imagery has been used given its free access and the availability for all the project test sites in the period 2014-2015. In particular, GE automatically displays the latest available data, but it allows to browse in time over all past historical images. The spatial resolution varies depending on the specific data source; in the case of SPOT imagery it is ~1.5m, for Digital Globe's WorldView-1/2 series, GeoEye-1, and Airbus' Pleiades it is in the order of ~0.5m resolution, whereas for airborne data (mostly available for North America, Europe and Japan) it is about 0.15m.
- **Spatial Assessment Unit:** A 3x3 block spatial assessment unit composed of 9 cells of 10x10m size has been used. Specifically, this choice is justified on the one hand by the fact that input data with different spatial resolutions have been used to generate the WSF2015 (i.e. 30m Landsat-8 and 10m S1). On the other hand, GE imagery exhibited in some cases a mis-registration error of the order of 10-15m, hence using a 3x3 block allows defining an agreement e.g. based on statistics computed over 9 pixels, thus reducing the impact of such shift.
- **Reference Labelling Protocol:** For each spatial assessment block any cell is finally labelled as **settlement** if *it intersects any building, lot or – just within settlements – roads and paved surface*. Instead, pixels not satisfying this condition are marked as **non-settlement**.
- **Definition of Agreement:** Given the classification and the reference labels derived as described above, three different agreement criteria have been defined:
 - 1) for each pixel, positive agreement occurs only for matching labels between the classification and the reference;
 - 2) for each block, a majority rule is applied over the corresponding 9 pixels of both the classification and the reference; if the final labels match, then the agreement is positive;
 - 3) for the classification a majority rule is applied over each assessment block, while for the reference each block is labelled as “settlement” only in the case it contains at least one pixel marked as “settlement”; if the final labels match, then the agreement is positive.

Crowd-sourcing was performed internally at Google. In particular, by means of an ad-hoc tool, operators have been iteratively prompted a given cell on top of the available Google Earth reference VHR scene closest in time to the year 2015 and given the possibility of assigning to each cell a label among: “building”, “lot”, “road/paved surface” and “other”. For training the operators, a representative set of 100 reference grids was prepared in collaboration between Google and DLR.

Sampling Design

The stratified random sampling design has been applied since it satisfies the basic accuracy assessment objectives and most of the desirable design criteria. In particular, stratified random sampling is a probability sampling design and it is one of the easier to implement; indeed, it involves first the division of the population into strata within which random sampling is performed afterwards. To include a representative population of settlement patterns, 50 out of the ~18.000 tiles of 1x1 degree size considered in the generation of the WSF2015 have been selected based on the ratio between the number of estimated settlements (i.e. disjoint clusters of pixels categorized as settlement in the WSF2015) and their area. In particular, the i -th selected tile has been chosen randomly among those whose ratio belongs to the interval $]P_{2(i-1)}; P_{2i}]$, $i \in [1; 50] \subset \mathbb{N}$ (where P_x denotes the x -th percentile of the ratio).

Table 5: Accuracies exhibited by the WSF2015 according to the three considered agreement criteria for different definitions of settlement.

Settlement =	Accuracy Measure	Agreement Criterion					
		1		2		3	
buildings	OA%	86.96		87.86		91.15	
	AA%	88.57		90.35		88.91	
	Kappa	0.6071		0.6369		0.7658	
	$UA_{NS}\% - UA_S\%$	98.11	54.69	98.73	56.76	94.84	80.58
	$PA_{NS}\% - PA_S\%$	86.24	90.90	86.72	93.98	93.32	84.51
buildings + lots	OA	88.08		88.94		91.26	
	AA%	88.64		90.19		88.71	
	Kappa	0.6510		0.6784		0.7716	
	$UA_{NS}\% - UA_S\%$	97.54	60.71	98.13	62.66	94.29	82.62
	$PA_{NS}\% - PA_S\%$	87.79	89.49	88.26	92.12	93.95	83.48
buildings + lots + roads / paved surface	OA	88.77		90.09		88.51	
	AA%	86.34		88.28		84.27	
	Kappa	0.6938		0.7317		0.7219	
	$UA_{NS}\% - UA_S\%$	94.49	72.20	95.35	75.06	88.13	89.60
	$PA_{NS}\% - PA_S\%$	90.78	81.91	91.62	84.94	96.04	72.51

As the settlement class covers a sensibly small proportion of area compared to the merger of all other non-settlement classes (~1% of Earth’s emerged surface), an equal allocation reduces the standard error of its class-specific accuracy. Moreover, such an approach allows to best address user’s accuracy estimation, which corresponds to the map “reliability” and is indicative of the probability that a pixel classified on the map actually represents the corresponding category on the ground. Accordingly, in this framework for each of the 50 selected tiles we randomly extracted 1000 settlement and 1000 non-settlement samples from the WSF2015 and used these as centre cells of the 3x3 reference block assessment units to label by photointerpretation. Such a strategy resulted in an overall amount of $(1000 + 1000) \times 9 \times 50 = 900.000$ cells labelled by the crowd.

Analysis

As measures for assessing the accuracy of the settlement extent maps, we considered:

- the percentage overall accuracy $OA\%$;
- the Kappa coefficient;
- the percentage producer's ($PA_S\%$, $PA_{NS}\%$) and user's ($UA_S\%$, $UA_{NS}\%$) accuracies for both the settlement and non-settlement class;
- the percentage average accuracy $AA\%$ (i.e., the average between $PA_S\%$ and $PA_{NS}\%$).

Results

Table 5 reports the accuracies exhibited by the WSF2015 according to the three considered agreement criteria for different definitions of settlement; specifically, we considered as “settlement” all areas covered by: i) buildings; ii) buildings or building lots; or iii) buildings, building lots or roads / paved surfaces. As one can notice, accuracies are always particularly high, thus confirming the effectiveness of the employed approach and the reliability of the final settlement extent maps. The best performances in terms of kappa are obtained when considering settlements as composed by buildings, building lots and roads / paved surfaces for criteria 1 and 2 (i.e., 0.6938 and 0.7317, respectively) and by buildings and building lots for criteria 3 (0.7716); the $OA\%$ follows a similar trend. This is in line with the adopted settlement definition. Moreover, agreement criteria 3 results in accuracies particularly high with respect to criteria 1 and 2 when considering as settlement just buildings or the combination of buildings and lots. This can be explained by the fact that when the detection is mainly driven by Landsat data then the whole 3x3 assessment unit tends to be labelled as settlement if a building or a lot intersect the corresponding 30m resolution pixel.

3.3.3 Accuracy Assessment of the Percentage Impervious Surface Product

In the following, the strategy designed for validating the PIS product is presented; specifically, details are given for all protocols adopted for each of the accuracy assessment components, namely response design, sampling design, and analysis. Results are discussed afterwards.

Response Design

The response design encompasses all steps of the protocol that lead to a decision regarding agreement of the reference and map classifications. The four major features of the response design are the source of information used to determine the source of reference data, the spatial unit, the labelling protocol for the reference classification, and a definition of agreement.

- **Source of Reference Data:** Cloud-free VHR multi-spectral imagery (Visible + Near Infrared) acquired at 2m spatial resolution (or higher) covering a portion of the AOI for which the Landsat-based PIS product has been generated;
- **Spatial Assessment Unit:** A 30x30m size unit has been chosen according to the spatial resolution of the Landsat imagery employed to generate the PIS product;
- **Reference Labelling Protocol:** As a first step, the NDVI is computed for each VHR scene followed by a manual identification of the most suitable threshold that allows to exclude all the vegetated areas (i.e. non-impervious). Then, the resulting mask is refined by extensive photointerpretation.
- **Definition of Agreement:** The above-mentioned masks are aggregated at 30m spatial resolution and compared per-pixel with the resulting VHR-based reference PIS to the corresponding portion of the Landsat-based PIS product.

Sampling Design

The entirety of pixels covered by the available VHR imagery over the given AOI is employed for assessing the quality of the Landsat-based PIS product.

Analysis

As measures for assessing the accuracy of the PIS maps, following indices are computed:

- the *Pearson's Correlation coefficient*: it measures the strength of the linear relationship between two variables and it is defined as the covariance of the two variables divided by the product of their standard deviations; in particular, it is largely employed in the literature for validating the output of regression models;
- The *Mean Error (ME)*: it is calculated as the difference between the estimated value (i.e., the Landsat-based PIS) and the reference value (i.e., the VHR-based reference PIS) averaged over all the pixels of the image;
- The *Mean Absolute Error (MAE)*: it is calculated as the absolute difference between the estimated value (i.e., the Landsat-based PIS) and the reference value (i.e., the VHR-based reference) averaged over all the pixels of the image.

Results

To assess the effectiveness of the method developed to generate the PIS maps, its performances over 5 test sites is analysed (i.e. Antwerp, Helsinki, London, Madrid and Milan) by means of WorldView-2 (WV2) scenes acquired in 2013-2014 at 2m spatial resolution. In particular, given the spatial detail offered by WV2 imagery, it was possible to delineate with a very high degree of confidence all the buildings and other impervious surfaces included in the different investigated areas. Details about acquisition date and size are reported in Table 6, along with the overall number of final 30x30m validation samples derived for the validation exercise. Such a task demanded a lot of manual interactions and transferring it to other AOIs would require extensive efforts; however, it can be reasonably assumed that the final quality assessment figures (computed on the basis of more than 1.9 million validation samples) shall be considered representative also for PIS maps generated in the framework of EO4SD-Urban. Table 6 reports the quantitative results of the comparison between the PIS maps generated using Landsat-7/8 data acquired in 2013-2014 and the WV2-based reference PIS maps. In particular, the considered approach allowed to obtain a mean correlation of 0.8271 and average ME and MAE equal to -0.09 and 13.33, respectively, hence assessing the great effectiveness of the Landsat-based PIS products. However, it is worth also pointing out that due to the different acquisition geometries, WV2 and LS8 images generally exhibit a very small shift. Nevertheless, despite limited, such displacement often results in a one-pixel shift between the Landsat-based PIS and the WV2-based reference PIS aggregated at 30m resolution. This somehow affects the computation of the MAE and of the correlation coefficient (which however yet resulted in highly satisfactory values). Instead, the bias does not alter the ME, which always exhibited values close to 0, thus confirming the capabilities of the technique and the reliability of the final products.

Table 6: Acquisition dates and size of the WV2 images available for the 5 test sites analysed in the validation exercise along with the number of corresponding 30x30m validation samples.

	Acquisition Date [DD.MM.YYYY]	Original Size [2x2m pixel]	Validation Samples [30x30m unit]
Antwerp	31.07.2014	5404 x 7844	188.280
Helsinki	21.04.2014	12468 x 9323	516.882
London	28.08.2013	7992 x 8832	313.937
Madrid	20.12.2013	10094 x 13105	588.202
Milan	14.05.2014	8418 x 7957	297.330

3.3.4 Accuracy Assessment of Urban Green Areas Product

The validation of the Urban Green Area mapping results is done in a similar way as the one for the Land Use Land Cover product.

500 sample points was randomly distributed among the entire map and overlaid on the VHR data of each epoch. At each sample point location, the reference data was collected by visual interpretation of the VHR data. The size of the area to be observed had to be related to the Minimum Mapping Unit (MMU) of the map product to be assessed. Finally, visual interpreted land cover type was compared with the mapping results and the numbers of correctly and not-correctly classified observations were recorded. From this information the specific error matrices and statistics were computed.

The confusion matrices showing the mapping errors for each relevant class and overall accuracy are provided within the Quality Control documentation in Annex 2. The user and producer accuracies for each class as well as the confidence interval at 95% confidence level are also made available.

The Urban Green Areas product covering AOI 1 & 2 within Lima for 2016 has an overall mapping accuracy of 97.77% with a CI ranging from 96.46% to 99.08% at a 95% CI.

3.3.5 Accuracy Assessment of Building Footprints Product

The validation of the Building Footprints mapping results is done in a similar way as the one for the Land Use Land Cover and Urban Green Areas products.

Sampling Design

The reference assessment units were logically building footprints themselves. A single stage stratified random sampling was applied which used the map product for the reference year 2016 as the basis for stratification. This ensured that all classes even very minor ones were included in the sample.

Regarding the sample size, a threshold of 3% of the total number of features had been set resulting to around 1600 sample units. Then, the sample size per stratum had been set to 20 by default, knowing that all features were included in the sample for the strata with less than 20 features. Finally, the number of sampling units related to *1100 - Residential* class were increased to reach the target of 1612 in total (see Table 7).

Table 7: Number of sampling units per stratum for the Building Footprints product.

Class Name	Class ID	No. of Sampling elements
Residential	1100	915
Building Facility - Residential	1170	123
Commercial	1211	91
Industry	1212	250
University	1213	20
School	1214	41
Military	1216	19
Hospital	1217	20
Public Building	1218	17
Non-Residential Urban Fabric	1219	20
Port	1250	20
Construction Site	1320	20

Building inside Urban Park	1410	20
Recreation Facility	1420	21
Cemetery	1430	15
Total	--	1612

Response Design

The calculated number of sampling units for each building class was randomly distributed within the stratum and overlaid on the VHR data of each epoch. The Figure 3 shows the subset of building footprints corresponding to the sampling units resulting from the strategy applied.

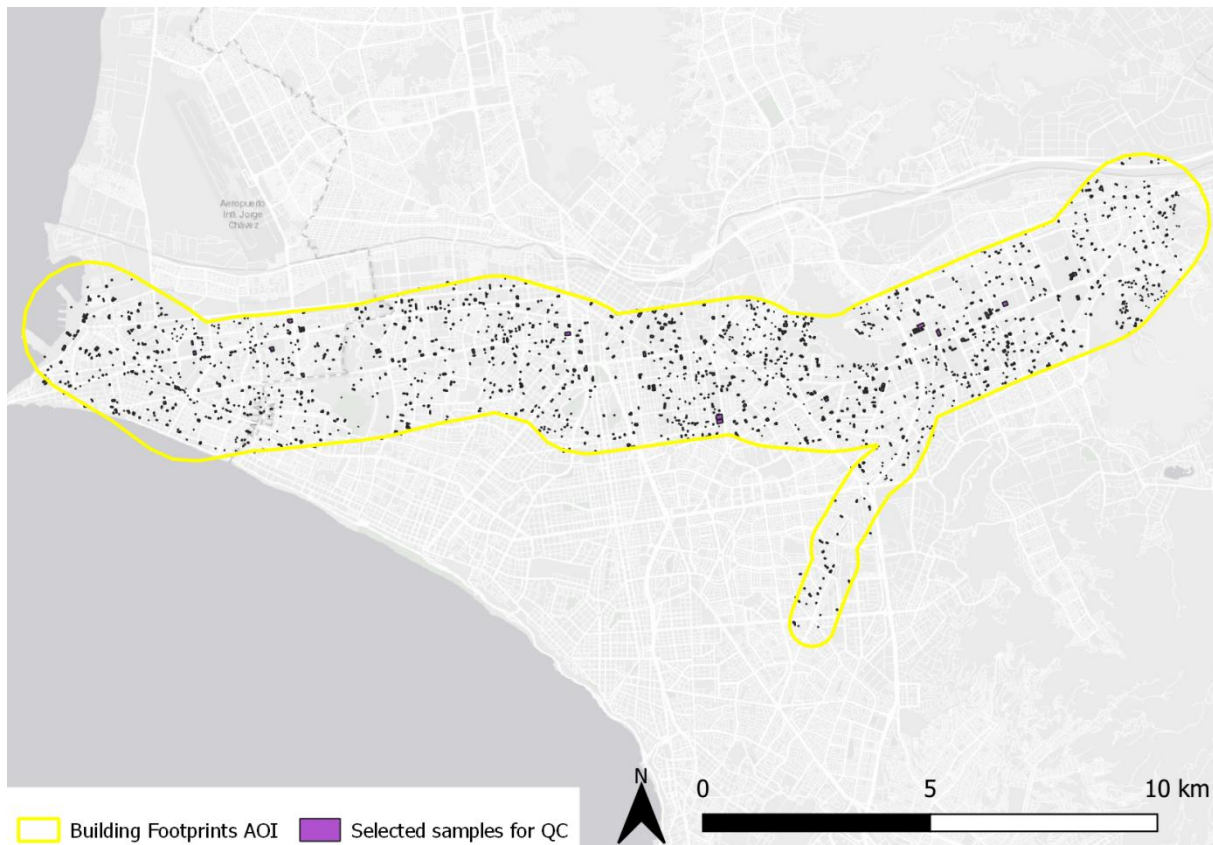


Figure 3: Subset of building footprints randomly distributed per stratum used for accuracy assessment.

In this way, for each sample unit (i.e. building footprint), the reference data was collected by visual interpretation of the VHR data. More precisely, the information collected is related to the presence/absence of the building and its thematic class/function. Then, the reference data was compared with the mapping results and the numbers of correctly and not-correctly classified observations were recorded for each class. From this information the specific error matrices and statistics were computed.

Analysis and results

The confusion matrices showing the mapping errors for each relevant class and overall accuracy are provided within the Quality Control documentation in Annex 2. The user and producer accuracies for each class as well as the confidence interval at 95% confidence level are also made available.

The Building Footprints product generated over the defined AOI in Lima for 2016 has an overall mapping accuracy of 93.76% with a CI ranging from 92.25% to 94.95% at a 95% CI.

3.4 Quality Control/Assurance

A detailed Quality Control and Quality Assurance (QC/QA) system has been developed which records and documents all quality relevant processes ranging from the agreed product requirements, the different types of input data and their quality as well as the subsequent processing and accuracy assessment steps. The main goal of the QC/QA procedures was the verification of the completeness, logical consistency, geometric and thematic accuracy and that metadata are following ISO standards on geographic data quality and INSPIRE data specifications. These assessments were recorded in Data Quality Sheets which are provided in **Annex 2**. The QC/QA procedures were based on an assessment of a series of relevant data elements and processing steps which are part of the categories listed below:

- Product requirements;
- Specifications of input data: EO data, in-situ data, ancillary data;
- Data quality checks: EO data quality, in-situ data quality, ancillary data quality;
- Geometric correction & accuracy, data fusion (if applicable), data processing;
- Thematic processing: classification, plausibility checks;
- Accuracy: thematic accuracy, error matrices
- Delivery checks: completeness, compliancy with requirements

After each intermediate processing step a QC/QA was performed to evaluate products appropriateness for the subsequent processing (see Figure 4).

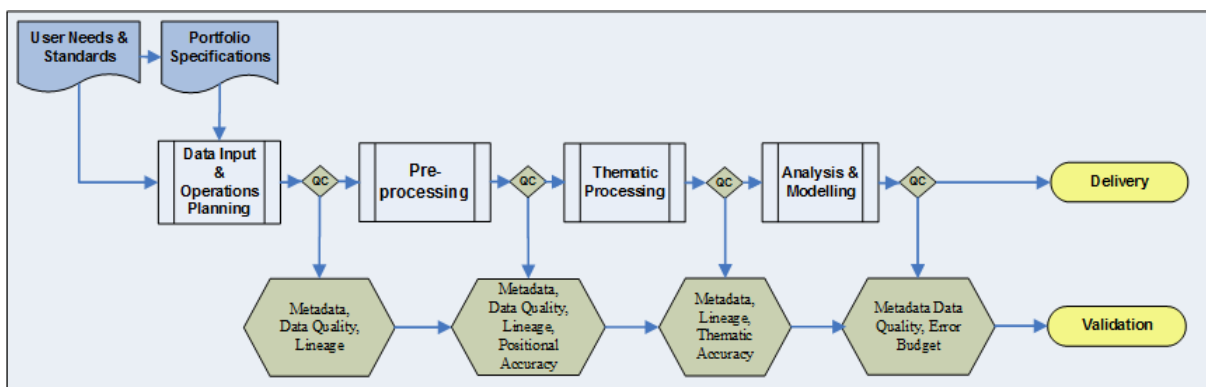


Figure 4: Quality Control process for EO4SD-Urban product generation. At each intermediate processing step output properties are compared against pre-defined requirements.

After the initial definition of the product specifications (output) necessary input data were defined and acquired. Input data include all satellite data and reference data e.g. in-situ data, reference maps, topographic data, relevant studies, existing standards and specifications, statistics. These input data were the baseline for the subsequent processing and therefore all input data had to be checked for **completeness**, **accuracy** and **consistency**. The evaluation of the quality of input data provides confidence of their suitability for further use (e.g. comparison with actual data) in the subsequent processing line. Data processing towards the end-product required multiple intermediate processing steps. To guarantee a traceable and quality assured map production the QC/QA assessment was performed and documented by personnel responsible for the Quality Control/Assurance. The results of all relevant steps provided information of the acceptance status of a dataset/product.

The documentation is furthermore important to provide a comprehensive and transparent summary of each production step and the changes made to the input data. With this information the user will be able to evaluate the provided services and products. Especially the accuracy assessment of map products and the related error matrices are highly important to rate the quality and compare map products from different service providers.

3.5 Metadata

Metadata provides additional information about the delivered products to enable it to be better understood. In the current project a harmonised approach to provide metadata in a standardised format applicable to all products and end-users was adopted. Metadata are provided as XML files, compliant to the ISO standard 19115 "Metadata" and ISO 19139 "XML Scheme Implementation". The metadata files have been created and validated by the GIS/IP-operator for each map product with the Infrastructure for Spatial Information in Europe (INSPIRE) Metadata Editor available at: <http://inspire-geoportal.ec.europa.eu/editor/>.

The European Community enacted a Directive in 2007 for the creation of a common geo-data infrastructure to provide a consistent metadata scheme for geospatial services and products that could be used not only in Europe but globally. The geospatial infrastructure called INSPIRE was built in a close relation to existing International Organization for Standardization (ISO) standards. These are ISO 19115, ISO 19119 and ISO 15836. The primary incentive of INSPIRE is to facilitate the use and sharing of spatial information by providing key elements and guidelines for the creation of metadata for geospatial products and services.

The INSPIRE Metadata provides a core set of metadata elements which are part of all the delivered geo-spatial products to the users. Furthermore, the metadata elements provide elements that are necessary to perform queries, store and relocate data in an efficient manner. The minimum required information is specified in the Commission Regulation (EC) No 1205/2008 of 3 December 2008 and contains 10 elements:

- Information on overall Product in terms of: Point of contact for product generation, date of creation
- Identification of Product: Resource title, Abstract (a short description of product) and Locator
- Classification of Spatial Data
- Keywords (that define the product)
- Geographic information: Area Coverage of the Product
- Temporal Reference: Temporal extent; date of publication; date of last revision; date of creation
- Quality and Validity: Lineage, spatial resolution
- Conformity: degree of conformance to specifications
- Data access constraints or Limitations
- Responsible party: contact details and role of contact group/person

These elements (not exhaustive) constitute the core information that has to be provided to meet the minimum requirements for Metadata compliancy. Each element and its sub-categories or elements have specific definitions; for example, in the element "Quality" there is a component called "Lineage" which has a specific definition as follows: "a statement on process history and/or overall quality of the spatial data set. Where appropriate it may include a statement whether the data set has been validated or quality assured, whether it is the official version (if multiple versions exist), and whether it has legal validity. The value domain of this element is free text," (INSPIRE Metadata Technical Guidelines, 2013). The detailed information on the Metadata elements and their definitions can be found in the "INSPIRE Metadata Implementing Rules: Technical Guidelines," (2013). Each of the EO4SD-Urban products will be accompanied by such a descriptive metadata file. It should be noted that the internal use of metadata in these institutions might not be established at an operational level, but the file format (*.xml) and the web accessibility of data viewers enable for the full utility of the metadata.

4 Analysis of Mapping Results

This Chapter will present and assess all results which have been produced within the framework of the current project, and provide the results of some standard analytics undertaken with these products including the following:

- Land Use / Land Cover - Status and Trends between 2007/2009 and 2016
- Urban Green Areas - Status and Change between 2007/2009 and 2016
- Building Footprints - Status and Change between 2007 and 2016

It is envisaged that these analytics provide information on general trends and developments in the AOIs which can then be further interpreted and used by Urban planners and the City Authorities for city planning.

The mapping results related to Flood Hazard & Risk Assessment are presented with the service operations separately in the dedicated Section 5 of this report due to the technical specifications and high level of complexity of such a study.

It should be noted that all digital data sets for these products are provided in concurrence with this City Report with all the related metadata and Quality Control documentation.

4.1 Land Use / Land Cover for 2007/2009 and 2016

This section will present the results of the LU/LC mapping for 2007/2009 and 2016 as well the statistical information on the changes between these two epochs.

4.1.1 LU/LC Mapping for AOI 1

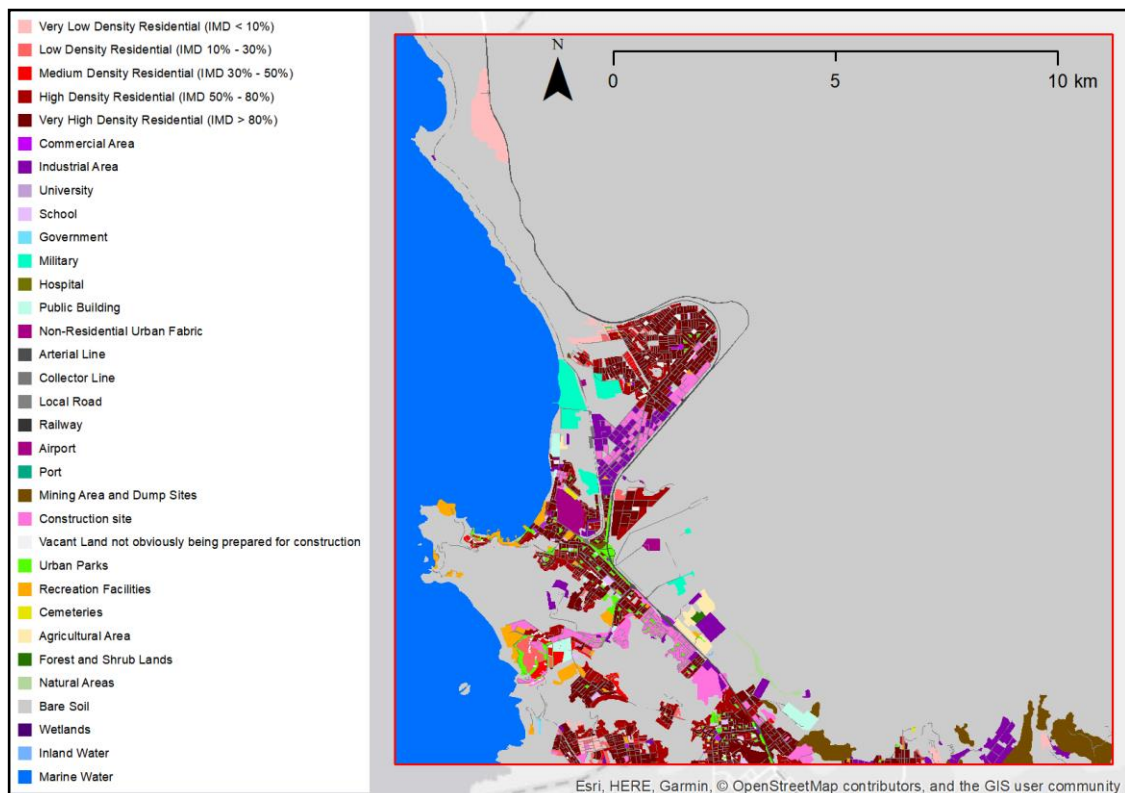


Figure 5: AOI 1 - Detailed Land Use Land Cover 2016 over Lima.

The LU/LC map generated for 2016 reference year over AOI 1 corresponding to Ancon District is depicted in Figure 5. A cartographic version of the map layout is provided as a pdf file in addition to the geo-spatial product.

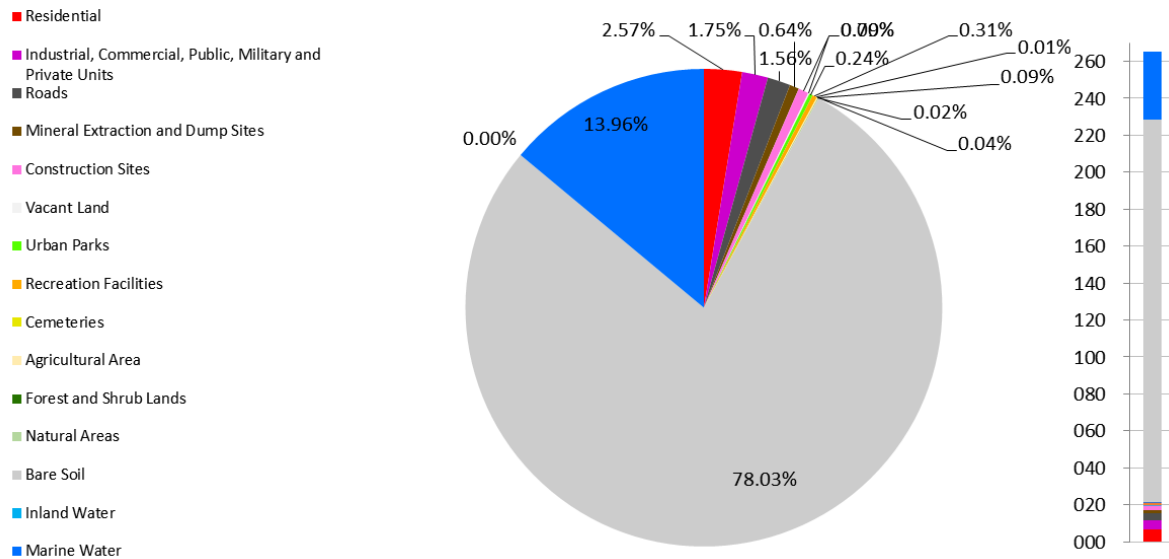


Figure 6: AOI 1 - Detailed Land Use Land Cover 2009 structure presented as Overall in % (left) and km² (right).

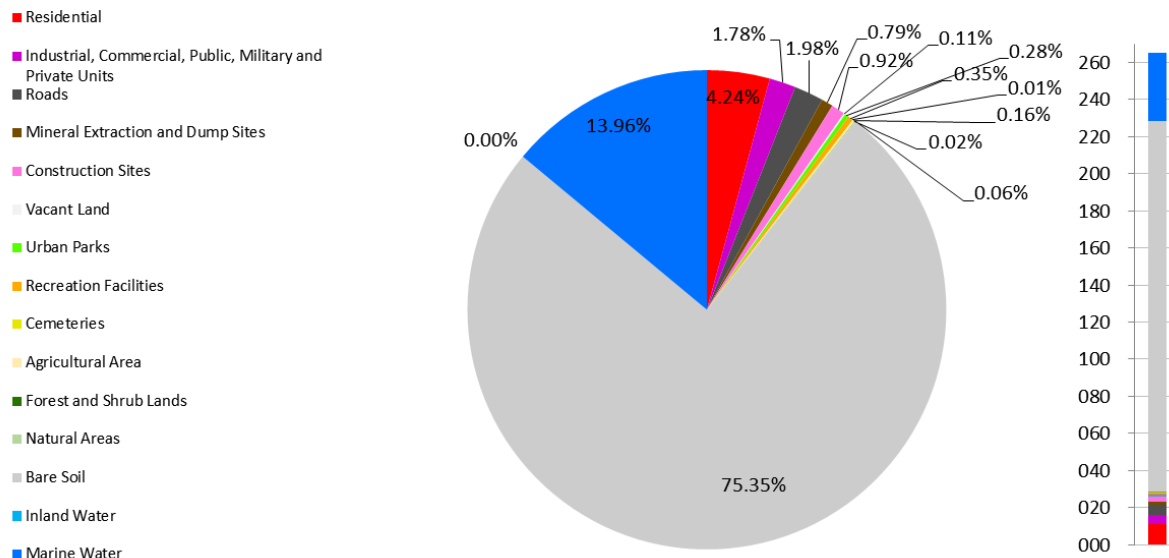


Figure 7: AOI 1 - Detailed Land Use Land Cover 2016 structure presented as Overall in % (left) and km² (right).

Figure 6 and Figure 7 provide more detailed information on the class disaggregation and area coverage for the epochs 2009 and 2016 respectively. AOI 1 covers Ancon District which is located in the north of the metropolitan area and where a project to establish a large public ecological park is initiated by the Peruvian Ministry of Environment. Therefore, it is not surprising to note that most of this territory is unexploited and covered with bare soil, still in 2016. The remaining part corresponds to artificial areas that develops near the coast along the major road and are mainly identified as residential areas mixed with industrial and military units. The most significant change over the period between 2009 and 2016 clearly is the building of new residential areas whose share increases from 2.6 to 4.2% in 8 years by consuming bare ground.

Table 8: AOI 1 - Detailed information on area and percentage of total area for each class for 2009 and 2016 as well as the changes.

LU/LC Classes	2016		2009		Change		Change per Year	
	sqkm	% of total	sqkm	% of total	sqkm	%	sqkm	%
1110 - Residential - Very Low Density	1.35	0.51%	0.14	0.05%	1.21	866.7%	0.17	123.8%
1120 - Residential - Low Density	0.50	0.19%	0.35	0.13%	0.15	41.9%	0.02	6.0%
1130 - Residential - Medium Density	0.42	0.16%	0.27	0.10%	0.15	53.7%	0.02	7.7%
1140 - Residential - High Density	2.85	1.07%	1.35	0.51%	1.50	111.1%	0.21	15.9%
1150 - Residential - Very High Density	6.14	2.31%	4.72	1.78%	1.42	30.0%	0.20	4.3%
1211 - Commercial	0.08	0.03%	0.08	0.03%	0.00	4.6%	0.00	0.7%
1212 - Industry	2.24	0.84%	2.43	0.91%	-0.19	-8.0%	-0.03	-1.1%
1214 - Schools	0.15	0.06%	0.14	0.05%	0.01	6.2%	0.00	0.9%
1215 - Government	0.02	0.01%	0.02	0.01%	0.00	0.0%	0.00	0.0%
1216 - Military	1.13	0.42%	1.13	0.42%	0.00	0.0%	0.00	0.0%
1217 - Hospitals	0.00	0.00%	0.00	0.00%	0.00	0.0%	0.00	0.0%
1218 - Public Buildings	0.53	0.20%	0.29	0.11%	0.24	83.7%	0.03	12.0%
1219 - Non-Residential Urban Fabric	0.58	0.22%	0.57	0.22%	0.00	0.4%	0.00	0.1%
1221 - Arterial	0.73	0.27%	0.73	0.27%	0.00	0.0%	0.00	0.0%
1222 - Collector	0.63	0.24%	0.63	0.24%	0.00	0.0%	0.00	0.0%
1223 - Local Road	3.90	1.47%	2.77	1.04%	1.12	40.5%	0.16	5.8%
1310 - Mineral Extraction and Dump Sites	2.09	0.79%	1.69	0.64%	0.40	23.5%	0.06	3.4%
1320 - Construction Sites	2.45	0.92%	1.86	0.70%	0.59	31.5%	0.08	4.5%
1330 - Vacant Land not obviously being prepared for construction	0.28	0.11%	0.23	0.09%	0.05	20.7%	0.01	3.0%
1410 - Urban Parks	0.73	0.28%	0.63	0.24%	0.10	16.0%	0.01	2.3%
1420 - Recreation Facilities (Sport Facilities, Stadiums, Golf Courses, etc.)	0.93	0.35%	0.82	0.31%	0.11	14.0%	0.02	2.0%
1430 - Cemeteries	0.04	0.01%	0.04	0.01%	0.00	2.8%	0.00	0.4%
2000 - Agricultural Area	0.42	0.16%	0.23	0.09%	0.19	82.2%	0.03	11.7%
3100 - Forest and Shrub Lands	0.05	0.02%	0.05	0.02%	0.00	0.0%	0.00	0.0%
3200 - Natural Areas (Savannah, Grassland)	0.15	0.06%	0.09	0.04%	0.06	61.1%	0.01	8.7%
3300 - Bare Soil	200.06	75.35%	207.16	78.03%	-7.11	-3.4%	-1.02	-0.5%

5100 - Inland Water	0.00	0.00%	0.00	0.00%	0.00	0.00	0.00	0.00%
5200 - Marine Water	37.07	13.96%	37.07	13.96%	0.00	0%	0.00	0%
Total	265.50	100%	265.50	100%	-	-	-	-

In addition to the overall LU/LC classification for the two epochs it is interesting to further assess the different trends between classes over the 7-year time. The quantitative figures for each class are first provided in Table 8 to get an overview. The next Section will highlight the LU/LC change information between the two epochs in more detail.

The area statistics of the LU/LC classes confirm the first preliminary analysis in terms of change dynamics. Indeed, artificial areas in general and residential density classes especially significantly increased over the period. The growth of densely and very densely populated residential areas is particularly strong (1.5 km², +111% and 1.4 km², +30% respectively). This trend is logically accompanied by the construction of public buildings (0.24 km², +84%) and service roads (1.1 km², 40.5%). The area covered by construction sites continues to increase (0.6 km², +31.5%), indicating that the trend to establish new residential areas goes on, while industrial areas are in slight decline (-0.2 km², -8%). As the urban expansion takes place in the desert, the proportion of bare soil within Ancon District decreases (-7.1 km², -3.4%).

4.1.2 Spatial Distribution of Main LU/LC Change Categories for AOI 1

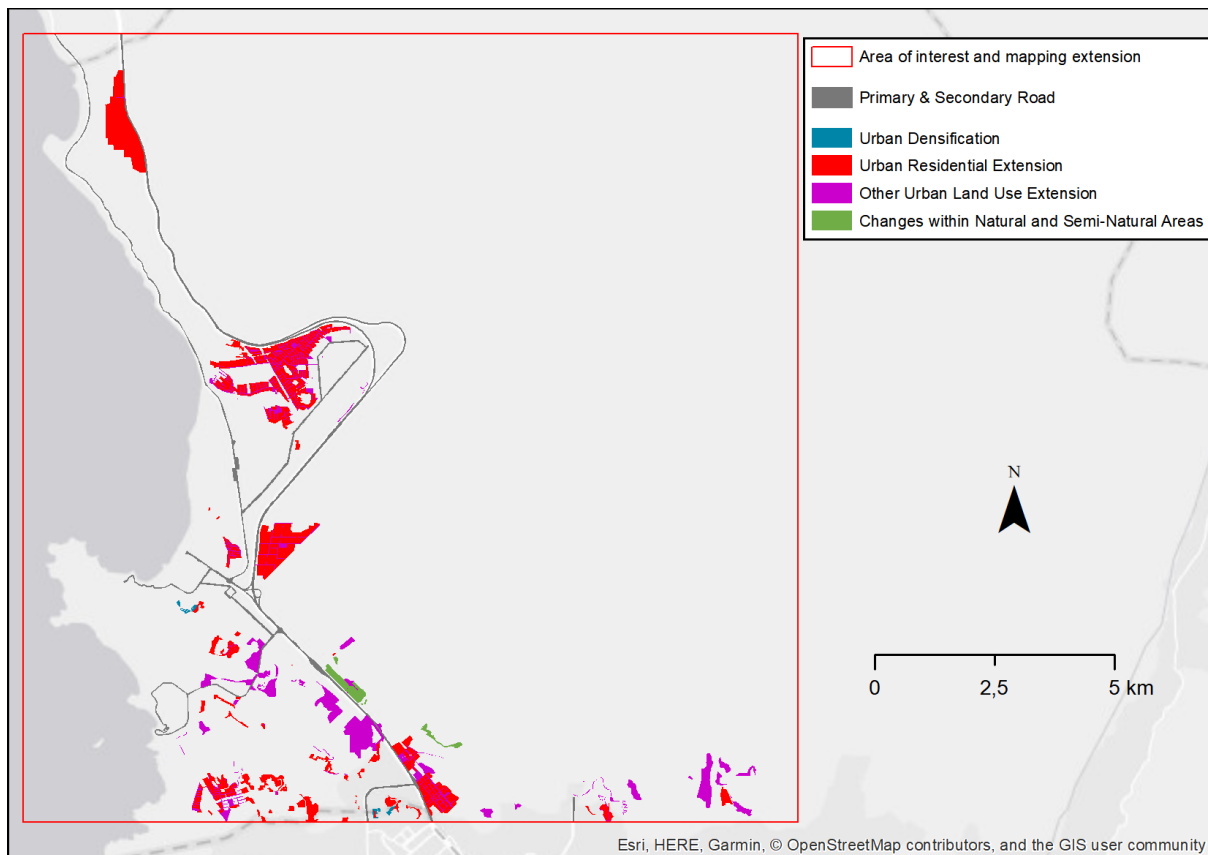


Figure 8: AOI 1 - Land Use Land Cover change types and spatial distribution.

In order to better analyse the growth trend and the spatial distribution of changes meaningful aggregations of the LU/LC classes in both epochs were used. The following categories were developed:

- Urban Densification: Changes from lower Density Residential Class into a higher one;
- Urban Residential Expansion: all changes from Non-Residential classes to a Residential one;
- Other Urban Land Use Expansion: all changes from Non-Urban or Urban Residential classes to Other Urban Land Use classes;
- Changes within Natural and Semi-Natural Areas: all changes in between the natural and semi-natural classes (e.g. Forest into Agriculture).

Overlay analysis of these aggregated categories of the epochs 2009 and 2016 is depicted in Figure 8.

The spatial distribution of the change types confirms the previously identified dynamic related to urban expansion, particularly stimulated by the development of new relatively large residential areas along the main roads.

The statistics of the Change categories are presented in Figure 9 and Table 9.

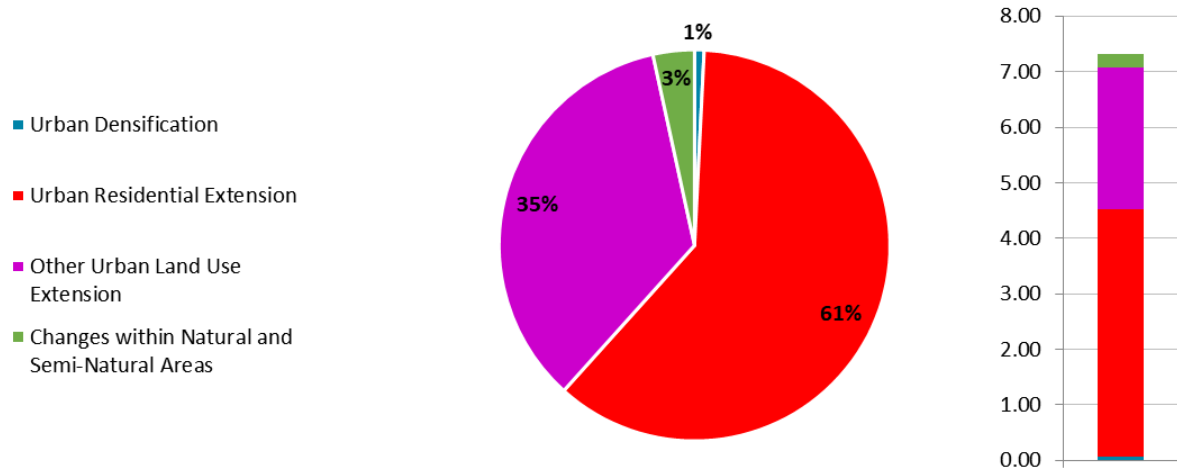


Figure 9: AOI 1 - Land Use Land Cover Change Types 2009-2016 presented in % (left) and km² (right).

The quantitative results show that the most dynamic changes which occurred between 2009 and 2016 were represented by the Urban Residential Expansion, i.e. changes from non-residential to residential classes with 60.9% from the total change area, and Other Urban Land Use Expansion, i.e. changes from non-urban to urban land use classes other than residential with 34.9%. Those changes represent 4.5 and 2.6 km² respectively over a total change area of 7.3 km². Urban Densification did not occur during the period (<1%) while changes within non-urban areas between natural and semi-natural classes were mainly limited to some new agricultural areas which remain marginal (0.25 km², 3.4%).

Table 9: AOI 1 - Overall Main LU/LC Changes Statistics.

Change Classes	Overall Change	
	sqkm	%
Urban Densification	0.06	0.8%
Urban Residential Expansion	4.46	60.9%
Other Urban Land Use Expansion	2.56	34.9%
Change within Natural and Semi-Natural Areas	0.25	3.4%
Total	7.33	100.0%

4.1.3 LU/LC Mapping for AOI 2

The LU/LC map generated for 2016 reference year over AOI 2 corresponding to the core urban area or city centre is depicted in Figure 10 and insight provided through Figure 11. A cartographic version of the map layout is provided as a pdf file in addition to the geo-spatial product.

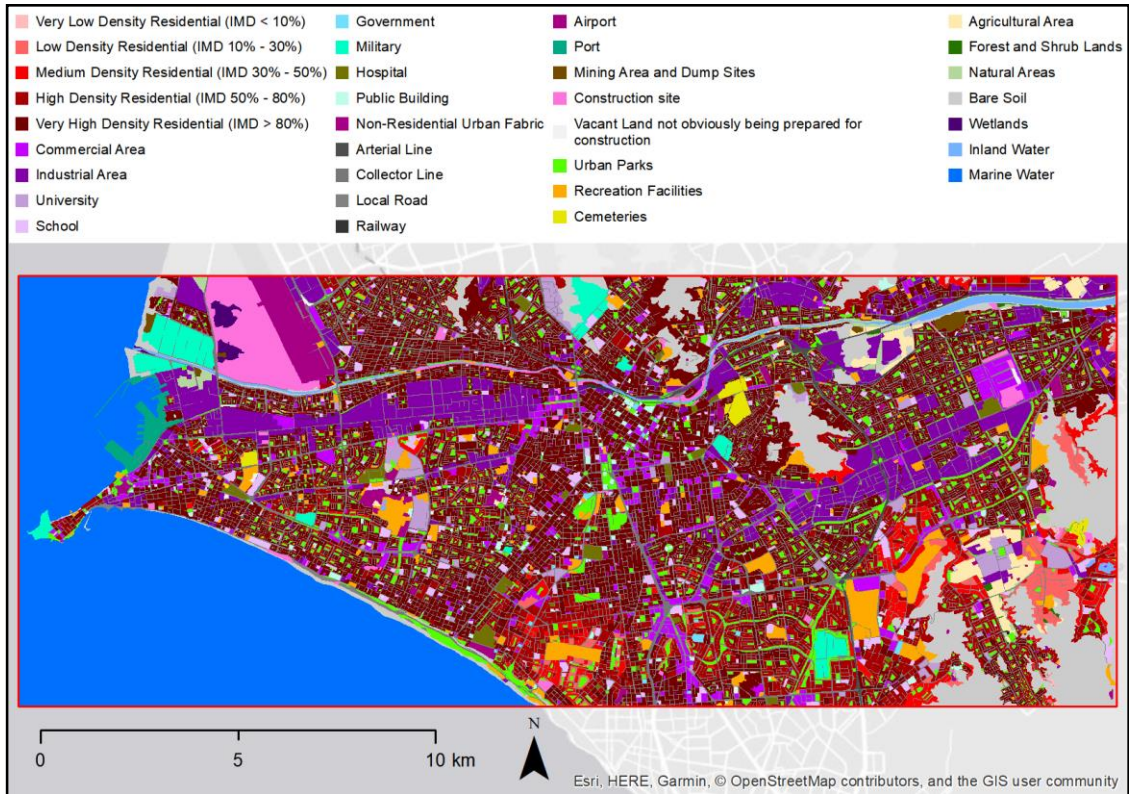


Figure 10: AOI 2 - Detailed Land Use Land Cover 2016 over Lima.



Figure 11: AOI 2 - Insight on the detailed Land Use Land Cover 2016 within the city centre.

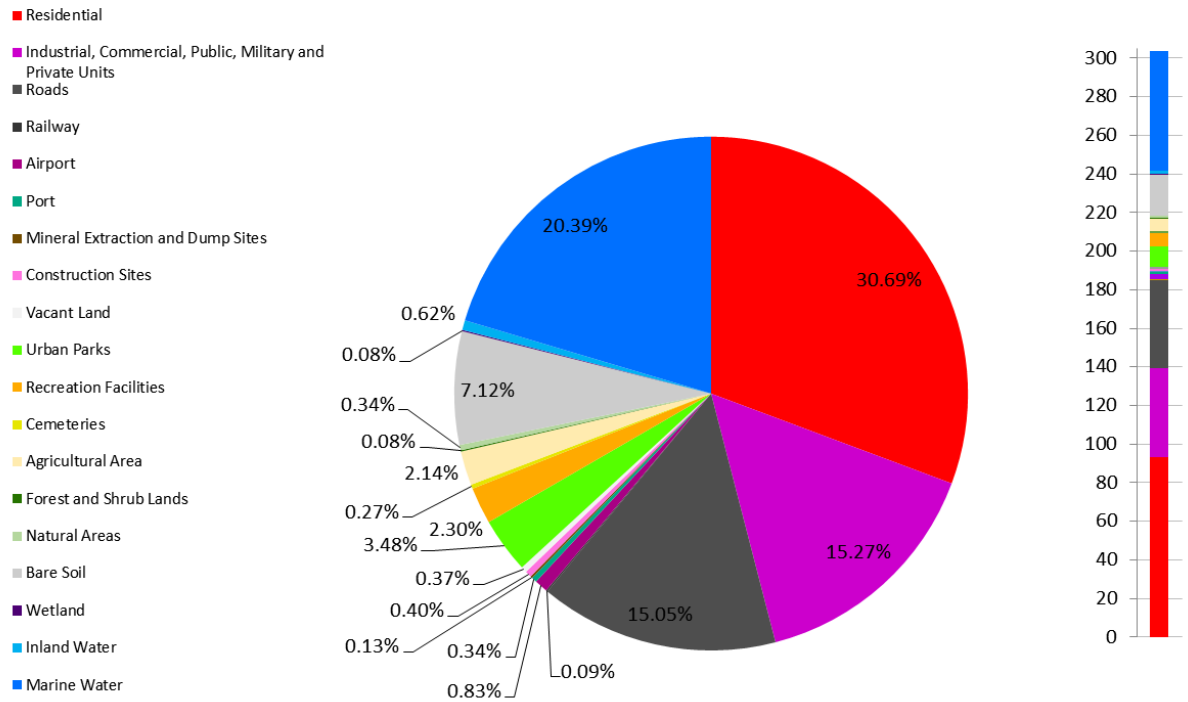


Figure 12: AOI 2 - Detailed Land Use Land Cover 2007 structure presented as Overall in % (left) and km² (right).

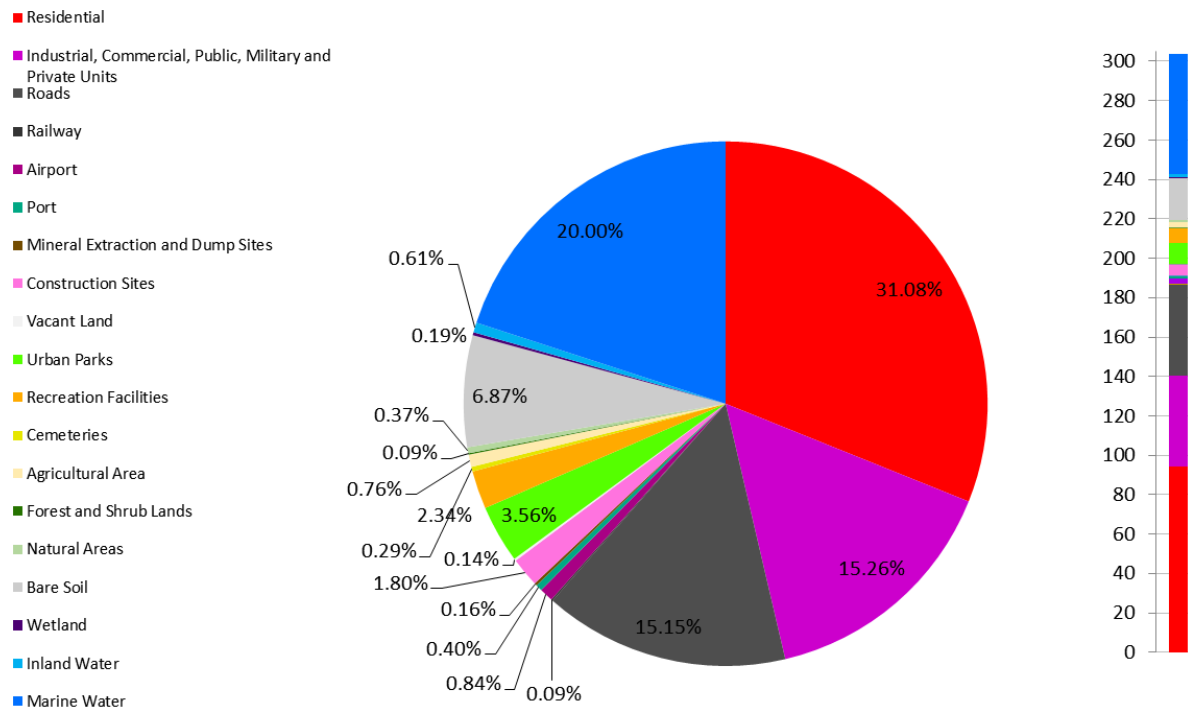


Figure 13: AOI 2 - Detailed Land Use Land Cover 2016 structure presented as Overall in % (left) and km² (right).

Figure 12 and Figure 13 provide detailed information on the class disaggregation and area coverage for the epochs 2007 and 2016 respectively. AOI 2 covers the city centre of the Peruvian capital where there are many urban challenges, e.g. population mobility and pollution, which require easy access to the public transport network and enough green spaces. Therefore, it is not surprising to note that most of this territory is covered by artificial areas largely dominated by residential areas (31% of the total area), industrial, commercial, public and private units (15%) and roads (15%). The other significant

urban areas correspond to parks (3.5%) and recreational facilities (2.3%). The remaining part mainly corresponds to bare soil with around 7% share. It is also relevant to note the high level of stability in the LU/LC distribution between 2007 and 2016 with very similar shares for most of the classes. The only one significant change dynamic over the period visible on those charts is the increase of construction sites (from 0.4 to 1.8%) at the expense of agricultural land (from 2.1 to 0.8%).

Table 10: AOI 2 - Detailed information on area and percentage of total area for each class for 2007 and 2016 as well as the changes.

LU/LC Classes	2016		2007		Change		Change per Year	
	sqkm	% of total	sqkm	% of total	sqkm	%	sqkm	%
1110 - Residential - Very Low Density	0.20	0.07%	0.33	0.11%	-0.12	-37.8%	-0.01	-4.2%
1120 - Residential - Low Density	2.82	0.93%	2.58	0.85%	0.24	9.4%	0.03	1.0%
1130 - Residential - Medium Density	6.11	2.01%	5.07	1.67%	1.04	20.4%	0.12	2.3%
1140 - Residential - High Density	20.61	6.79%	21.00	6.92%	-0.39	-1.9%	-0.04	-0.2%
1150 - Residential - Very High Density	64.59	21.28%	64.17	21.14%	0.41	0.6%	0.05	0.1%
1211 - Commercial	7.51	2.47%	7.74	2.55%	-0.23	-3.0%	-0.03	-0.3%
1212 - Industry	21.61	7.12%	21.72	7.15%	-0.10	-0.5%	-0.01	-0.1%
1213 - University	3.49	1.15%	3.36	1.11%	0.13	3.8%	0.01	0.4%
1214 - Schools	4.78	1.57%	4.82	1.59%	-0.04	-0.9%	0.00	-0.1%
1215 - Government	0.25	0.08%	0.28	0.09%	-0.03	-10.0%	0.00	-1.1%
1216 - Military	3.73	1.23%	3.74	1.23%	-0.01	-0.3%	0.00	0.0%
1217 - Hospitals	1.82	0.60%	1.76	0.58%	0.07	3.7%	0.01	0.4%
1218 - Public Buildings	1.41	0.46%	1.40	0.46%	0.00	0.2%	0.00	0.0%
1219 - Non-Residential Urban Fabric	1.73	0.57%	1.53	0.51%	0.19	12.5%	0.02	1.4%
1221 - Arterial	1.43	0.47%	1.43	0.47%	0.00	0.0%	0.00	0.0%
1222 - Collector	6.89	2.27%	6.66	2.19%	0.23	3.4%	0.03	0.4%
1223 - Local Road	37.66	12.41%	37.58	12.38%	0.08	0.2%	0.01	0.0%
1230 - Railway	0.28	0.09%	0.28	0.09%	0.01	2.5%	0.00	0.3%
1240 - Airport	2.56	0.84%	2.53	0.83%	0.03	1.3%	0.00	0.1%
1250 - Port	1.23	0.40%	1.03	0.34%	0.20	19.7%	0.02	2.2%
1310 - Mineral Extraction and Dump Sites	0.49	0.16%	0.39	0.13%	0.10	25.3%	0.01	2.8%
1320 - Construction Sites	5.48	1.80%	1.22	0.40%	4.26	349.5%	0.47	38.8%
1330 - Vacant Land not obviously being prepared for construction	0.41	0.14%	1.14	0.37%	-0.72	-63.7%	-0.08	-7.1%

1410 - Urban Parks	10.81	3.56%	10.57	3.48%	0.24	2.3%	0.03	0.3%
1420 - Recreation Facilities (Sport Facilities, Stadiums, Golf Courses, etc.)	7.12	2.34%	6.99	2.30%	0.12	1.8%	0.01	0.2%
1430 - Cemeteries	0.88	0.29%	0.81	0.27%	0.07	8.4%	0.01	0.9%
2000 - Agricultural Area	2.31	0.76%	6.50	2.14%	-4.19	-64.4%	-0.47	-7.2%
3100 - Forest and Shrub Lands	0.26	0.09%	0.25	0.08%	0.01	3.4%	0.00	0.4%
3200 - Natural Areas (Savannah, Grassland)	1.11	0.37%	1.03	0.34%	0.09	8.5%	0.01	0.9%
3300 - Bare Soil	20.85	6.87%	21.60	7.12%	-0.75	-3.5%	-0.08	-0.4%
4000 - Wetlands	0.56	0.19%	0.25	0.08%	0.32	128.7%	0.04	14.3%
5100 - Inland Water	1.84	0.61%	1.87	0.62%	-0.03	-1.6%	0.00	-0.2%
5200 - Marine Water	60.70	20.00%	61.90	20.39%	-1.20	-1.9%	-0.13	-0.2%
Total	303.52	100%	303.52	100%	-	-	-	-

In addition to the overall LU/LC classification for the two epochs it is interesting to further assess the different trends between classes over the 9-year time. The quantitative figures for each class are first provided in Table 10 to get an overview. The next Section will highlight the LU/LC change information between the two epochs in more detail.

The area statistics of the LU/LC classes confirm the first preliminary analysis in terms of change dynamics. Indeed, very few classes are concerned by a change area of more than 1 km² and only two classes show signs of real dynamics: construction sites multiplied during the period (4.26 km², +350%), whereas their presence was limited in 2007 (1.22 km²) and settled on land formerly dedicated to agriculture (-4.19 km², -64%). Nevertheless, it seems also relevant to highlight a slightly more noticeable evolution of medium-density residential areas (1.04 km², +20%) and a surface of 1.20 km² of land reclaimed from the sea (5200 - Marine Water).

4.1.4 Spatial Distribution of Main LU/LC Change Categories for AOI 2

As for AOI 1, in order to better analyse the growth trend and the spatial distribution of changes meaningful aggregations of the LU/LC classes in both epochs were used. The following categories were developed:

- Urban Densification: Changes from lower Density Residential Class into a higher one;
- Urban Residential Expansion: all changes from Non-Residential classes to a Residential one;
- Other Urban Land Use Expansion: all changes from Non-Urban or Urban Residential classes to Other Urban Land Use classes;
- Changes within Natural and Semi-Natural Areas: all changes in between the natural and semi-natural classes (e.g. Forest into Agriculture).

Overlay analysis of these aggregated categories of the epochs 2007 and 2016 is depicted in Figure 14.

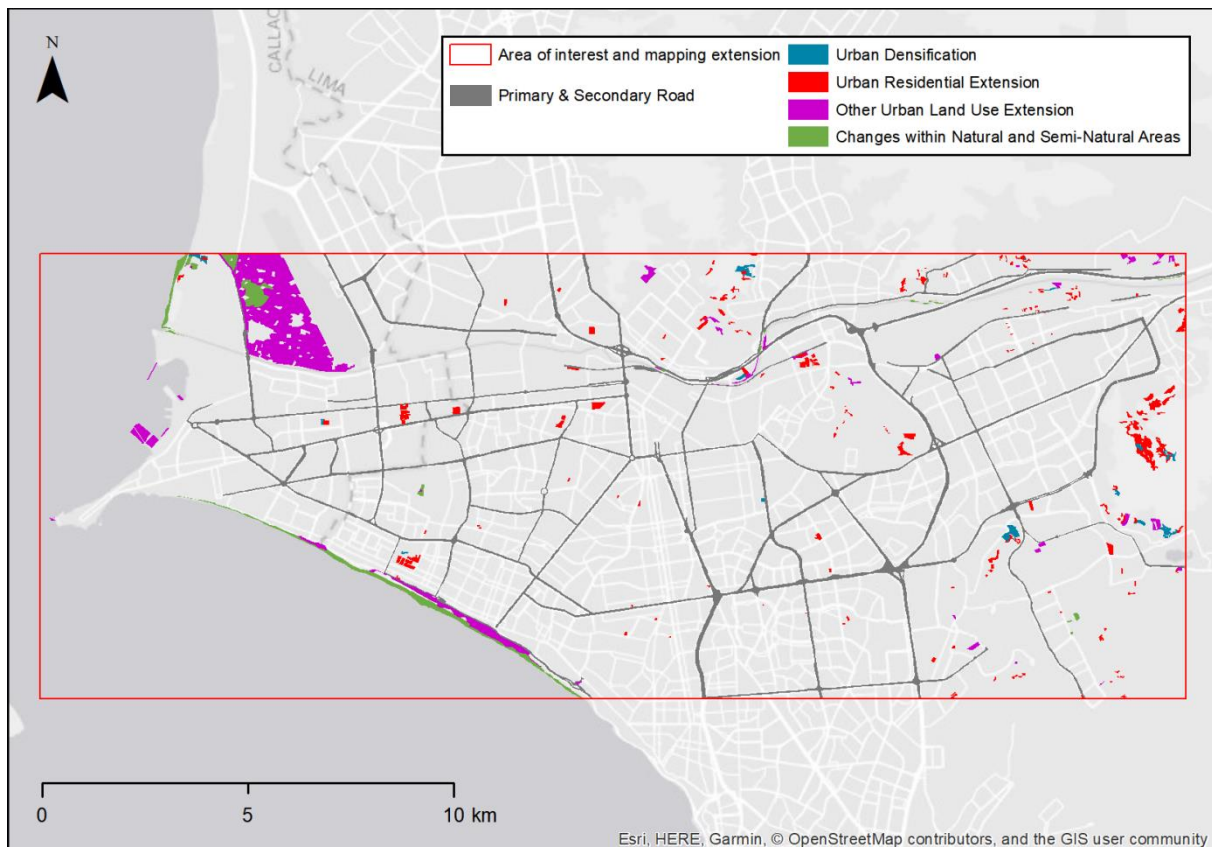


Figure 14: AOI 2 - Land Use Land Cover change types and spatial distribution.

The spatial distribution of the change types confirms the analysis in the sense that urban densification is almost non-existent and urban residential expansion quite limited which can be summarized as a few new small units scattered throughout this very urban territory. Otherwise, this change mapping highlights the location and extent of the land where agriculture or sea have given way to human activities other than residential ones:

- Located in the northeast of the AOI, near the coast, the expansion of Lima Jorge Chávez International Airport still under construction in 2016 largely explains the reduction in agricultural land present in 2007.
- Located at the extreme east of the area of interest, the Callao Port was extended by the sea.
- The southeast coast has also undergone significant changes as land has been reclaimed from the sea to create a beach lined with green spaces and recreational facilities.

The statistics of the Change categories are presented in Figure 15 and Table 11.

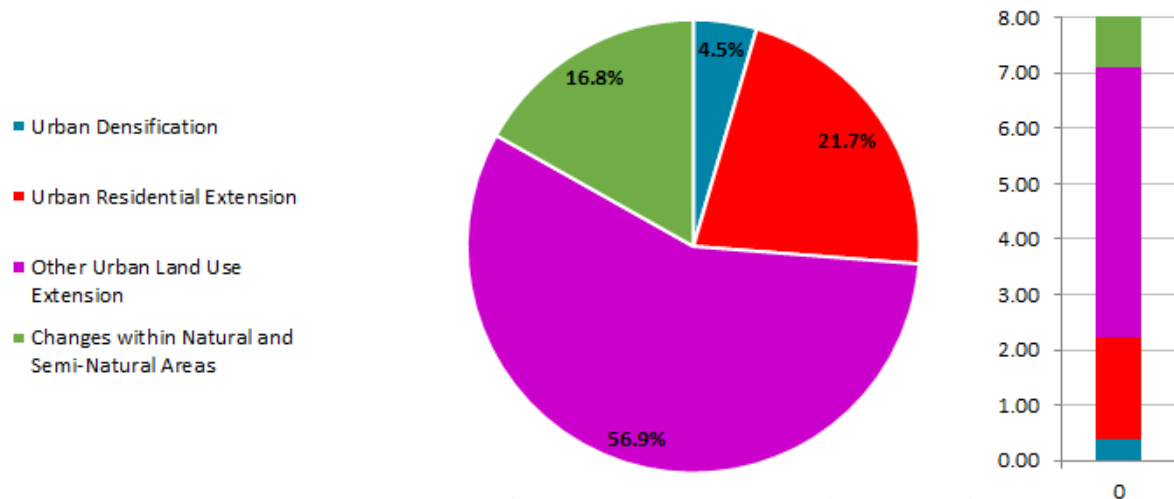


Figure 15: AOI 2 - Land Use Land Cover Change Types 2007-2016 presented in % (left) and km² (right).

The quantitative results also reveal the limited extent of the changes that occurred during the period, since they represent only 8.5 km² over an area of interest of 304 km². Most of the change areas are related to the three sites of infrastructure development identified previously which are not related to residential use and represent 73.7%, i.e. 6.3 km². Finally, new residential units were built only over 1.85 km² representing 21.7% of the total change area while urban densification is insignificant (4.5%).

Table 11: AOI 2 - Overall Main LU/LC Changes Statistics.

Change Classes	Change Overall	
	sqkm	%
Urban Densification	0.39	4.5%
Urban Residential Extension	1.85	21.7%
Other Urban Land Use Extension	4.85	56.9%
Change within Natural and Semi-Natural Areas	1.44	16.8%
Total	8.53	100.0%

4.2 Urban Green Areas

Urban green areas refer to land within and on the edges of a city that is partly or completely covered with grass, trees, shrubs, or other vegetation. The product delivered provides accurate information (1 m resolution) on the spatial location and extent of green areas located within the urban extent (Level I class: 1000 – Artificial Surfaces) derived from the baseline LU/LC information product. This section will present the results of the urban green areas mapping for 2007/2009 and 2016 focusing on the spatial and statistical information related to the changes between these two epochs.

4.2.1 Urban Green Areas for AOI 1

The Urban Green Areas change map generated over AOI 1 Ancon District is depicted in Figure 16. A cartographic version of the map layout is provided as a pdf file in addition to the geo-spatial product.

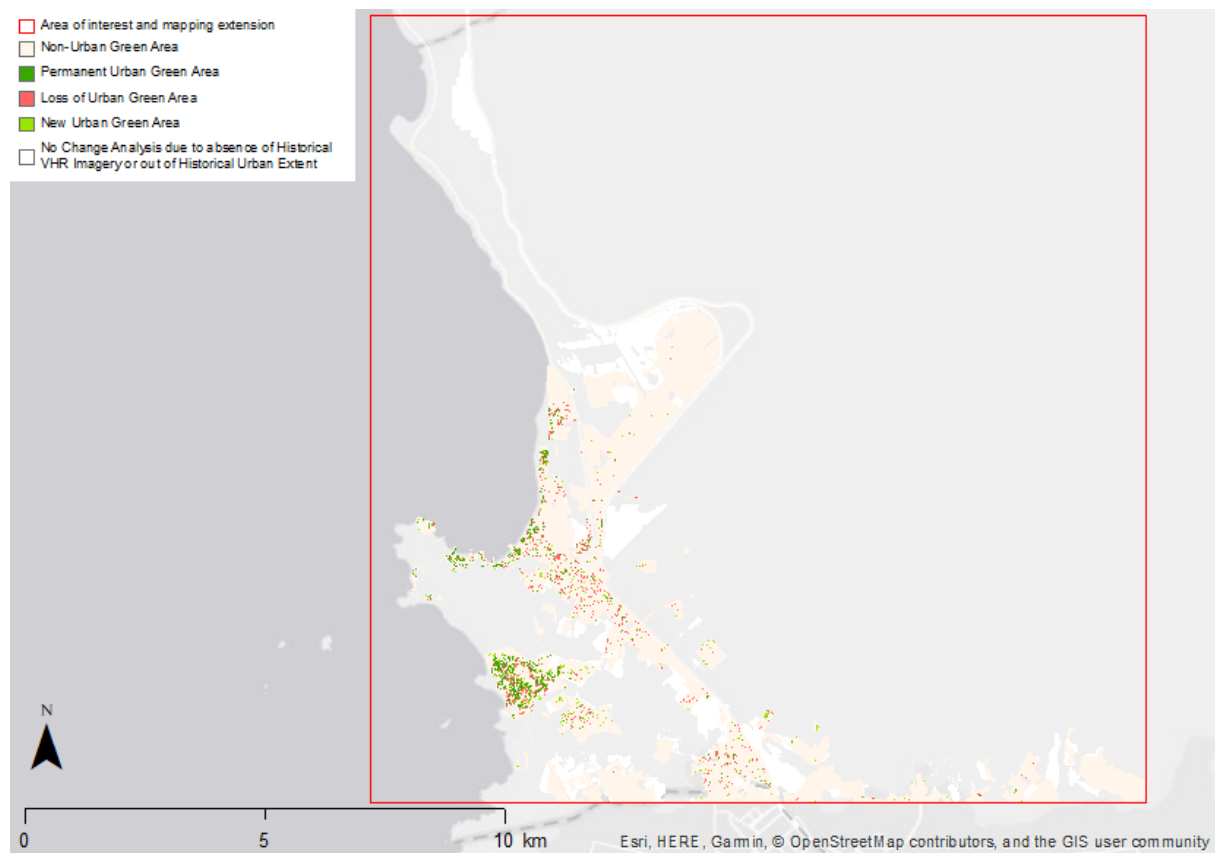


Figure 16: AOI 1 - Urban Green Areas changes and spatial distribution.

The urban extent over AOI 1 is limited to the areas along the coastline and most of the territory remains covered by bare soil. Green areas seem to be quite homogeneously distributed within this urban extent with a stronger trend for decreasing over time.

The quantitative results are presented in Figure 17 and Figure 18. The urban extent in 2016 was larger of around 7 km² comparing with the one in 2009 which explains why changes were not analysed over a quarter of 2016 urban extent. Nevertheless, the permanent green spaces over the period represent 1.75% of the entire area, or 0.5 km². But while urban expansion is significant over the 7-year period, the same cannot be said for the evolution of green coverage, at least over the historical urban extent of 2009. Indeed, the loss in green areas represents 2.3% for a gain of only 1.2%, reducing the overall coverage of urban vegetation from 1.13 km² to 0.82 km², i.e. 0.3 km² decrease.

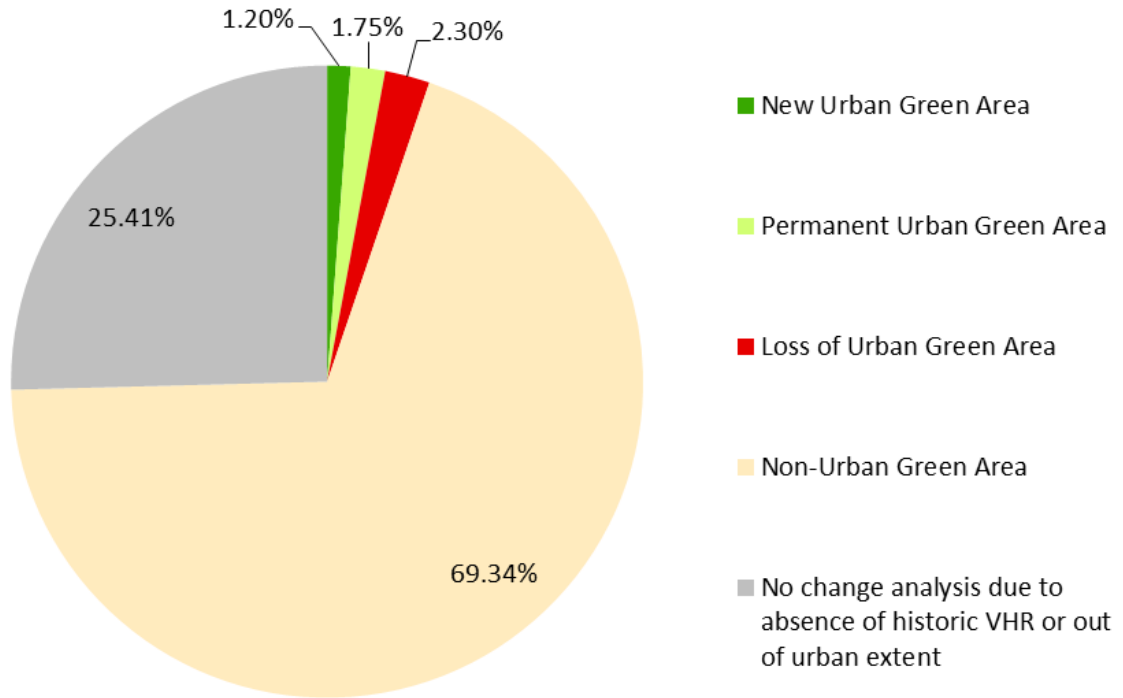


Figure 17: AOI 1 - Status and change of urban green areas in-between 2009 and 2016 expressed in %.

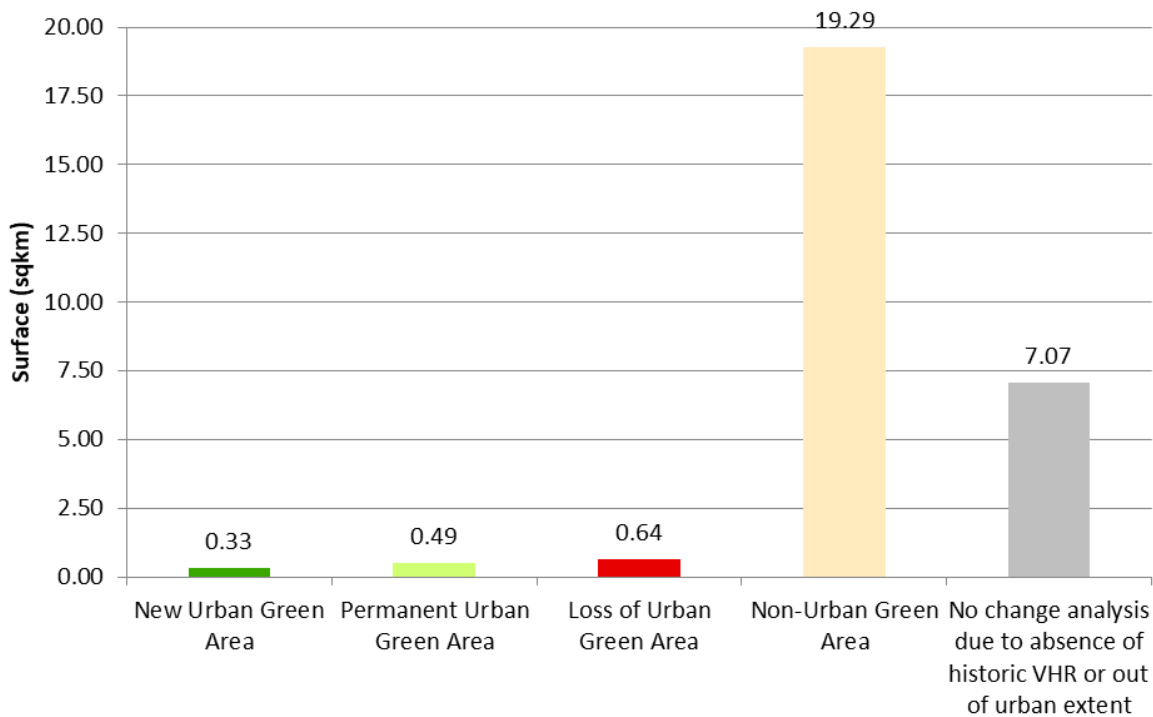


Figure 18: AOI 1 - Status and change of urban green areas in-between 2009 and 2016 expressed in area.

4.2.2 Urban Green Areas for AOI 2

The Urban Green Areas change map generated over AOI 2 corresponding to the core urban area of Lima is depicted in Figure 19. A cartographic version of the map layout is provided as a pdf file in addition to the geo-spatial product.



Figure 19: AOI 2 - Urban Green Areas changes and spatial distribution.

The urban extent logically covers most of the area of interest with very low level of urban expansion between 2007 and 2016 allowing a more complete change analysis than for AOI 1. The spatial distribution of green areas seems to be quite homogeneous with higher presence in the southern part and reveals a trend for decreasing over time.

The quantitative results illustrated in Figure 20 and Figure 21 confirm this preliminary analysis. Indeed, the area of green spaces lost over the period (21.06 km², 9.84%) is equivalent to that of permanent green spaces (19.79 km², 9.25%), while the gain is much lower (5.83 km², 2.73%). In contrast to the slightly increasing urban area from 170.76 km² to 187.98 km² (+17.22 km²), green coverage decreased between 2007 and 2016 in the heart of Lima, from 41.18 km² to 25.87 km² (-15.31 km²).

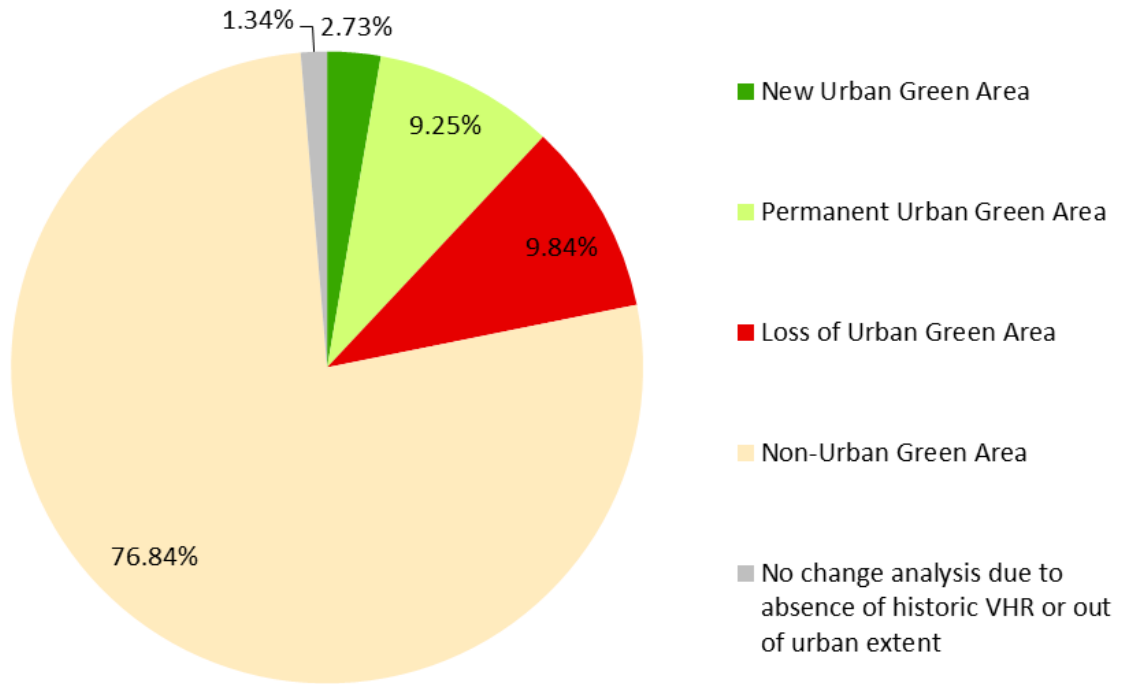


Figure 20: AOI 2 - Status and change of urban green areas in-between 2007 and 2016 expressed in %.

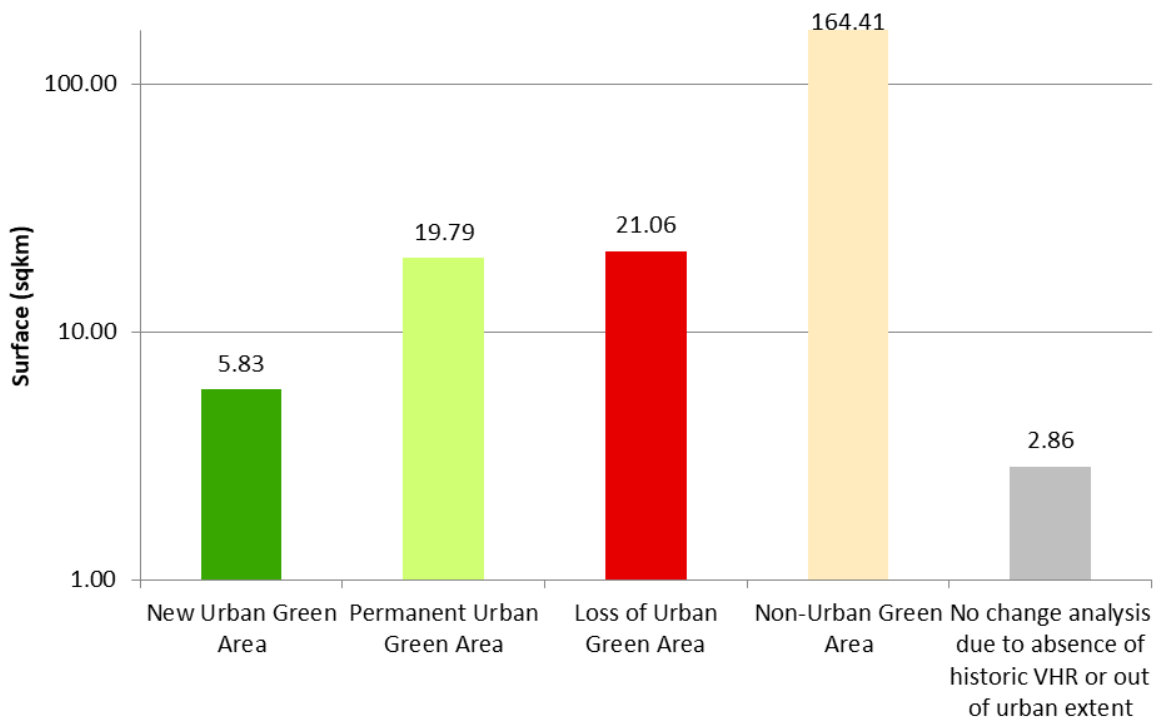


Figure 21: AOI 2 - Status and change of urban green areas in-between 2009 and 2016 expressed in area.

4.3 Building Footprints

The product provides information on the spatial distribution, number and size of building footprints which are defined as the contour of houses and other manmade buildings as they are commonly represented in cadastral systems. Not only the building footprint was extracted from VHR satellite imagery, but also the use/function of buildings was determined considering the LU/LC classification within artificial areas.

Building Footprints product has been generated only over a subset of AOI 2 defined alongside the metro line 2 crossing the city from west to east and an irrigation canal, because this is a costly product firstly aiming in this case at providing insight on building density and types and the proportion of population served by public transport. This section will present the results of the Building Footprints mapping for 2007 and 2016 as well the changes between these two epochs.

4.3.1 Mapping Results for 2016

The resulting map for 2016 is depicted in Figure 22 and a cartographic version of the map layout is provided as a pdf file in addition to the geo-spatial product.

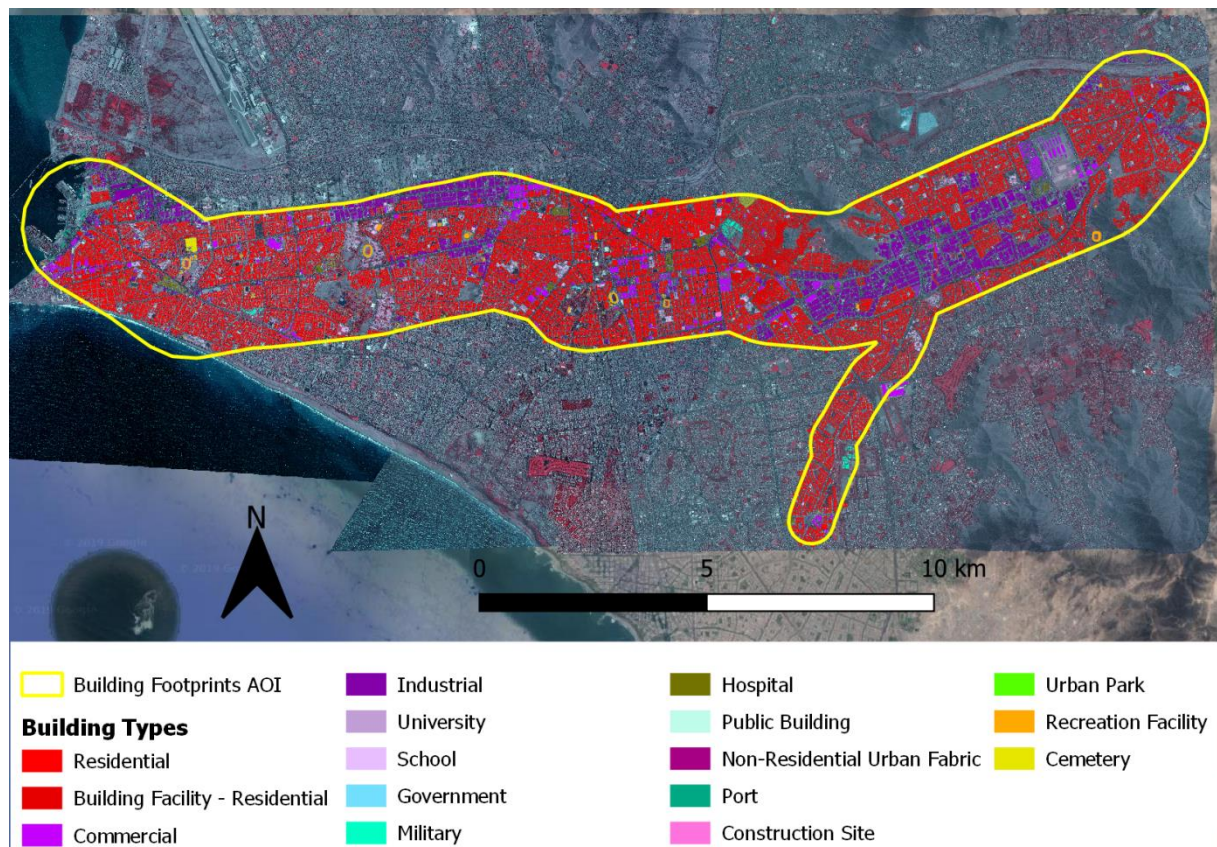


Figure 22: Mapping of Building Footprints in the heart of Lima in 2016.

The area of interest is mostly covered by artificial surfaces with a high building density and mainly used for residential purpose. If commercial buildings as well as buildings linked to public services and facilities are homogeneously distributed, industrial buildings are generally organised into large activity zones especially in central-eastern part.

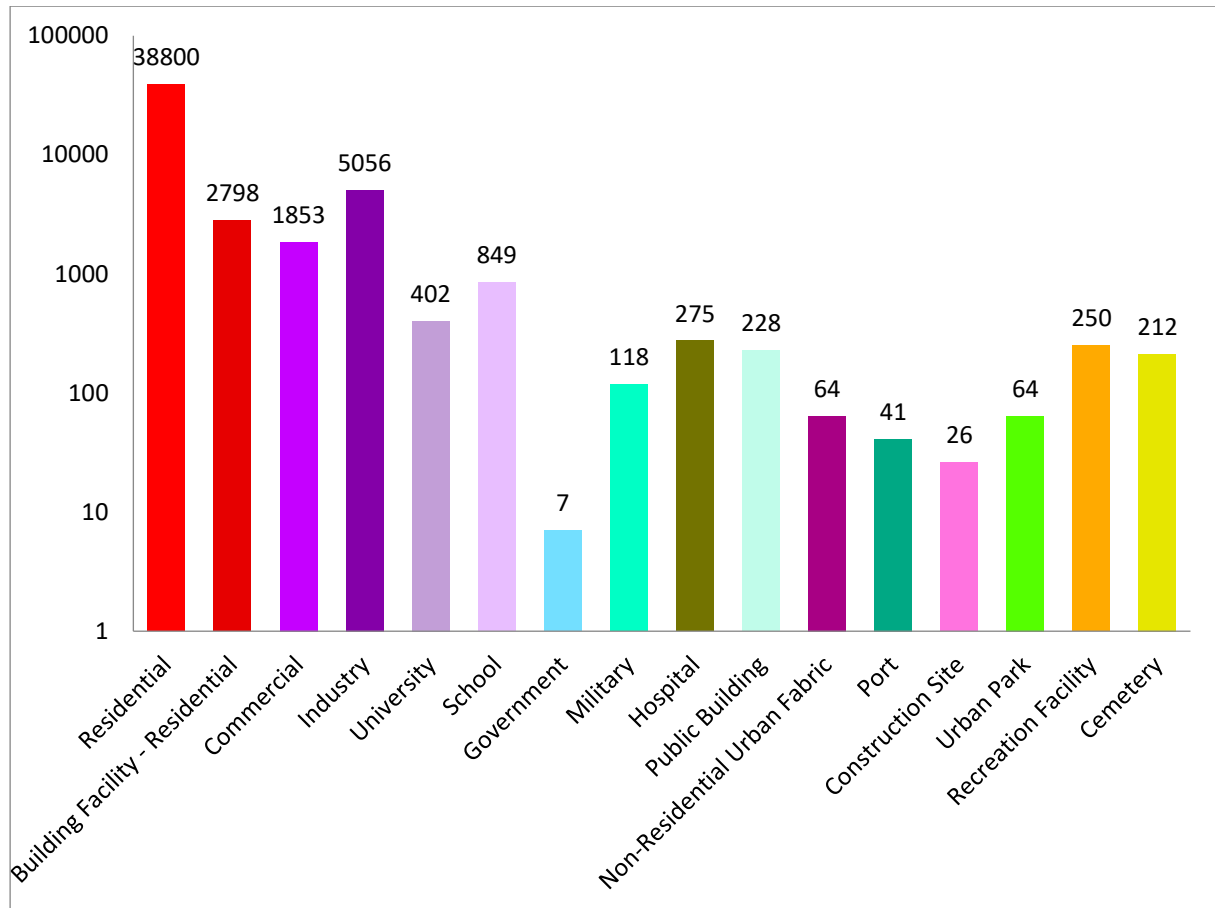


Figure 23: Number and type of buildings in the heart of Lima in 2016.

Figure 23 shows the number of building footprints extracted by type of use/function. 51,043 buildings have been extracted over an area of interest of 84 km² and the quantitative results clearly confirm the dominance of the residential buildings which represent 81.5% of the total (41,598 features including building facilities as defined in section 2.8). Industrial buildings are also numerous with more than 5,000 footprints extracted which is coherent considering the large activity zones detected on the map. Commercial buildings (1,853 features) and buildings related to public services and infrastructure finally complete the population of the dataset, particularly for education (1,251 features combining both schools and universities).

4.3.2 Mapping Results for 2007

The resulting map for 2007 is depicted in Figure 24 and a cartographic version of the map layout is provided as a pdf file in addition to the geo-spatial product.

The visual analysis of the mapping results for 2007 leads to the same conclusions as for 2016 regarding both building density and spatial distribution according to the use/function classification.

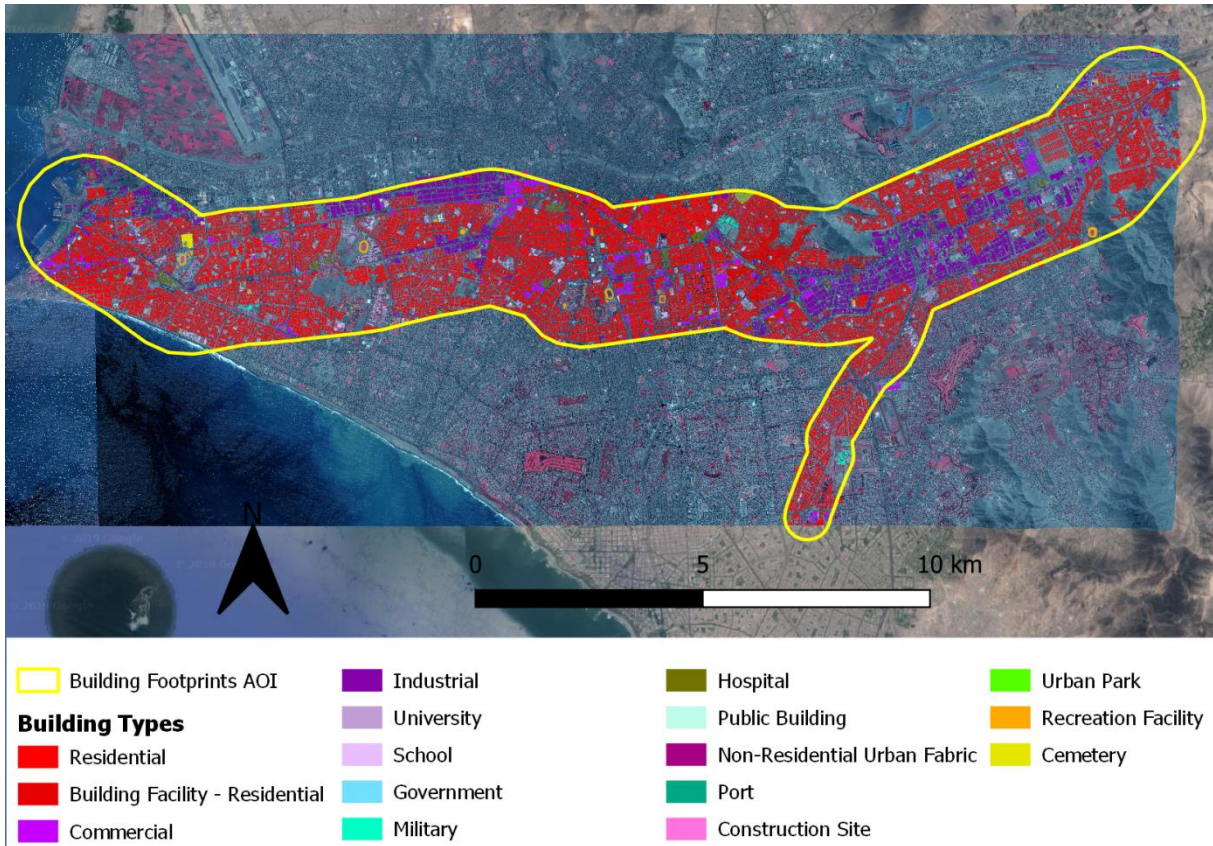


Figure 24: Mapping of Building Footprints in the heart of Lima in 2007.

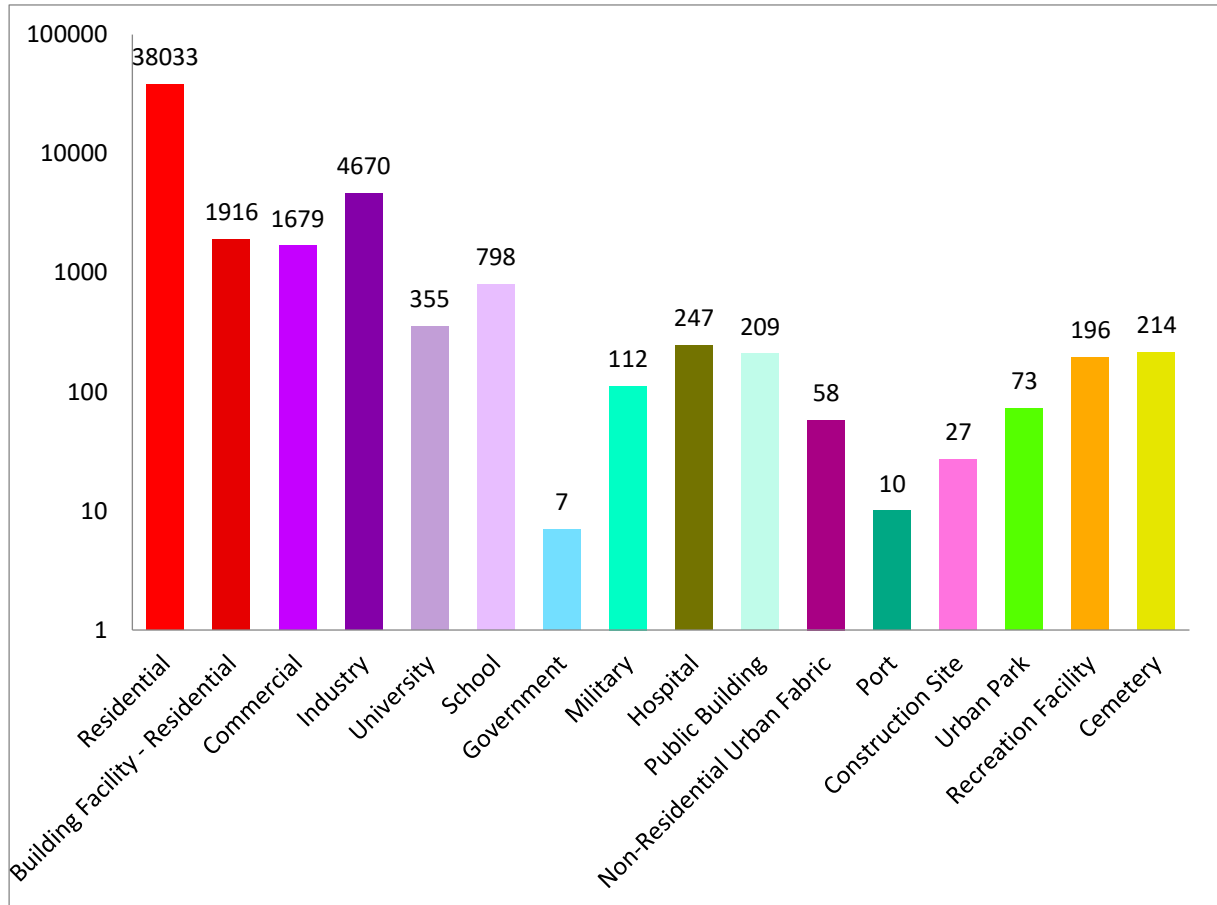


Figure 25: Number and type of buildings in the heart of Lima in 2007.

Figure 25 shows the number of building footprints extracted by type of use/function. 48,604 buildings have been generated over the area of interest which is a slightly lower number in comparison with 2016. This reveals a relatively low building rate over the decade: 2,439 features more in absolute difference, or +5%. Otherwise, residential buildings were also predominant as they represent 82.2% of the total (39,949 features including building facilities as defined in section 2.8). Near 5,000 industrial buildings were extracted mainly within the large activity zones. Commercial buildings (1,679 features) and buildings related to public services and infrastructure finally complete the population of the dataset, particularly for education (1,153 features combining both schools and universities). In conclusion, the overall distribution per building type remained stable over time.

4.3.3 Change Mapping Results

Figure 26 shows the spatial distribution of the changes occurred over the period regarding the building footprints. The changes seem to be quite homogeneously distributed with a higher proportion in the eastern part. As confirmed by Figure 27, the proportion of new buildings (61.8%, +3,000) is much higher than the one of destroyed buildings (34.2%, -1,600). It is also worth to highlight the fact that a few dozen buildings have been modified, involving a change in their footprint.

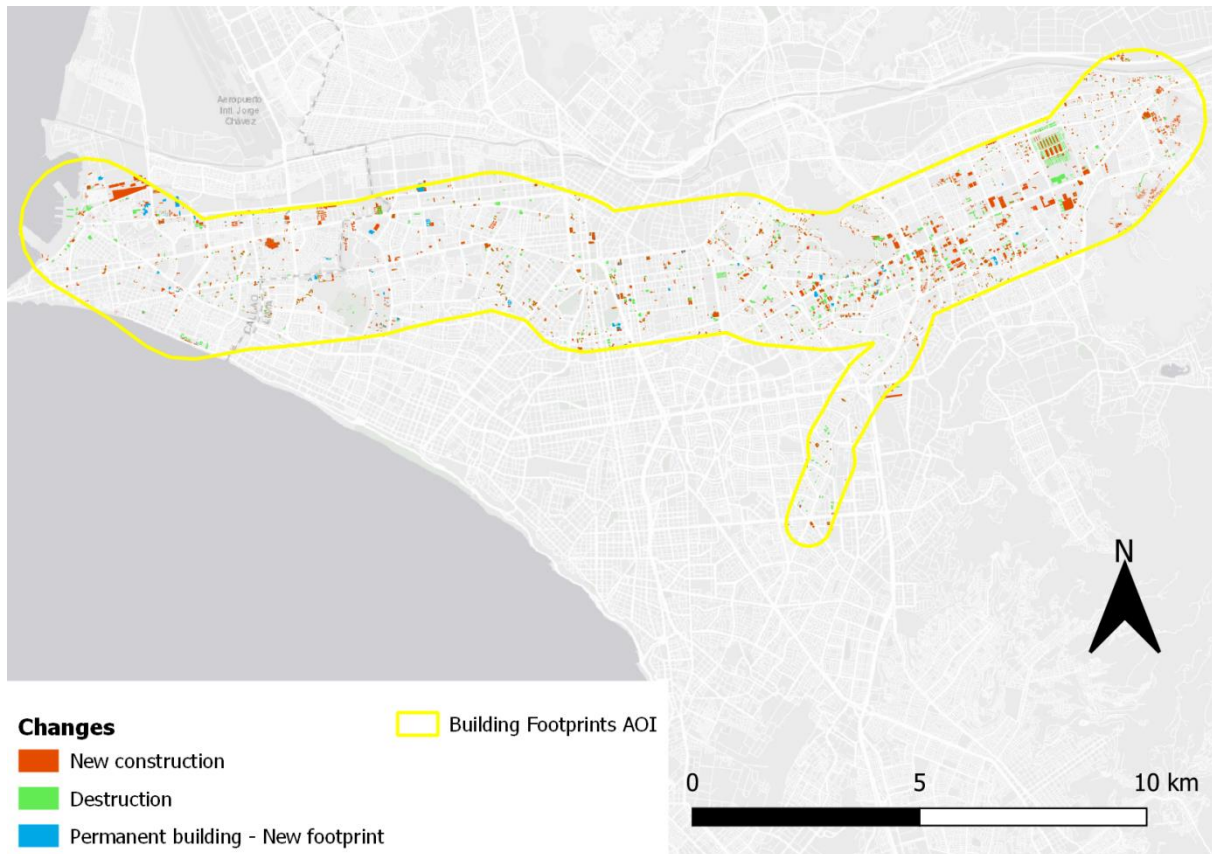


Figure 26: Building Footprints changes in the heart of Lima between 2007 and 2016.

Looking deeper and comparing with the baseline land use / land cover product, the most significant changes are related to industrial facilities. Other changes concerned new building construction for residential use mainly, highlighting the recent growth of this urban district. At the end, the overall number of buildings increased by 5% over the decade.

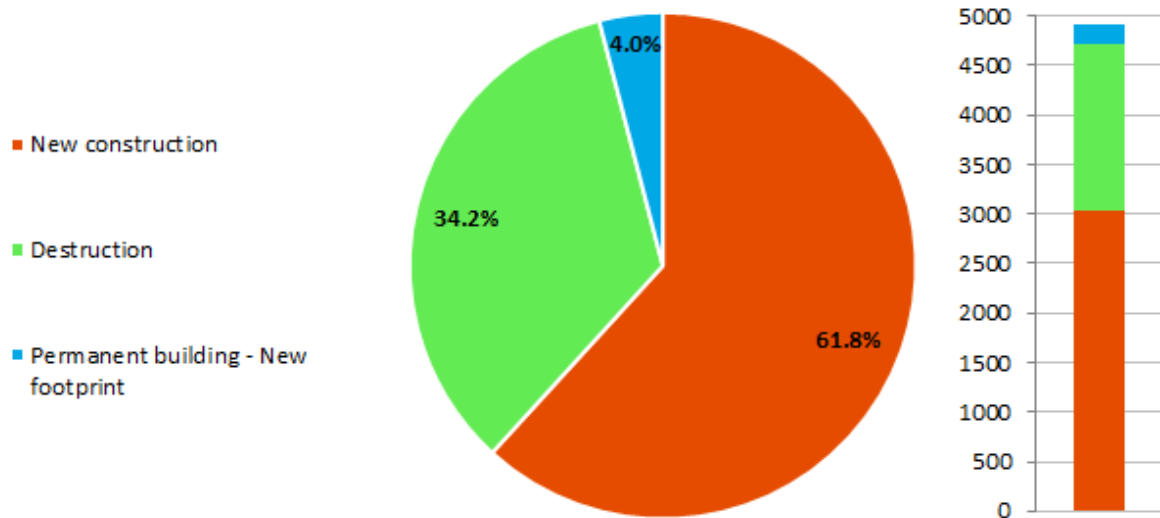


Figure 27: Relative proportion and area of changes related to building footprints-between 2007 and 2016.

Figure 28 is an example of a significant change occurring within an industrial area. Buildings have been destroyed and replaced mainly by urban green areas around a single large building.

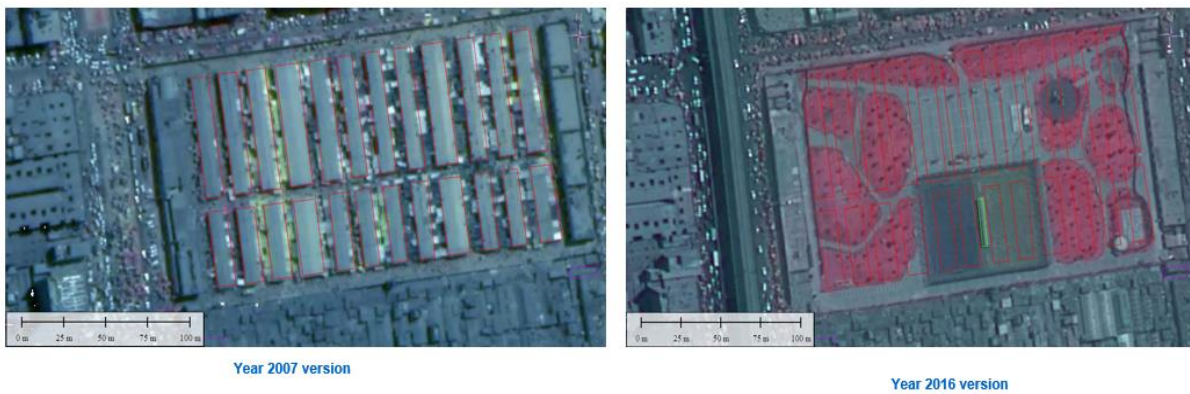


Figure 28: Example of significant change between 2007 and 2016.

4.4 Sustainable Development Goal 11 Indicators

A main objective of the EO4SD-Urban Product Portfolio is to support the reporting requirements of Urban Development Policies and Strategies. One of the most important policy frameworks that countries are trying to implement are the UN Sustainable Development Goals (SDGs). Seventeen SDGs were developed with a focus on “ending extreme poverty; fighting inequality & injustice; and addressing climate change,” by 2030. To achieve the 17 goals there are 169 targets and for each target, indicators will be used to assess the level of achievement of the countries.

The SDG Goal 11 “Make cities and human settlements inclusive, safe, resilient and sustainable” is specifically dedicated to Sustainable Urban Development. A list of Urban Sustainability Indicators specific to the SDG Goal 11, have been defined in March 2016 by the UN and are described in the UN-Habitat “SDG Goal 11 Monitoring Framework Report (UN, 2016a)”.

The EO4SD-Urban project supports seven GPSC cities, namely Bhopal and Vijayawada in India, Campeche in Mexico, Saint-Louis and Dakar in Senegal, Abidjan in Ivory Coast and Lima in Peru. For these seven cities, the indicators for which the needed input data is available were calculated and are described in the following subsections. The EO4SD-Urban products can be fully or partly used for the calculation of four SDG 11 indicators (see Table 12).

Table 12: SDG 11 indicators measurable with the support of EO4SD-Urban products.

TARGETS	INDICATORS
Target 11.1: By 2030, ensure access for all to adequate, safe and affordable housing and basic services and upgrade slums	11.1.1: Proportion of urban population living in slums, informal settlements or inadequate housing
Target 11.2: By 2030, provide access to safe, affordable, accessible and sustainable transport systems for all, improving road safety, notably by expanding public transport, with special attention to the needs of those in vulnerable situations, women, children, persons with disabilities and older persons	11.2.1: Proportion of the population that has convenient access to public transport by sex, age and persons with disabilities
Target 11.3: By 2030, enhance inclusive and sustainable urbanization and capacity for participatory, integrated and sustainable human settlement planning and management in all countries	11.3.1: Ratio of land consumption rate to population growth rate
Target 11.7: By 2030, provide universal access to safe, inclusive and accessible, green and public spaces, in particular for women and children, older persons and persons with disabilities	11.7.1: Average share of the built-up area of cities that is open space for public use for all, by sex, age and persons with disabilities

A short description of the calculation as well as the needed input data and the achieved outputs are described in the next sections for the indicators 11.2.1 and 11.3.1. For Lima, it is not possible to calculate the Indicators 11.1.1 and 11.7.1, as the needed input data is not available.

More information including the exact calculation steps of each indicator are described in the UN-Habitat Methodological Guidance document to monitor and report on the SDG Goal 11 indicators (UN-Habitat, 2016).

4.4.1 SDG 11 Indicator 11.2.1

The 11.2.1 Indicator calculates the *Proportion of the population that has convenient access to public transport by sex, age and persons with disabilities* and describes the Target 11.2: “By 2030, provide access to safe, affordable, accessible and sustainable transport systems for all, improving road safety, notably by expanding public transport, with special attention to the needs of those in vulnerable situations, women, and children, persons with disabilities and older persons.”

The indicator aims to monitor the use and access of public transportation system and move towards reaching a convenient access for all. According to UN-Habitat and described in the Methodological Guidance document (UN-Habitat, 2016) the access to public transport is considered convenient when an officially recognised stop is accessible within a distance of 0.5 km from a reference point such as home, school, workplace, market, etc.

The indicator is calculated by using the following formula:

$$\% \text{ with access to public transport} = \frac{100 \times (\text{population with convenient access to public transport})}{\text{city population}}$$

At a diagnosis phase, this indicator helps urban planners in identifying areas that are underserved and to be put as a priority in the Master Plans for the localisation of transport stations and addition of new transport lines (bus, metro, tramway, train).

Calculating this indicator considering parameters such as sex, age and persons with disabilities would require additional census data, as not available through EO data. However, the indicator can be calculated over the Larger Urban Area using the Global Human Settlement Population Layer and the OpenStreetMap (OSM) transportation features (bus and subway stations and stops, railway stations, ferry terminals), both available for the reference year 2015. It provides a first good estimate of the proportion of the population that has convenient access to public transport.

The results are presented in Figure 29 below. For comparative reasons the graphic shows the indicator results for all GPSC cities, but Bhopal and Vijayawada. The proportion of the population that has convenient access to public transport is estimated nearly 50% of the total population of Lima which is a slightly lower value than for Dakar, while this indicator is lower for Abidjan and Saint-Louis with a value close to 30% and for Campeche with 20%.

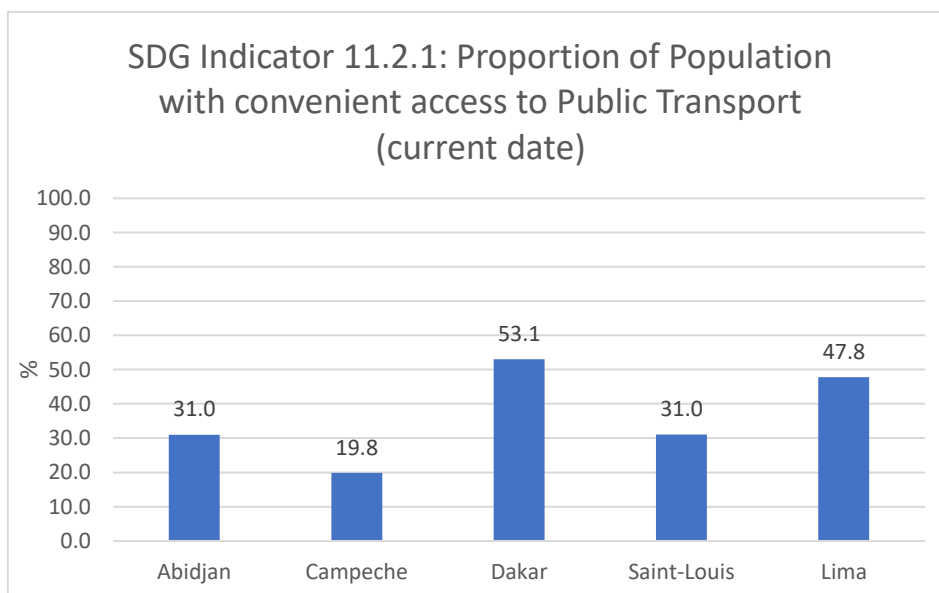


Figure 29: Proportion of population with convenient access to public transport.

4.4.2 SDG 11 Indicator 11.3.1

The 11.3.1 Indicator calculates the *Ratio of land consumption rate to population growth rate* and describes the Target 11.3: “By 2030, enhance inclusive and sustainable urbanization and capacity for participatory, integrated and sustainable human settlement planning and management in all countries.”

The indicator needs the definition of the two components population growth and land consumption rate. According to the UN-Habitat Methodological Guidance document (UN-Habitat, 2016) the population growth rate (PGR) is the increase of population in a country during a specific period, usually one year. The PGR is expressed as a percentage of the population at the start of that period.

Further, the land consumption rate includes a) the expansion of build-up area that can be directly measured and b) the absolute extent of land that is subject to exploitation by agriculture, forestry or other economic activities and c) the over-intensive exploitation of land that is used for agriculture and forestry.

The indicator is calculated by using following formula:

$$\text{Ratio of land consumption rate to population growth rate (LCRPGR)} = \frac{\text{Land consumption rate}}{\text{Annual population growth rate}}$$

The ratio of land consumption rate to population growth rate is an indicator for measuring land use efficiently and is intended to answer the questions of whether the remaining undeveloped urban land is being developed at a rate that is less than or greater than the prevailing rate of population growth. As the ratio of land consumption rate to population growth rate is dimensionless and not straightforward in its interpretation, several countries report the urban expansion and the population growth rate in terms of percentage change instead of using the ratio values (Nicolau et. al., 2018).

In the following, the ratio (see Figure 30) and the percentage change values (see Figure 31) for all GPSC cities were calculated. For the calculation of the population growth rate the Global Human Settlement Population Layer available for the years 2000 and 2015 were used. For the calculation of the land consumption rate the built-up area extracted from the Larger Urban Area LU/LC classification is taken by dissolving all artificial classes.

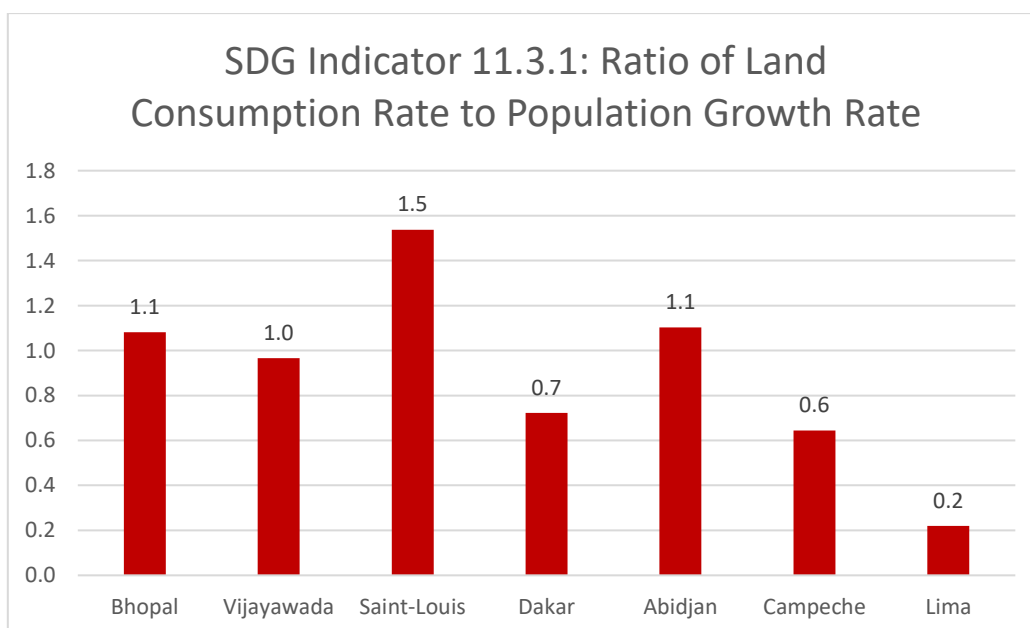


Figure 30: Ratio of land consumption rate to population growth rate between 2005 and 2015.

Figure 30 shows the ratio of land consumption rate to population growth rate for all GPSC cities. All GPSC cities are visualised in the bar chart for comparative reasons. Lima, even more than Campeche and Dakar, has a value significantly below one, which means that the population growth rate is higher than the land consumption rate and let assume that the land is efficiently used.

Cities with values close to one have a population growth rate similar to the land consumption rate. This indicates that the land is efficiently used too.

On the contrary, cities with values significantly above one have a higher land consumption rate than a population growth rate. This indicates that the land is not as efficiently used as for example in Lima.

European countries, for comparison very often have values below zero. This means that either the population or the land consumption shows a decrease.

Looking at the percentage change values of population and land consumption between 2000/2007 and 2015/2016 all cities have a growing population and a growing urban extent, which is typical for cities in developing countries. Lima’s population grew by 34% between 2000 and 2015. Its land consumption grew by 6.6% between 2007 and 2016. This means that the population grew faster than the built-up area of the city and indicates also that the city seems to grow in a compact way.

In Saint-Louis for example, it is the other way around. Here the land consumption grew by 21% while the population grew by only 17%, indicating that the city had a less compact growth in the last years.

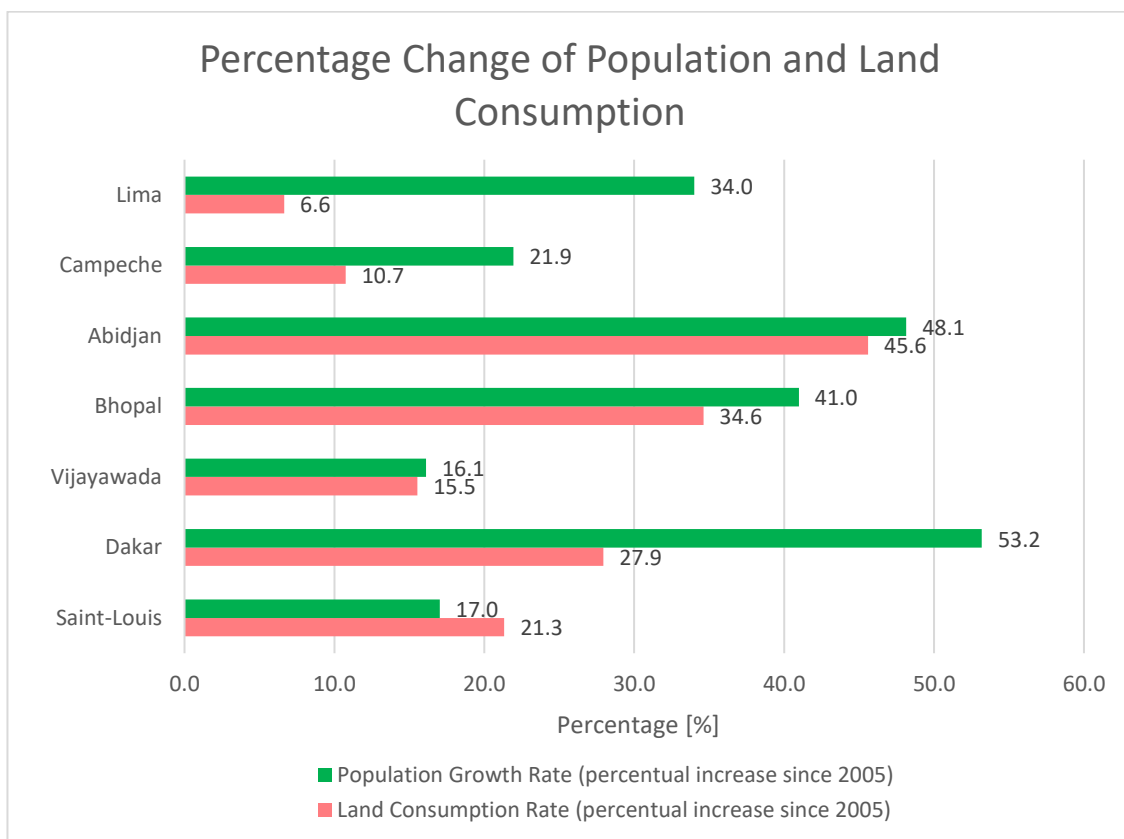


Figure 31: Percentage change of population and land consumption between 2005 and 2015.

A significant limitation of this indicator is that the approach captures only the urban extent change, not the internal city dynamics.

4.5 Concluding Points

This Chapter 4 presented only a summary and overview of what is possible in term of analytics with the geo-spatial datasets provided for Lima in the current project. This Report is a living document and will be complemented with further analysis during the project when relevant. Important would be to further analyse the EO4SD Urban datasets with the main stakeholder, i.e. the Peruvian Ministry of Environment in charge of urban development policies, in order to enhance the latter for planning purposes.

5 Flood Hazard and Risk Assessment

Flood Hazard and Risk Mapping is a vital component for appropriate land use planning in flood-prone areas. First of all, Flood Hazard and Risk Maps are designed to increase awareness of the likelihood of flooding among the public, local authorities and other organisations.

Specific flood regimes and underlying causes for the flooding events in the area of interest have to be analysed carefully, as these can be very varied in different regions.

For the metropolitan area of Lima basically three main flood scenarios have to be considered:

- Tsunamis in coastal areas generated by major earthquakes in close proximity to the Peruvian coast
- River Floods after heavy rainstorms in the upper catchment parts of the main rivers crossing the metropolitan area (mainly December – March)
- Short-term local Flash Floods and Mud and Debris Flows in mountainous Eastern parts of Lima (mainly December – March)

The latter two scenarios may occur together.

Because of the fundamental cause – effect relationships the flood hazard analysis is performed separately for the processes (1) Tsunami inundations and (2) River and Flash Floods (including Mud and Debris Flows).

5.1 General Characteristics of the Study Area

The city of Lima stretches for 60 km from north to south along the Pacific Ocean, and for more than 30 km from west to east from the Pacific Ocean to the Andes Mountains. The seaport and town of Callao is considered as part of the city of Lima and forms the Lima Metropolitan Area.

Lima's estimated population is about 10,000,000. Since the ocean and mountains bind the city, further expansion is difficult.

The study area covers about 1,153 km² and altitudes between 0 and approx. 2,300 m asl (cf. Fig 1).

Most of Metropolitan Lima is located on the Pacific Coastal Plain on dissected alluvial cones formed by the Chillón, Rímac and Lurín rivers having its source in the Western Cordillera of the Central Andes. The eastern parts of the city, however, extend over the foothills and valleys of the Andean Mountains.

The Western Cordillera of the Andes Mountains rises abruptly east of the city and reaches altitudes of 6,100 m only 130 km from the Pacific Ocean.

The geology of the Lima region reflects the active subduction of the Nazca Plate under the South American Plate and consequent uplift and volcanic activity. The Andes in Central Peru are relatively young mountains with the oldest exposed rock being pyroclastics of the upper Jurassic. These are overlain by lower Cretaceous shales and quartzites, followed by limestone of lower to middle Cretaceous age. In middle and upper Cretaceous time, volcanism resumed and andesites and pyroclastics were deposited which form the bedrock at the highest stratigraphic level. The overlying alluvial cones and beach sediments formed during the rapid rise of the Andes have been dissected by rejuvenated down-cutting to as much as 20 m at Lima (Karakouzian et al. 1997).

Western South America is the only major subduction zone where an entire oceanic slab descends under a continent. Here, the oceanic Nazca Plate subducts beneath the South American continent. The interaction of these two gigantic plates is the main reason for very high seismic activity in this region. With the exception of Japan, the Pacific continental border of South America has the highest seismic activity in the world. Major earthquakes with magnitudes greater than 8.0 occur every 5–10 years in this region (Kulikov et al. 2005).



Figure 32: Lima, Peru – Service Area (Image: DigitalGlobe 22/02/2017, 13/05/2016; DHM: ALOS World 3D – 30m, version 2.1 - ©JAXA)

Lima is located in the great desert that runs along the Pacific Coast of South America. To the east, the Andean Mountains prevent the transport of moisture from the Amazonas basin. Rain and snow mostly fall on the eastern side of the range casting a rainless shadow over the western slopes.

Due to the cold Humboldt ocean current (Peru current) flowing north along the western coast of South America and carrying fresh, cold Sub-Antarctic surface water, temperatures are much lower than expected. The effect of the cold water of the Humboldt current is enhanced by up-welling taking place along the coast of Peru. Despite Lima’s location in the tropics about 12 degrees south of the equator and in a desert, the climate can be classified as a desert climate with subtropical temperature ranges (Capel Molina 1999). It is characterized by a warm season from December to April, and a cool, humid and cloudy season from June to October, with May and November as transition months. Marine air is cooled by the current and thus is not conducive to generating precipitation (although clouds and fog are produced).

While relative humidity is high, rainfall is very low due to strong atmospheric stability (Garreaud & Aceituno 2007). Inland districts receive anywhere between 10 and 50 mm of rainfall per year, which accumulates mainly during the winter months. Coastal districts receive only 10 to 30 mm (Ministerio De Agricultura 2010). Winter precipitation occurs in the form of persistent morning drizzle events - locally called 'garúa'. Summer rain is infrequent and occurs in the form of isolated light and brief showers which generally occur during afternoons and evenings when leftovers from Andean storms arrive from the east (Capel Molina 1999). However, the amount of precipitation increases significantly when approaching the Andean mountains, resulting in a semiaride climate which is characterized by occasional heavy local storms in summer season (Villacorta et al. 2015).

Lima's climate (like that of most of coastal Peru) gets severely disrupted in El Niño events. El Niño–Southern Oscillation (ENSO) is an irregularly periodic variation in winds and sea surface temperatures over the tropical eastern Pacific Ocean, affecting the climate of much of the tropics and subtropics. The warming phase of the sea temperature is known as El Niño and the cooling phase as La Niña. The two periods last several months each (typically occurring every few years) and their effects vary in intensity (MetOffice 2019). Mechanisms that cause the oscillation remain under study.

The average annual precipitation in the catchment areas of the three main rivers crossing Metropolitan Lima (Chillón, Rímac and Lurín River) varies between values near zero in the coastal area and more than 1000 mm in the highest part of the catchment area (cf. Figure 33).

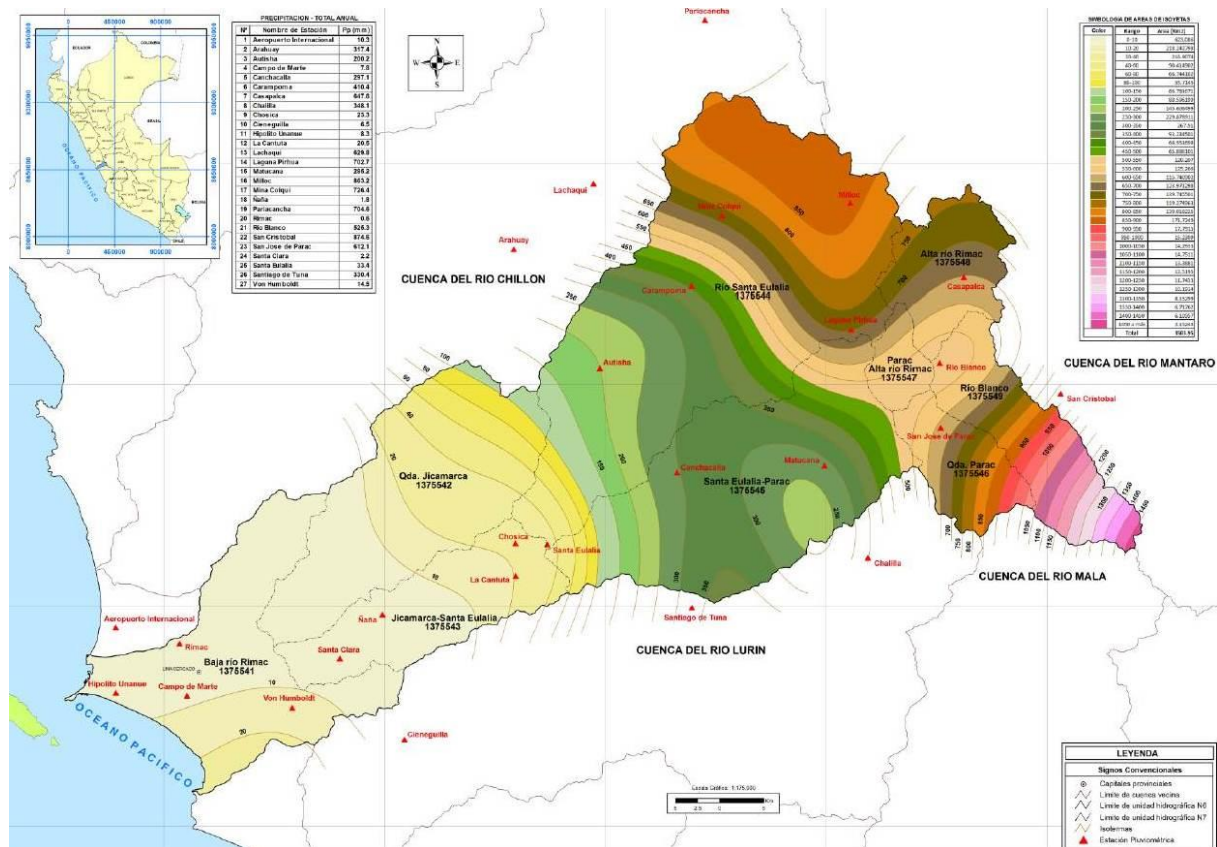


Figure 33: Spatial distribution of the total annual precipitation (isohyets) in the catchment area of the Rímac River in the period 1964 - 2009 (Ministerio De Agricultura 2010)

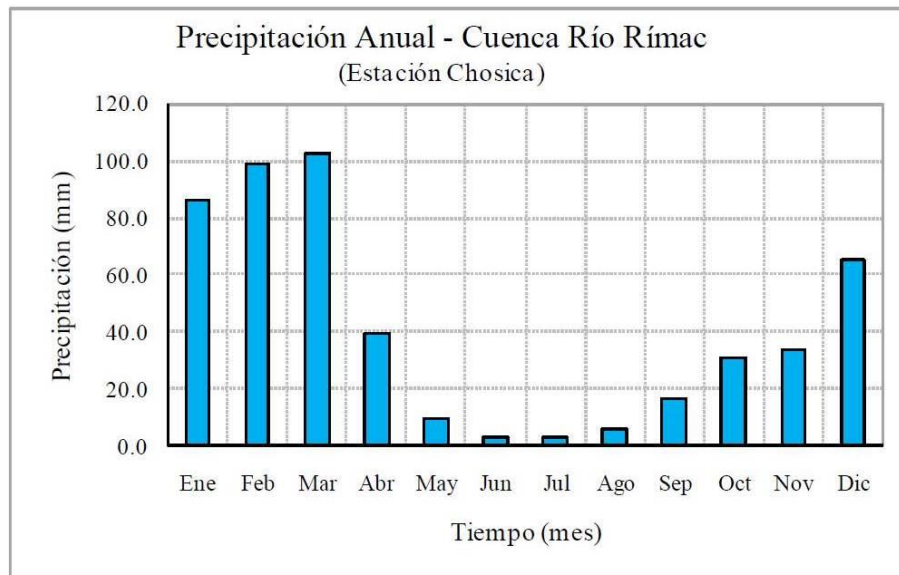


Figure 34: Monthly distribution of average total precipitation in the Rímac River basin – based on the method of Thiessen polygons for the Chosica weather station (Ministerio De Agricultura 2010).

The maximum precipitation in the Rímac River basin within 24 hours between 1964 and 2009 was recorded in 1970 at Santiago de Tuna weather station (close to the watershed between Rímac and Lurín Rivers) with approx. 90 mm (Ministerio De Agricultura 2010).

The maximum 24 h precipitation within the study area between 1964 and 2009 was 37.2 mm in La Cantuta near Chosica (2002) and 30.7 mm in Chosica (2002). In the coastal area 16.0 mm at the Hipólito Unanue weather station and 9.7 mm at the Von Humboldt weather station (both on 15-01-1970) are outstanding.

Three major rivers cross Metropolitan Lima all having its sources in the Western Cordillera of the Central Andes Mountains and flowing into the Pacific Ocean (cf. Figure 35). These are from north to south:

- Chillón River (Catchment Area: 2,296 km², Flow Length: 126 km)
- Rímac River (Catchment Area: 3,663 km², Flow Length: 160 km)
- Lurín River (Catchment Area: 1,825 km², Flow Length: 109 km)

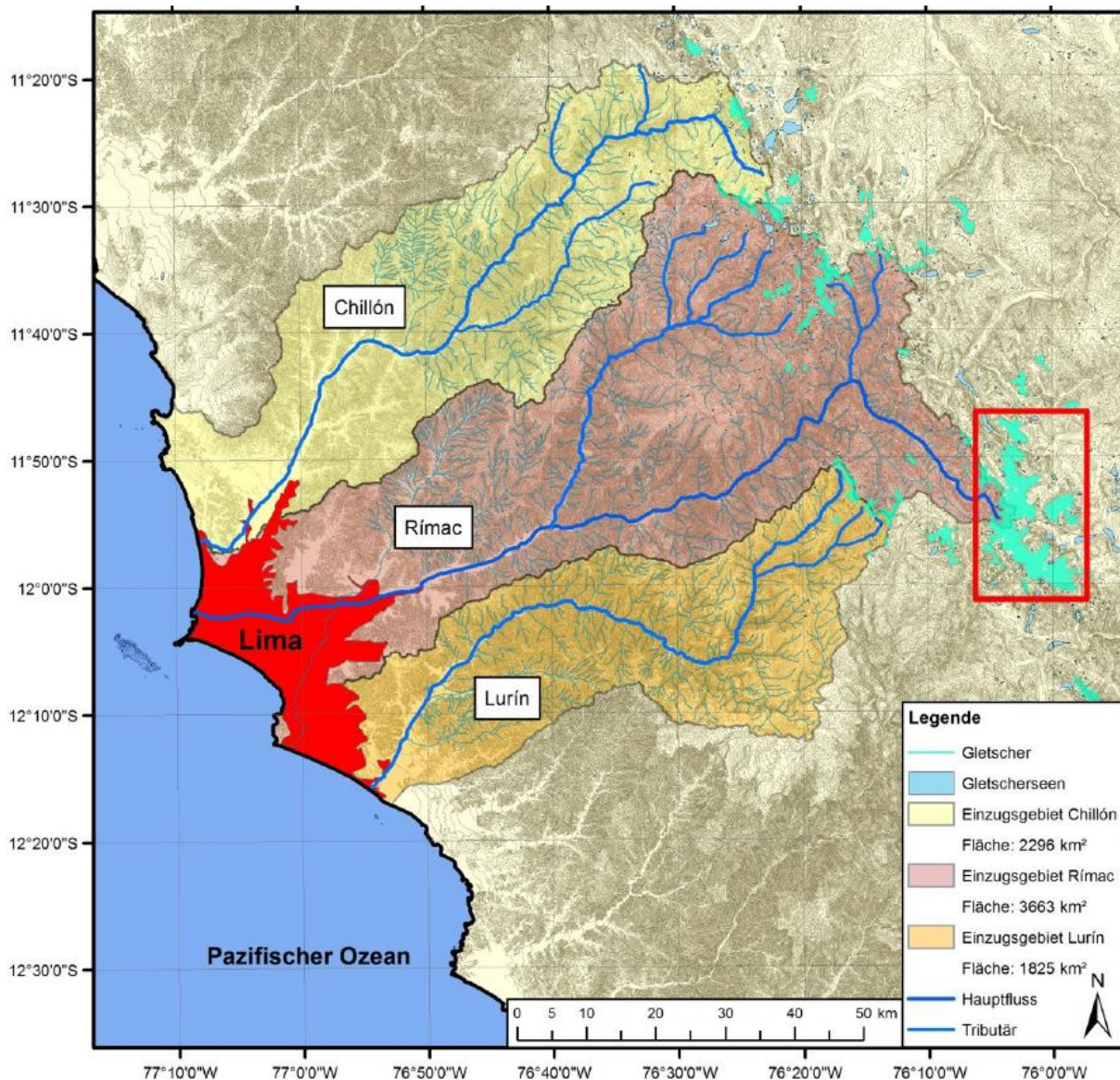


Figure 35: The catchment areas of the Rivers Chillón, Rímac and Lurín on the western slopes of the Central Andes (Drenkhan 2010)

Within the basins of the three rivers all kind of humidity provinces from super-arid to super-humid can be found.

Whereas the Chillón River and the Lurín River touch the study area only marginally, the lower part of the catchment area of the Rímac River lies within the study area completely. The largest tributary within the study area is the Rio Huaycoloro flowing into the Rímac River from the north in Santa Maria de Huachipa.

Numerous smaller tributaries most of them to be categorized as torrents (*'quebradas'*) run into the Rímac River from both sides of the valley. Typically these torrents are dry over long periods (years over even decades) and are activated only in times of heavy precipitations producing devastating flash floods and debris flows.

The Rímac River which brings melt- and rainwater from the Central Andes is a vital resource for the city, since it carries what will become drinking water for its inhabitants and fuels the hydroelectric dams that provide electricity to the area. Due to irregular flow characteristics (significant seasonal rainfall variations in the Andean mountains, cf. Figure 34) the water supply in Metropolitan Lima is very challenging (Schütze et al 2018).

Today the flow of the Rimac River has been drastically altered by the installation of five hydroelectric plants and by the transfer of water from the Mantaro basin. In the drinking water treatment plants of La Atarjea, the water is stored and distributed in such a way that in the dry period of winter almost all the water from the river is diverted to the municipal network. In these months, most of the remaining water observed in the river downstream of La Atarjea comes from unauthorized drainage.

(<https://elcomercio.pe/opinion/colaboradores/rimac-rio-fenomeno-nino-avenidas-martha-bell-noticia-565031>)

The original area of interest was slightly extended and smoothed in the northern part to include both sides of the Chillon River in the district of Puente Piedra (cf. Figure 36).

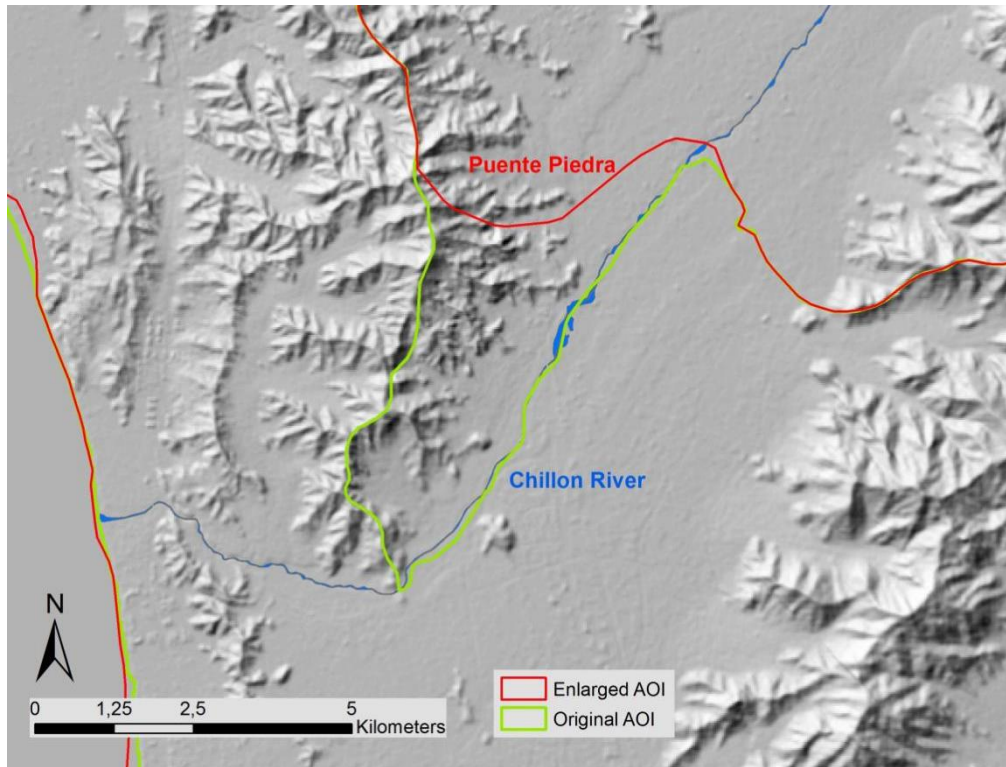


Figure 36: Adaptation of AOI in the northern part of Metropolitan area of Lima aiming at covering both sides of flood prone lower course of Chillon River

5.2 EO Data Used

In general, there are two types of data available for this purpose: optical and Radar data. Available HR optical data from the sensors Landsat 5, Landsat 7, Landsat 8, ASTER and Sentinel-2 covering the period from 2000 to 2018 was downloaded and analysed with regard to regional and/or local flooding. Unfortunately, no information about flooding could be obtained from this data as most of the River and Flash Flood events are characterized by short or very short duration. Consider, that Lima is situated in a coastal desert!

VHR Imagery purchased for the generation of the other products was also used by Joanneum Research (JR) for conducting this study even if covering only parts of the urban area (cf. Figure 38):

- QuickBird 2007 / 2009
- Pléiades 2016

This data gives a good impression of the rapid development and expansion of Lima but no information about flooding could be obtained.

Radar data from the current European Space Agency (ESA) Sentinel-1 data is acquired constantly and it is free of charge. Sentinel-1 Radar Data covering the 2017 major flood event (period from 2017-03-17 to 2017-03-24; 3 datasets) was downloaded and processed with regard to water extent. The data tend to give unreliable results in urban environment due to the high number of low backscattering objects.

The flood risk product is a combination of hazard with Land Use / Land Cover (LULC) information. The latter is derived from the Very High Resolution (VHR) satellite data based LULC product and thus these datasets are also indirectly used for this product.

For the areas which are not covered by the VHR LULC classification based on 2016 Pleiades imagery classification results from the EOWORLD project delivered by IABG and based on 2013 satellite data were used.

Flooding and damages from short-term River and Flash Floods can only be detected by visual interpretation of VHR optical data. Normally, such data is available only, when ordered directly in case of emergency as was the case in the March 2017 event.

For the 2017 event WorldView-2 imagery (acquisition date 18/03/2017 and 21/03/2017) is available in Google Earth and can be used for visual interpretation of flood extent and damage assessment (cf. Fig. 14 and 15).

The ALOS Global Digital Surface Model "ALOS World 3D - 30m (AW3D30)", version 2.1 (©JAXA) was used for physiographic and hydrographic analyses.

Whereas still no LiDAR based Digital Surface and Terrain Models with very high spatial resolution are available for the area of Metropolitan Lima, some small isolated VHR DSMs were generated based on aerial drone survey (e.g. Chosica – cf. Figure 37, Chaclacayo, San Juan de Miraflores, Mi Perú District (Callao). The data can be downloaded from the Sistema de Información para la Gestión del Riesgo de Desastres (SIGRID), maintained by the Centro Nacional de Estimación, Prevención y Reducción del Riesgo de Desastres (Cenepred) and provides at least a useful base for the accuracy assessment of some of the results (<http://sigrid.cenepred.gob.pe/sigridv3/drones>).

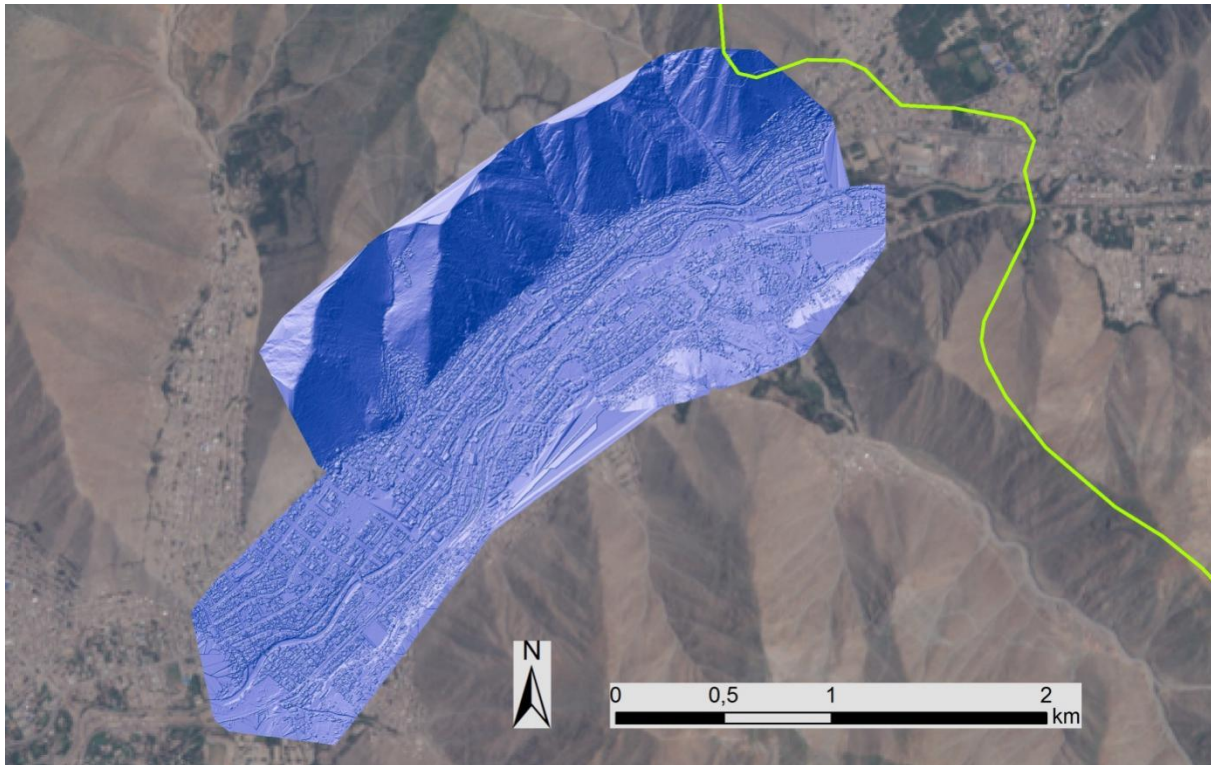


Figure 37: VHR DSM mosaic based on aerial drone survey (acquisition date 07/04/2015 and 20/01/2017, Source: Cenepred, Sistema de Información para la Gestión del Riesgo de Desastres - SIGRID) Background Image: Sentinel 2 – acquired 20/02/2017.

5.3 Short Description of Methodological Approach

Flood extent mapping based on EO data heavily depends on available data sets as well as on types of floods in focus. Whereas there is a good chance to identify large-scale River Floods, normally no information regarding short-term local floods (Flash-Floods) can be obtained from EO data due to short duration and/or cloud cover.

In some cases, short-term local floods can be recorded and localized based on reports (e.g. in social media) and press releases.

The modelling option which was taken into consideration originally, depends on the availability of an up-to-date DEM with sufficient resolution and accuracy. After testing available datasets based on SRTM, ASTER and ALOS we came to the conclusion that the modelling approach will not give reliable results. The same is true for any approach based on Digital Elevation Models, like e.g. the height above nearest drainage (HAND) index (Rennó et al., 2008).

Due to the relatively low frequency of catastrophic Tsunamis, no remote sensing data exist showing the run-up of the waves and resulting damages in the study area. Hazard assessment and mapping therefore is based on historical data and on modelling results where different approaches have been applied in former studies.

By mono-temporal analysis of Sentinel-1 GRD scenes from the 2017 major flood event (17/03/2017 and 24/03/2017) standing water could not be recognized by traditional approach based on decrease of backscattering and combined thresholding/region-growing. The following main reasons may be decisive in this regard:

- Objects and structural patterns in complex urban environment may increase SAR backscatter, and
- River and Flash Floods occurred in the area with only short-term inundation by standing water. Sentinel-1 images were acquired during or shortly after the flood peak, when water could already have receded.

The SAR change detection option was taken into consideration for the 2017 event, but detected changes obtained with this methodology do not refer to flooding only, but also to other natural or artificial processes and thus give unreliable results - so this idea was rejected.

Finally, delimitation of flood extent by visual interpretation of WorldView-2 imagery (acquisition date 18/03/2017 and 21/03/2017) was performed as alternative approach to derive the maximum visible extent of the flood.

To overcome the drawbacks of EO data an intensive research for ancillary data was performed.

For Peru, the SIGRID database (Sistema de Información para la Gestión del Riesgo de Desastres) which is maintained by CENEPRED (Centro Nacional de Estimación, Prevención y Reducción del Riesgo de Desastres) provides a large number of technical documents as well as (interactive) maps.

The ALOS Global Digital Surface Model "ALOS World 3D - 30m (AW3D30)", version 2.1 (©JAXA) was used for physiographic and hydrographic analyses.

Landforms were classified using different SAGA tools. Finally, the classification according to Iwahashi & Pike (2007) was used for the identification of areas prone to Flash Floods and Mud and Debris Flows. The classification into 12 terrain types is based on three morphometric variables - slope gradient, local convexity, and surface texture. The resulting classes are undefined and have to be calibrated empirically by subsequent analysis. According to the event history from the SIGRID database, Class 2 (steep slope, coarse texture, high convexity) was used for the identification of flash flood hazardous areas.

For further differentiation of the Flash Flood Hazard climatological considerations were taken into account as precipitation events triggering such processes can be observed mainly in the Eastern part of Metropolitan area of Lima (valleys of Huyacoloro and Rímac River).

For estimation of River Flood Hazard, watercourse lines of tributaries were generated from the DEM using ArcMap's hydrologic tools. Note that the results obtained do not always agree with what it is seen on the optical imagery, but this makes sense. Hydrologic features are usually redirected or channelized when crossing urban areas. Places where both datasets do not match can be explained as places where the physiography pushes the water to follow a path that humans have modified. The trajectories of the main rivers were taken from the EOWORLD LULC dataset.

After classification in two classes based on Stream Order the lines were buffered with 50 m (Stream Order (Strahler) 1 and 2) and 100 m respectively (Stream Order (Strahler) 3 and 4, main rivers) to roughly estimate potential flooding zones.

Risk is defined as a combination of probability and consequences. A detailed and uniform land-use map is an important prerequisite to perform flood risk calculations, since it determines what is damaged in case of flooding.

Two different datasets regarding the urban land use / land cover were made available for this analysis:

- LULC classification (delivered by IABG through the EOWORLD project) based on 2013 imagery covering the whole AOI (approx. 1,153 km²)
- LULC product generated by SIRS through EO4SD-Urban covering only a part of the total AOI in the centre of Lima (cf. Figure 38) based on 2016 VHR imagery (approx. 244.56 km²)

The exposition is classified following an approach developed by NEO (based on: Dasgupta et al. 2015) integrating economic costs, social damage, physical damage and flood duration. Four land use damage levels (A, B, C, D) are defined based on this estimation.

Both land-use classification results were recoded to pre-defined categories (as given in Table 13) and merged after categorization.

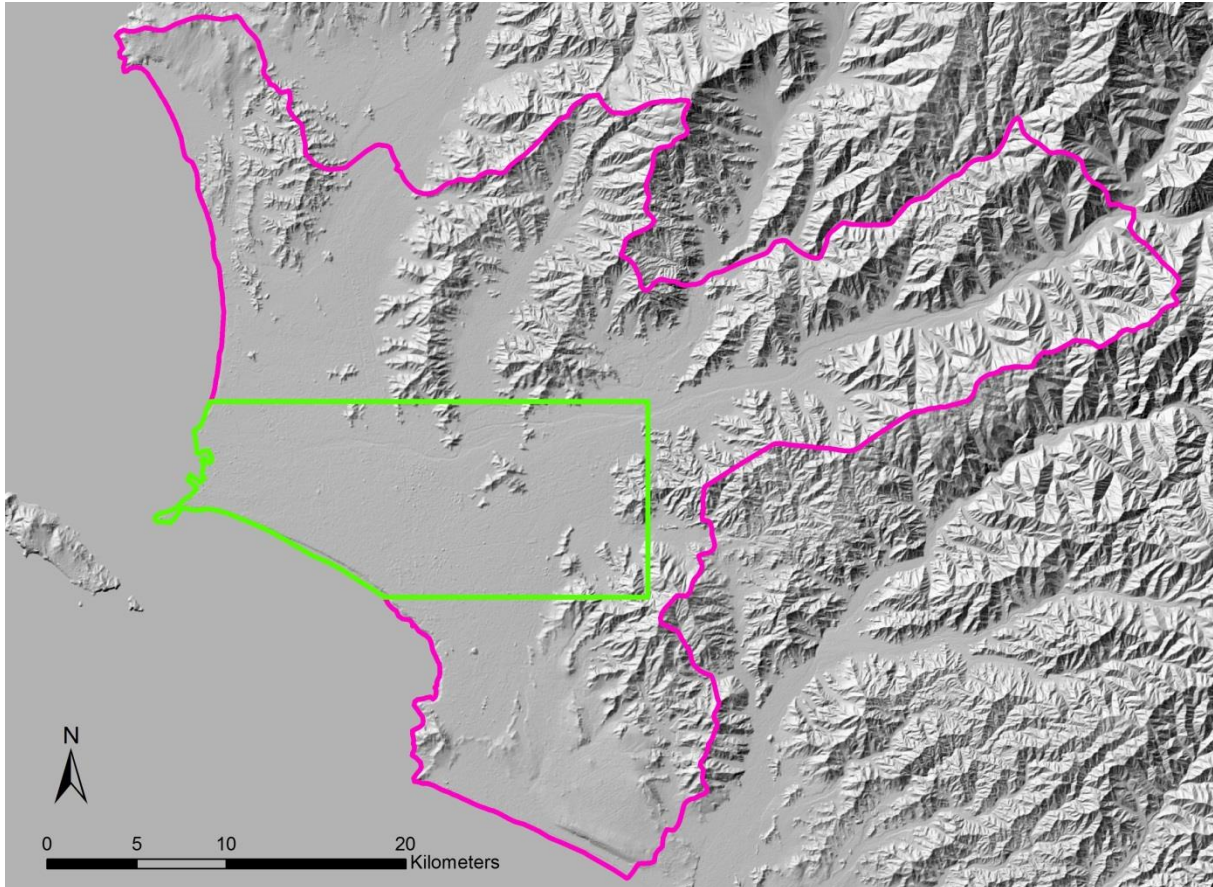


Figure 38: Metropolitan area of Lima covered by EOWORLD LULC classification (full AOI – pink) and area of EO4SD-Urban LULC classification (green) (Background: Hillshade ALOS World 3D – 30m (AW3D30), version 2.1)

Whereas it is possible to parallelize the two datasets for the classification of these four levels of exposition, it is not feasible to join all land use classes from the two different datasets as the nomenclature is too different – thus the detailed statistical analysis was restricted to the AOI subset in Lima centre.

New VHR imagery as available in Google Earth indicates, that most of the Construction Sites (2013 as well as 2016) now have changed to Continuous urban fabric or Commercial and Industrial Units and were classified higher (C) than the original value A as defined by NEO for Construction Sites.

Table 13: Land use classes and reclassification to pre-defined damage levels

Classes	Damage				Total	Level
	Economic Costs 0-2	Social Damage 0-2	Physical Damage 0-2	Flood Duration 0-2		
Agricultural Land	1.5	0.5	0	1	3	B
Commercial and Industrial Units	2	0.5	1	0.5	4	B
Construction Sites 2013/2016	1.5	1	1	1	4.5	C
Dump site	0	1.5	0.5	0	2	A
Forests and Shrub Lands	0.5	0	0	0	0.5	A
Formal medium and high density residential - Continuous urban fabric (Sealing level: 50%-100%)	1.5	1.5	2	1.5	6.5	D
Formal low density residential - Discontinuous urban fabric (Sealing level: 10%-50%)	1.5	1	2	1	5.5	C
Land Without Current Use	0	0	0	0	0	A
Mineral Extraction site	1	0	0.5	0.5	2	A
Military	1	0.5	1	1	3.5	B
Non-Residential Urban Fabric	1	1	0.5	1	3.5	B
Other Natural and Semi-Natural Areas including Wetlands	0	0	0	0	0	A
Roads and associated land, Railways	1.5	1	2	1.5	6	C
Port Area	2	1	0.5	1.5	5	C
Airport	2	0.5	1.5	1.5	5.5	C
Sports and leisure facilities	0.5	0.5	0	0.5	1.5	A
Other Urban / Artificial Area	1.5	1.5	1	0.5	4.5	C
Urban Greenery, Cemeteries	0.5	0.5	0.5	1	2.5	B
Village Settlements, very low density residential (Sealing level 1-10%)	1.5	1.5	0.5	1.5	5	C
Water Bodies	0	0	0	0	0	A

The Flood Risk matrix is generated based on pre-defined damage levels on land use classes and flood hazard classified into three hazard levels. The flood risk level is classified in four qualitative classes based on the combination of flood hazard and land use damage as shown in Table 14.

Table 14: Flood Hazard and Risk classification

		Damage cost on land use			
		A	B	C	D
Flood Hazard	1 (low)	1A	1B	1C	1D
	2 (medium)	2A	2B	2C	2D
	3 (high)	3A	3B	3C	3D
Flood Risk classification					
Low Risk	1A 1B 2A				
Medium Risk	1C 1D 2B 2C 2D 3A 3B				
High Risk	2D 3C				
Very high Risk	3D				

5.4 Product Description

There are three final layers in this product: (1) the raw data on past flood extents as derived from EO data and ancillary data (flood history – only River and Flash Floods included), (2) the Flood Hazard map which summarizes past flood events and thus gives information about the likelihood of future events, and (3) the Flood Risk map combining this data with information on urban and peri-urban land use and its damage potential in case of flooding. The coordinate reference system of the Vector files is UTM18S (datum WGS84) (EPSG: 32618) as for all the other products delivered.

Because of the fundamental cause – effect relationships the following description is given separately for the processes (1) Tsunami inundations and (2) River and Flash Floods (including Mud and Debris Flows).

5.4.1 Tsunami Inundations

Flood History

Most Tsunami events worldwide are induced by offshore earthquakes. According to the map of tsunamigenic earthquakes for the period 1562–1960 produced by Soloviev and Go (1975), almost the entire coast of South America is a zone of high tsunami hazard.

Four types of tsunamis are capable of impacting the study region (Kulikov et al. 2005):

(1) Trans-Pacific tsunamis

Trans-Pacific tsunamis were reported for the coasts of Peru and Chile in 1946, 1952, 1957, 1960, 1964, 1968, 1975, and 1994. Maximum observed wave heights were 3–4 m (Lockridge, 1985). However, the probability of a catastrophic trans-Pacific tsunami with wave heights exceeding several meters for the Peruvian coast is estimated to be low.

(2) Regional tsunamis

Regional Tsunamis are tsunamis generated by major earthquakes near the coast of Central and South America but relatively far from the Lima region. Regional tsunamis are a serious threat to the coast of Peru. Depending on the source region, tsunami warning times of approx. one hour after the recording of the main earthquake shock may be realistic.

(3) Local tsunamis

Local Tsunamis are those generated by major earthquakes in close proximity to the Area of Interest. Since wave arrival times would be significantly less than an hour, local tsunamis are a major threat for people in the susceptible zones.

(4) Landslide-generated tsunamis.

The possibility of catastrophic landslide-generated tsunamis has received little attention for the coast of South America. There have been several cases where relatively small earthquakes have been accompanied by significant tsunamis. For example, the 1960 Peruvian earthquake with magnitude $M = 6.9$ produced a tsunami run-up of 9 m. One of the possible reasons for these unusually strong tsunamis is that earthquakes could trigger massive submarine landslides on the continental slope of Peru. This type of combined source may be responsible for unusual tsunamis. The possibility of landslide-generated tsunamis for the coast of Peru therefore needs to be examined (Kulikov et al. 2005).

Seismic events accompanied by large tsunamis along coastal central Peru have been reported since the era of the Spanish occupation of the Inca Empire in the 16th century.

Major events are recorded:

- 1586 (9th of July),
- 1604 (24th of November),
- 1687 (20th of October),
- **1746 (28th of October),**
- 1828 (28th of March)
- 1940 (24th of May)
- 1942 (24th of August)
- 1966 (17th of October)
- 1970 (31st of May)
- 1974 (3rd of October)
- 2007 (15th of August)

The 1746 earthquake is considered one of the most catastrophic seismic events in Peruvian history. The epicentre was located in front of the central area of Peruvian coast. The moment magnitude for this event has been estimated between 8.8 and 9.0 and the reported tsunami run-up height was between 15 m and 24 m (Dorbath et al. 1990). According to historical sources, the city of Lima was completely destroyed by ground shaking and the subsequent tsunami flood. In Callao only 221 out of the 5,000 inhabitants survived the Tsunami (Mas et al. 2014). The 1974 earthquake that occurred in front of Lima city, had a local tsunami height of 1.6 m (Dorbath et al. 1990).

Due to the relatively low frequency of catastrophic tsunamis in the study area, no EO data exist showing the run-up of the waves and resulting damages. Hazard assessment and mapping therefore is based on historical data and on modelling results where different approaches have been applied in former studies.

Flood Hazard

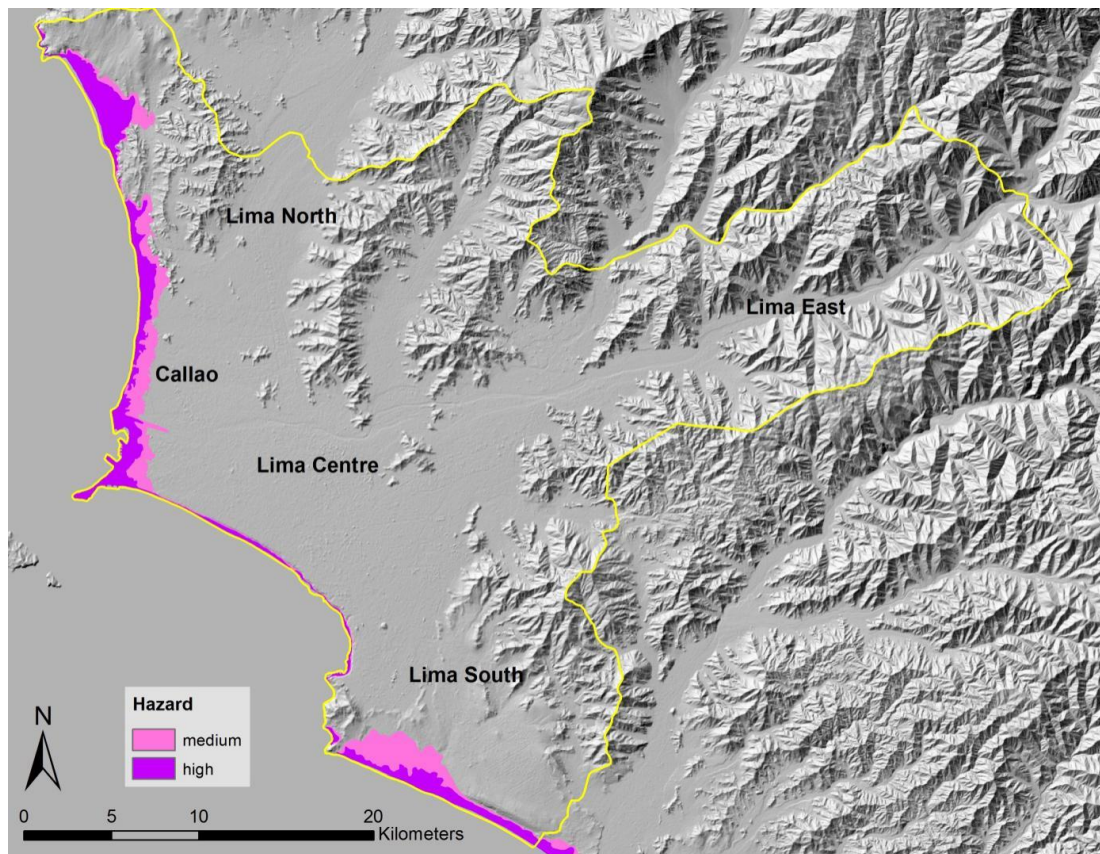


Figure 39: Tsunami Flood Hazard Map for Metropolitan area of Lima. Yellow line: limits of Area of Interest (Background: Hillshade ALOS World 3D – 30m (AW3D30), version 2.1)

In a regional approach, the best estimates of extreme tsunami wave heights and respective return periods still are to be obtained using observed tsunami data. Almost 500 years of observational data on tsunami run-up allow to apply the Extreme Statistics theory directly for tsunami heights and to estimate tsunami risk for this region based on these data. For the whole section of the Peruvian and Northern Chile coast, the event corresponding to a 50-year recurrence period is about 15 m while the tsunami run-up corresponding to a 100-year return event is 25 m.

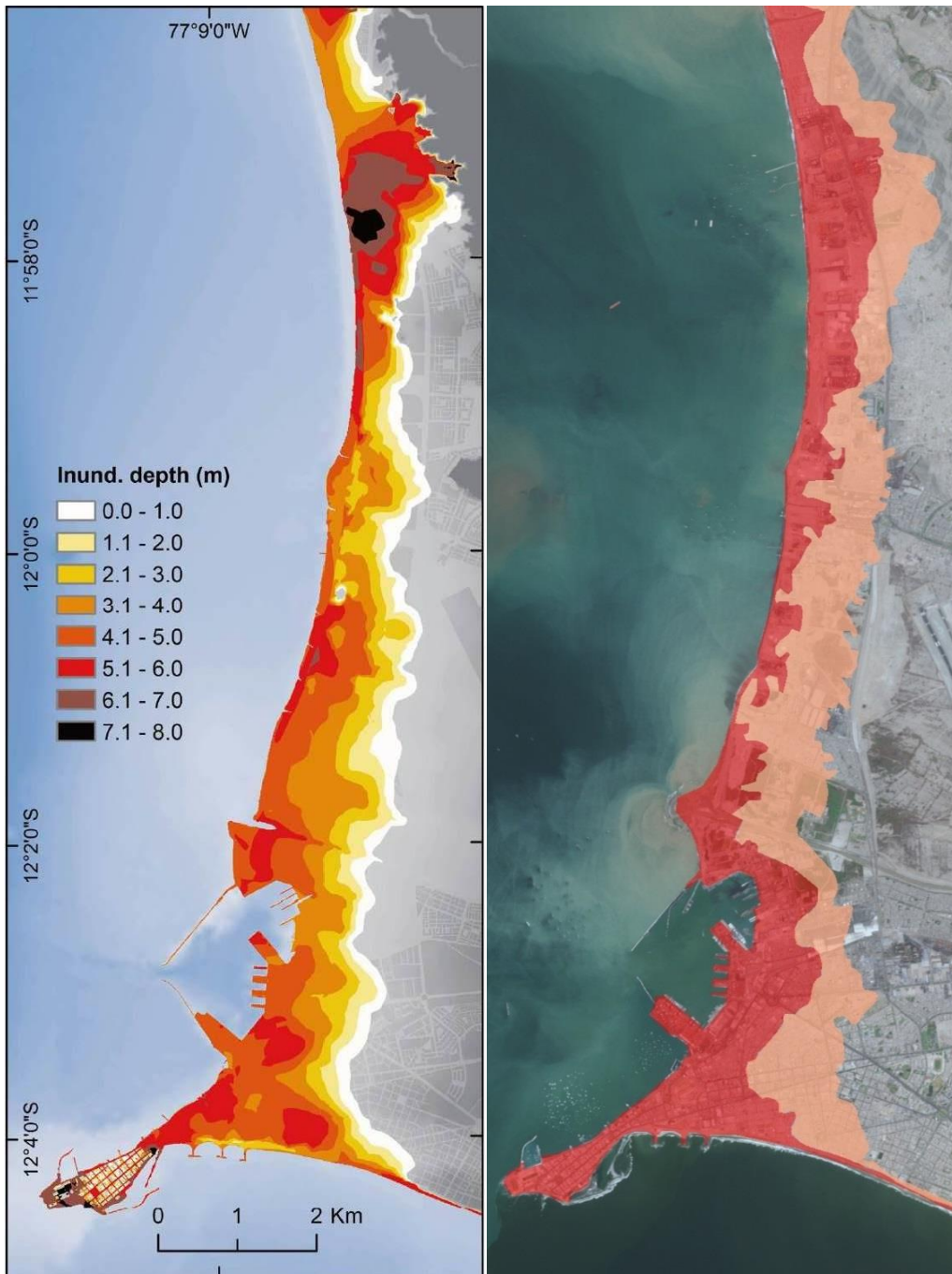


Figure 41: left: Tsunami Inundation Hazard Map for the Callao – La Punta area based on the maximum inundation from 12 scenarios (Mas et al. 2014); right: Comparison with result of DHN modelling: red: most probable inundation scenario, orange: scenario according to the 1746 event.

More recent studies aimed at determining the tsunami inundation area for the coastal region of Lima by adopting different seismic source scenarios through numerical modelling and a detailed topography model that includes roughness values and LULC classification (Adriano et al. 2013, Mas et al. 2014).

The resulting Hazard Map for the Callao area, which is based on the outputs of 12 different numerical tsunami simulations, show maximum inundation depths of approx. 8 m which is not in accordance with the historical data from the 1746 earthquake as well.

It can be assumed that the accuracy of any model output would benefit considerably from the availability of LiDAR based Digital Surface Models with very high spatial resolution.

Flood Risk

The coastal areas which are endangered by Tsunamis are characterized by important infrastructure (e.g. port of Callao, traffic lines), industrial areas, high density residential and commercial areas, public buildings and recreation facilities (e.g. on the beaches).

La Punta peninsula, which is more or less surrounded by the ocean, would be the most vulnerable area, and has rather long and exposed evacuation routes (cf. Figure 42). To the north, the coastline of Callao forms a long sweeping bay. Halfway between Callao and the town of Pachacutec there is the mouth of Lurín River. The coastal areas north of Callao port are dominated by industrial and commercial buildings with some residential areas as well as construction sites. To the back of the International Airport Jorge Chavez, a zone with agricultural fields, bare land and some natural vegetation can be found. Agricultural use as well exists to the south of the town of Pachacutec.



Figure 42: Aerial sight of Callao - La Punta which obviously is the most vulnerable area of metropolitan Lima in case of a Tsunami (Source: Arvo Corporación)

To the south of La Punta, the coastline is characterized by high cliffs (approx. 50 m; Costa Verde), which means that only the beaches and the infrastructure below the cliffs are endangered by Tsunami waves. What must be taken into account, is the fact that the beaches may be very crowded on summer days and that the number of roads and stairs for climbing the cliffs is rather low. Furthermore, an important traffic line (the “Circuito de Playas”) runs on the beaches below the cliffs. In case of a major earthquake rockfalls and landslides from the cliff are very likely and were reported even after minor events (cf. https://archivo.elcomercio.pe/sociedad/lima/temblor-lima-fotografiaron-deslizamientos-costa-verde-noticia-1733945?ref=flujo_tags_516037&ft=nota_124&e=titulo).



Figure 43: Crowded beaches of the Costa Verde on a summer day (Source: <http://www.peru4you.de/tsunami.html#>)



Figure 44: Visualization of a possible tsunami at the Costa Verde of Lima (Bahia de Miraflores) where high cliffs protect the built up area (Source: MINAM Ministerio del Ambiente / Ministry of Environment)

The southern districts (Chorrillos, Villa El Salvador, Lurin and Pachacamac) again are characterized by a coastal plain which is endangered by Tsunami waves. These zones are used as residential areas, sports and leisure facilities (parks and beaches) and as industrial and commercial areas in the southeastern parts. Some parts of the Panamericana Sur are also within the potential inundation zones.

Generally, the Peruvian authorities are well aware of the high vulnerability and risk regarding the occurrence of major earthquakes and catastrophic Tsunami waves. Thus, there are constant efforts to develop effective prewarning and evacuation concepts for such case.

In Peru, the Sistema Nacional de Alerta de Tsunamis (SNAT), stationed in Callao and under the responsibility of the Direccion de Hidrografia y Navegacion (DHN) of the Peruvian Navy, is responsible for tsunami warnings. It cooperates closely with the Pacific Tsunami Warning Center (PTWC) in Hawaii. PTWC tsunami warnings in Peru are first sent to Jorge Chavez International Airport via the Aeronautical Fixed Telecommunication Network (AFTN) and then further coordinated by DHN. The Institute for Geophysics of Peru (IGP), which is involved in the communication, evaluates measured data of the earthquakes and decides whether there is a tsunami threat. In the event of a tsunami risk, the emergency operations centre of the Instituto Nacional de Defensa Civil (INDECI) is informed, issuing a warning to the population and initiating possible evacuation measures. The DHN in turn informs all ports in Peru.

New efforts include:

- an interactive map developed by the Peruvian-Japanese Center for Seismic Research and Disaster Mitigation (Cismid) showing the zones of Lima which are most vulnerable to the occurrence of a tsunami. This map, which is in permanent update, also includes the zones of vertical refuge - buildings qualified as resistant in case of a seismic event. If these buildings resist the earthquake, they are planned to be occupied by the inhabitants of the area in the event of a tsunami. The evacuation routes as well as photos of these routes are displayed as well.
- The Peruvian Navy has developed a new tool to help civilians take preventive measures to protect themselves against tsunamis. Through the "Cambiemos Las Cifras" (Let's Change the figures) campaign, which was launched in 2016 by the Navy's Hydrography and Navigation Bureau (DHN), civilians can download an app that provides evacuation routes and the location of shelters before a tsunami hits land (Diálogo 2016).

Since a Tsunami wave from a local seismic event may reach the coast within 10 to 30 minutes, it is obvious that most prewarnings from the involved authorities will not leave sufficient time for the complete evacuation of exposed zones. The earthquake itself therefore has to be the prewarning for exposed people. Most inhabitants of the coastal areas are well aware of this fact. However, the practicability of any evacuation concepts in case of a catastrophic earthquake is difficult to be evaluated. In case of a 9.0 Mw earthquake close to the Peruvian coast, the authorities expect the earthquake and tsunami to have an impact of around 51,000 fatalities and 686,000 persons injured in the Lima and Callao area (Centro de Estudios y Prevención de Desastres – PREDES 2009).

Examples of the Flood Risk Products are shown in the section 5.6 for all types of floods.

5.4.2 River Floods and Flash Floods

Flood History

For the Lima Metropolitan area short-term local floods and river floods after heavy rainstorms in the upper catchment parts of the rivers which cross the city are typical and have been reported in many years although Lima is situated in a coastal desert characterized by very low precipitation.

Every few years, connected with the El Niño phenomenon, significant rain does fall in parts of the desert, including Lima. Especially strong El Niños struck in 1925, 1983, and 1997/98. The maximum rain event in the last decades in urban Lima itself was characterized by a rain amount of only 16 mm - even this being sufficient for widespread flooding (mainly due to the absence of an adequate drainage system) and still referred to as “catastrophic event of biblical dimensions” (<http://blog.pucp.edu.pe/blog/juanluisorrego/2010/03/>).

Normally, no information regarding short-term local floods (Flash-Floods) can be obtained from EO data due to short duration and/or cloud cover. Only one event from the past can be detected and analysed from such data (March 2017). The following list therefore is based on reports (e.g. in social media), press releases and technical reports from local authorities. Furthermore, the SIGRID database (Sistema de Información para la Gestión del Riesgo de Desastres) which is maintained by CENEPRED (Centro Nacional de Estimación, Prevención y Reducción del Riesgo de Desastres) provides a large number of technical documents as well as maps. Nevertheless, such inventory never will meet the claim to be complete.

It is known that during the years 1863, 1891 and 1894 there were important flood events, but there are no data on damages available. In April 1891 Rímac River flooded San Francisco and Monserrate in Lima Centre (<http://blog.pucp.edu.pe/blog/juanluisorrego/2010/03/>). Further destructive river and flash floods, most of them connected with mud and debris flows are reported for the years 1909, 1915, 1925, 1926, 1936, 1939, 1967, 1971, 1972, 1975, 1976, 1983, 1987, 1989 and 1994. The area which was hit most frequently, was the town of Chosica in the Rímac River valley where different torrents (“*quebradas*”) were activated repeatedly (e.g. *Quebradas Quirio, Pedregal, Libertad, Carossio, Rayos de Sol and Cashahuacra*) (Chira La Rosa 2016). One of the most severe events of the 20th century was that of March 9th, 1987, between 4:00 and 7:30 p.m., when flash floods and mud flows (“*huaycos*”) were produced in a number of torrential basins of the district of Lurigancho-Chosica. More than 100 inhabitants were killed and the material damage was valued at 12.5 million dollars (Garcia Chaca 2016).

According to reports and press releases, the following flood events have happened within the past 20 years:

1998

Flooding from Chillón, Rímac, Lurin and Huaycoloro Rivers – January to March

23/02/1998 - 24/02/1998: Flash floods in torrents on righthand side of Rímac River (Chosica)

2000

Flash flood and debris flow, Jicamarca/Lurigancho

2008

February – April: Flash and flash floods in Lima – Ñaña, Carabayllo, San Martín de Porres and parts of Lurín

2009

February: Local flash flood in Chosica

March: Flooding of Chillón River (San Diego in San Martin de Porres)

2010

02/01/2010: Local flash flood and debris flows in Districts of Lurigancho and Comas

2012

10/03/2012: Flash floods and mud / debris flows in Lima – Chosica

05/04/2012: 28 mm rain were recorded at the weather station of Chosica. Activation of torrents on both sides of Rio Rimac producing flash floods as well as destructive mud and debris flows (Lima - Chosica, Chaclacayo). (Zavala et al 2012)

2015

09/02/2015: the torrents Huampani, Chacrasana, Santa María, Quirio, San Antonio, Mariscal Castilla y California (Chosica), La Ronda (Ricardo Palma) and La Floresta (Chaclacayo) were activated.

23/03/2015: flash floods and landslides in Lurigancho Chosica from the overflowing of the following creeks: Pedregal, Carossio, Rayos del Sol, Quirio, San Antonio, California, La Trinchera, Buenos Aires, La Cantuta, Moyopampa, La Libertad and Mariscal Castilla; an emergency was declared in the District of Lurigancho - Chosica.

2017

Heavy rains affected nearly all of Peru in February and March 2017, leading to catastrophic flooding and landslides. More than 100 people died, nearly 158,000 were displaced and 210,000 homes were damaged in the whole country, according to Peru's emergency operations centre. In Lima, the riverside areas of the province of Lima suffered the overflows of the rivers Chillón, Huaycoloro, Rímac, Lurín and Surco. Damages from flooding and bank erosion heavily struck infrastructure as well as residential, commercial and industrial zones.

According to articles and photos from online newspapers, flash floods in the area culminated between 16th and 19th of March. Photos with water pouring through the streets are mostly tagged with 17th of March. In photos from 19th rapid flood water is not captured but damages are (Indra Sistemas S.A. 2017). Areas most concerned were between Chosica and Chaclacayo (Rímac River), north of Villa San Luis (Rímac River), north of Lurigancho (Huaycoloro River), Santa María de Huachipa (Huaycoloro River) and area south of Pampa de los Perros (Chillón River). Flooding also was reported from the Districts of Santa Anita and Ate (Surco River).

The identification of the maximum flood extent is based mainly on visual interpretation of WorldView-2 Images that cover the metropolitan area of northern Lima, acquired on 18th and 21st of March 2017 (available online via Google Earth). The Flood Extent Map shows water in river banks and maximum inundation extent (cf. Figure 51). Because, according to reports and press releases, flood peak occurred between 18th and 19th of March, extent of water visible in the imagery may be smaller than during flood peak. The main areas where flooding evidences were detected in these images are along Rímac River. The area of Carapongo/Santa María de Huachipa is the largest one, representing almost the 90% of the total area detected. It is an area mainly occupied by industrial activities, although the western part of it is also residential. Second largest area is Cajamarquilla, located to the north of Carapongo area, upstream of Huaycoloro River.

Activated torrents were mainly situated in Chosica – Lurigancho, Chaclacayo (INGEMMET 2017). Based on the information from reports and press releases, some of the damages can still be identified on WorldView2 VHR data acquired on 17th of April 2017 and available on Google Earth (although many of the damages were repaired within the time between the event and the acquisition date one month later, cf. Figure 47 and Figure 48).

2018

Floodwaters from the overflowing Rimac River hit Lurigancho - Chosica, east of Lima on 23rd of January 2018.



Figure 45: Rímac River in sector of San Antonio de Carapongo (District of Lurigancho) – pre-event situation on 3rd of March 2017 (Image © DigitalGlobe)



Figure 46: Rímac River in sector of San Antonio de Carapongo (District of Lurigancho) – post-event situation on 21st of March 2017 (Image © DigitalGlobe)



Figure 47: Quebrada Yanacoto, Lurigancho District (Eastern Lima): pre-event situation on 3rd of March 2017 (Image © DigitalGlobe)



Figure 48: Quebrada Yanacoto, Lurigancho District (Eastern Lima): post-event situation on 17th of April 2017 (Image © DigitalGlobe)

Smaller affected areas were identified along Chillón River at San Martín de Porres, Comas, Puente de Piedra, Sol de Carabayllo and la Rinconada Condominium. The extent of these ones is limited, although a number of buildings were washed away by the runoff in the sector of Puente Piedra (cf. Figure 49 and Figure 50).



Figure 49: Chillon River in sector of Puente Piedra (District of Comas) – pre-event situation on 11th of March 2017 (Image © DigitalGlobe)



Figure 50: Chillon River in sector of Puente Piedra (District of Comas) – post-event situation on 21st of March 2017 (Image © DigitalGlobe)

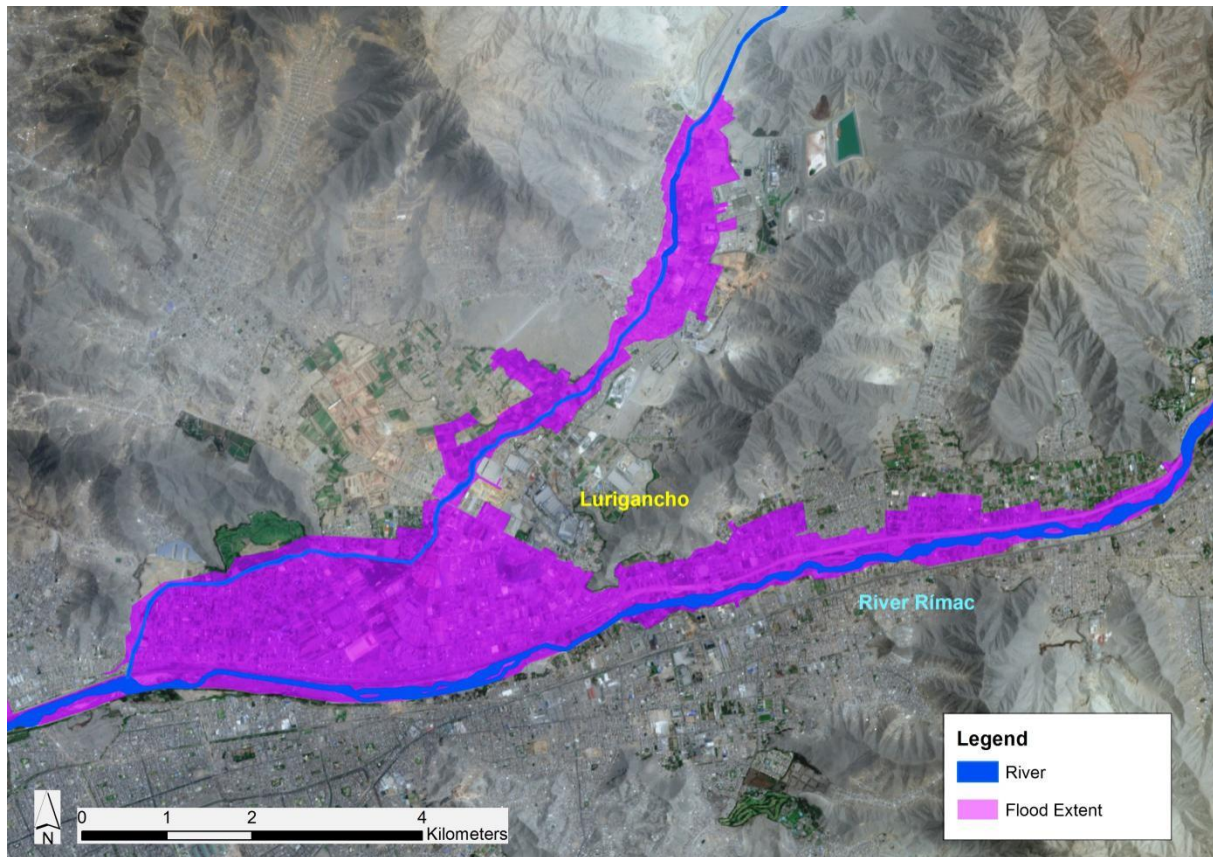


Figure 51: Subset of flood extent map showing the flood extent in Carapongo/Santa María de Huachipa and Cajamarquilla (Lima). Visual interpretation of WorldView-2 Images acquired on 18th and 21st of March 2017. Background Image: Sentinel 2 – acquired 20/02/2017.

Flood Hazard

The Flood Hazard Map for River and Flash Floods (cf. Figure 52) was generated based on the occurrence of flood events during the past 20 years. It is taking into account all available data sources (EO based flood extents, reports and press releases, results of modelling of potential flooding along rivers and waterways, ancillary data) aiming at covering all areas which are potentially endangered by flooding. The classification in three qualitative hazard levels is expert-based under consideration of reported frequencies of floods.

The map aims to give an idea about the flood presence in terms of both frequency and extent in Metropolitan Area of Lima, and illustrates which part is in general flooded more often than other areas.

The Hazard assessment takes the 2017 event as a benchmark. This event is rated as most severe event at least since the 1997/98 El Niño phenomenon (INGEMMET 2017).

However, the analysis of extreme flow conditions of the Rímac River based on data from the period between 1912 and 2009 at the water gauge of Chosica indicates that significantly higher levels may occur.

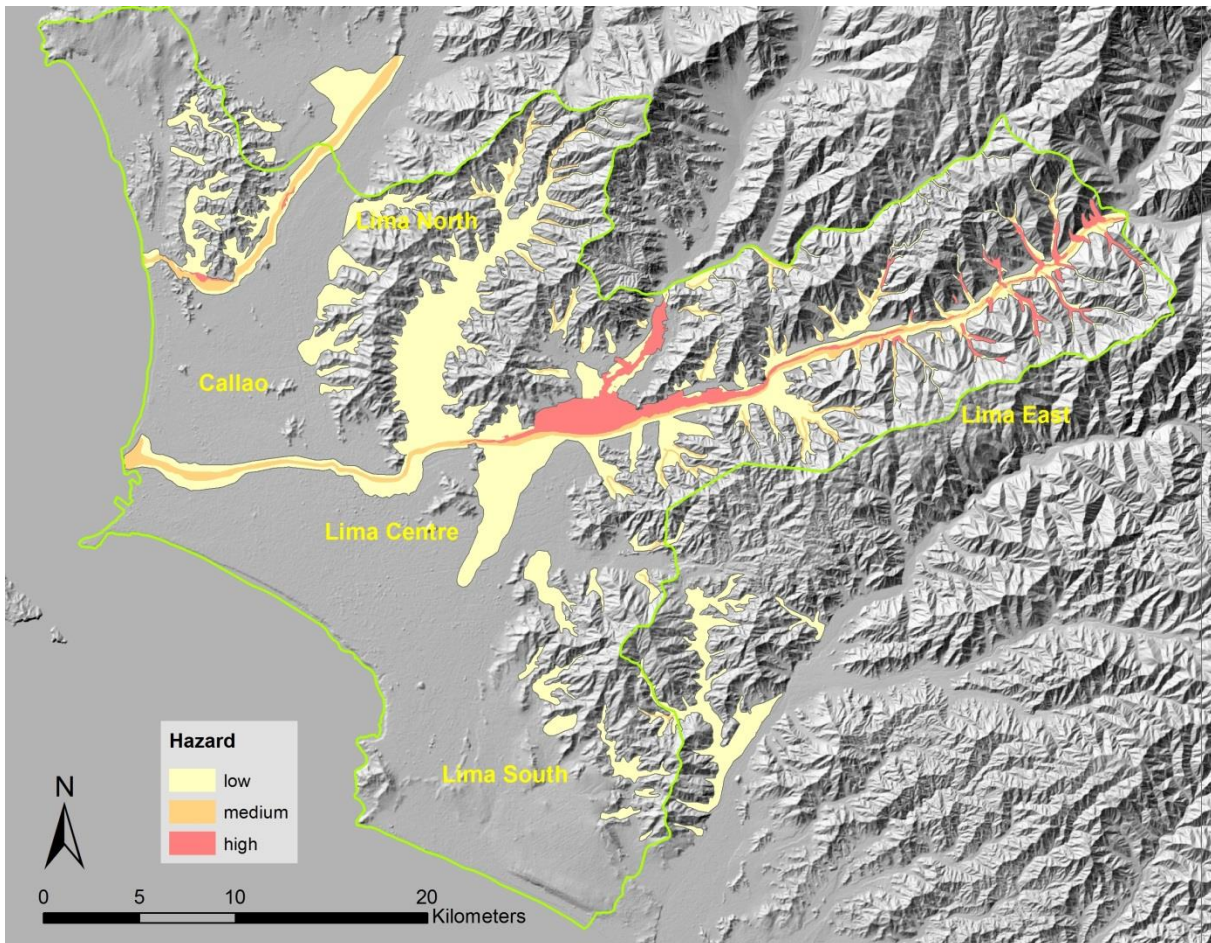


Figure 52: River and Flash Flood Hazard Map for Metropolitan area of Lima. Green line: limits of Area of Interest (Background: Hillshade ALOS World 3D – 30m (AW3D30), version 2.1)

Due to the increase in rainfall in the Andean region in the summer season (December – March), especially during El Niño periods the rivers that cross the city (Chillón, Rímac and Lurín) swell. Floods may occur even when there is no or very little rain in Metropolitan area of Lima itself as short horizontal distances result in significant effects with regard to precipitation (Municipalidad Metropolitana de Lima / SGDC, 2013).

However, local showers in the populated foothills of the Andes may activate torrents having been dry for long periods triggering Flash Floods as well as Mud and Debris Flows (“huaycos”). Because of the specific weathering processes, resulting in the accumulation of residual soil and colluvial deposits on the slopes of these small tributaries where almost no natural vegetation can be found, rather low precipitation amounts are sufficient for the activation of high-energetic runoff processes. Critical thresholds of rainfall generating floods and mud flows in the torrents are as low as 10 mm/day and 3 mm/hour.

Data from the water gauge of Chosica presenting daily averages from the period between 1912 and 2009 show the very irregular flow characteristics of the Rímac River not only because of the significant seasonal rainfall variations in the Andean mountains but also from year to year. The maximum flow volumes were recorded in March 1941 with 325 m³/s. More recent data show maxima in March 2003 (128.61 m³/s) and in March 2009 (139.17 m³/s) (Chira la Rosa 2016).

The critical level (red alarm) when inundations have to be expected, is defined with a flow volume of 95 m³/s at the water gauge of Chosica. This level was exceeded again in February and March 2017 (more than 130 m³/s, cf. Figure 53).

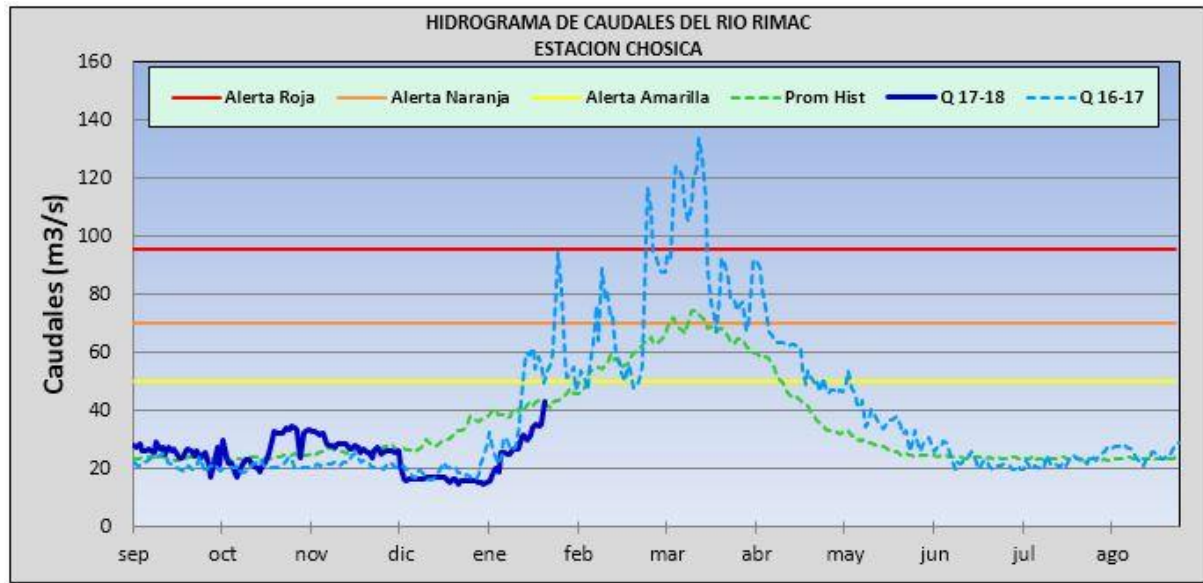


Figure 53: Hydrograph of the Rimac River at the Chosica water gauge, dated 22nd of January 2018 (SENAMHI - National Meteorology and Hydrology Service of Peru): the different alarm levels (yellow: 50 m³/s, orange: 70 m³/s, red: 95 m³/s) are shown as well as the hydrograph for 2016/2017 (dotted blue line) with its maximum in March 2017.

The Chillón River which triggers inundations in the northern part of the study area (e.g. San Martín de Porres, Carabayllo, Puente Piedra) is characterized by a flow regime which is similar to that of Rimac River. Its catchment area is smaller than that of the Rímac River (cf. Figure 35) and so are its flow rates. In very humid years (triggered by the El Niño phenomenon) maximum flows greater than 200 m³/s were reported (e.g. in 1940/41).

Only the lower parts of the catchment area, forming a fluvial plain, are situated within the study area. Besides agricultural areas, this zone is characterized by the strong urban expansion of Lima. The districts on the right-hand river side (e.g. Ventanilla, Puente Piedra and Carabayllo) are among those which grow fastest, mostly without sound urban planning (Municipalidad Metropolitana de Lima 2013).

The floodplain is at permanent risk of flooding as a result of the low carrying capacity of the river. This is enhanced by the presence of excavation materials and rubbish in the lower part of the Chillón River, locally reducing the channel to < 8,00 m and inducing damming and risk of extensive overflows and floods in the agricultural and urban areas.

The zones which are most endangered by Flash Floods as well as Mud and Debris flows from smaller tributaries are mainly in the Eastern part of Lima (Districts of Lurigancho, Chaclacayo, Ate and Chosica). A number of small and steep valleys can also be found in the coastal mountains in the districts of Comas, Los Olivos and Independencia.

Torrents almost always have dry beds; runoffs only occur when there are significant rain events triggered by El Niño events. In these conditions, flash floods and destructive mud and debris flows are produced.

The River and Flash Flood Hazard classification involved the following considerations:

High Hazard:

- areas which were flooded by Rivers Rímac, Chillón or Huaycoloro or hit by Flash Floods in the 2017 event (cf. Flood Extent Map)

- areas where Flash Floods (and Mud and Debris Flows) were reported and/or mapped at least once within the last 20 years.

Medium Hazard:

- zones close (< 50 m) to small tributaries (Stream Order (Strahler) 1 and 2) as derived from watercourse generation from the ALOS DEM in the Eastern part of Metropolitan area of Lima with semi-arid climate conditions (Districts of San Juan de Lurigancho, Lurigancho, Chaclacayo, Ate)
- Potential flooding zones (defined by 100 m Buffer) of main rivers (Chillon, Rímac, Huaycoloro) as derived from watercourse generation from the ALOS DEM which were not flooded in the 2017 event

Low Hazard:

- landforms identified as prone to Flash Floods and Mud and Debris Flows according to classification following the approach of Iwahashi & Pike (2007) – alluvial fans , mudflow cones
- Potential flooding zones (defined by 200 m Buffer) of main rivers (Chillon, Rímac, Huaycoloro) as derived from watercourse generation from the ALOS DEM which were not flooded in the 2017 event

An additional zone of low hazard was defined in the Districts of Santa Anita and Ate where – according to reports and press releases - flooding occurs occasionally caused by the Surco River – actually an artificial canal bearing water of the Rímac River and normally used for irrigation purposes.

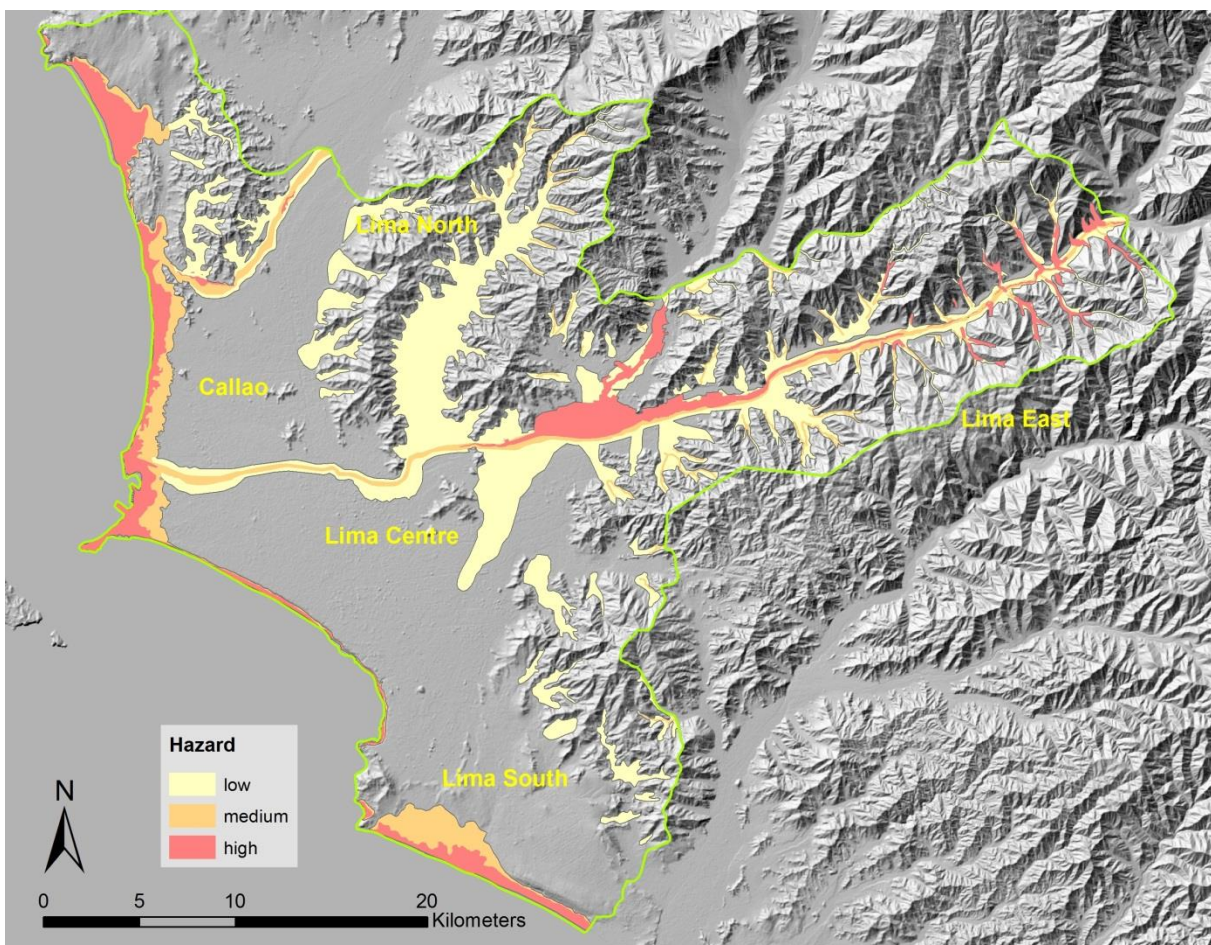


Figure 54: Flood Hazard Classification in Metropolitan Lima merged for Tsunami Hazard and River and Flash Flood Hazard. Green line: limits of Area of Interest (Background: Hillshade ALOS World 3D – 30m (AW3D30), version 2.1)

Residential and Public Urban Fabric with high damage potential was analyzed more detailed and combined with the Flood Hazard Map both in the area covered by the EO4SD-Urban LULC classification (Central Lima) as well as in the total Metropolitan area.

The statistics for Residential and Public Urban Fabric in the area covered by the EO4SD-Urban LULC classification (Central Lima) is shown in Figure 55; based on these statistics, approx. 9.1% of Lima Residential and Public Urban Fabric is situated in medium and high Flood Hazard zones. Additional 16% of this land use class is situated in low Flood Hazard Zones.

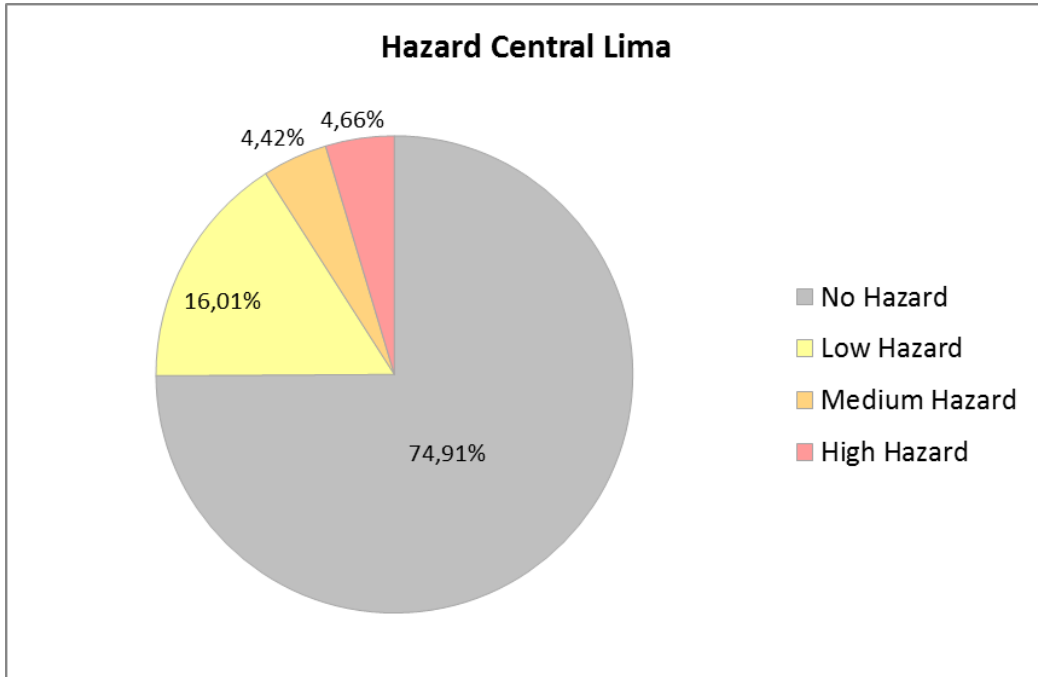


Figure 55: Flood Hazard Classification displaying proportions of areas prone to flooding in area of EO4SD-Urban LULC classification only (cf. Figure 38)

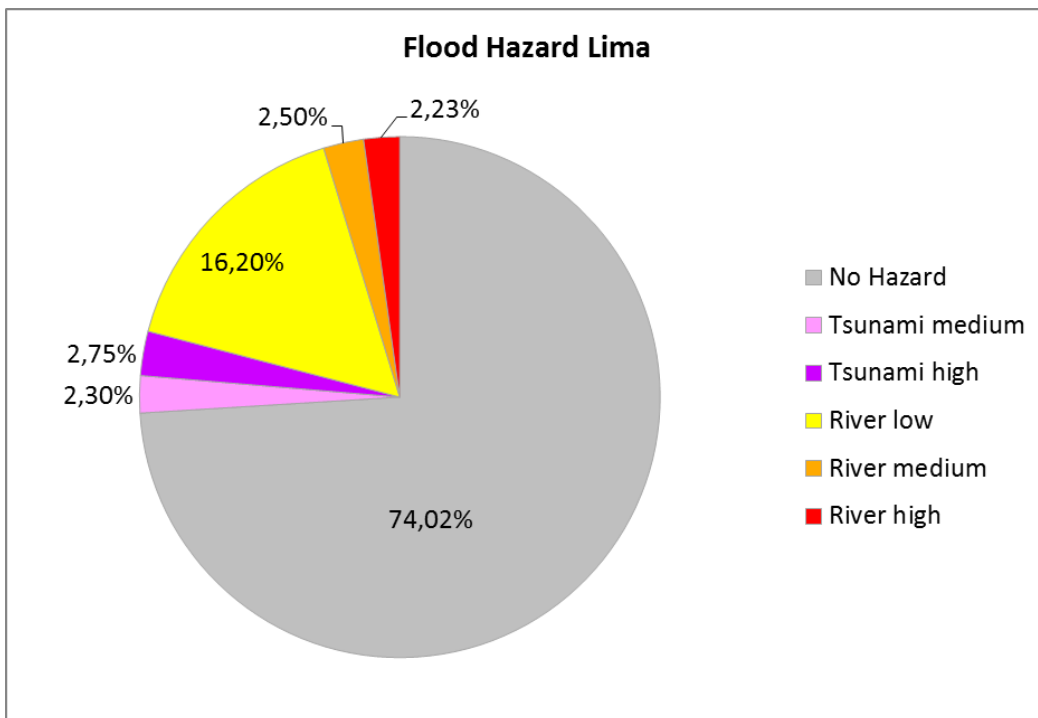


Figure 56: Flood Hazard Classification displaying proportions of areas prone to flooding in Metropolitan Lima area – shown separately for Tsunami Hazard and River and Flash Flood Hazard

The same analysis for the total Metropolitan area of Lima, subdivided in Tsunami and River and Flash Flood Hazard zones, gives a similar result as shown in Figure 56 with approx. 9.8% of Residential and Public Urban Fabric being situated in Medium and High Hazard zones – whereby the ratio of the hazard emanating from Tsunami inundations is similar to that emanating from River and Flash Floods. Again, an additional 16% of this land use class is situated in low Flood Hazard Zones (emanating from River and Flash Floods).

The extreme flooding scenario to be considered is a destructive earthquake during El Niño periods with landslides damming the high-water bearing Rímac River followed by bursting of the natural dams thus inducing water surges in the Rímac valley. This scenario seems to be quite realistic, as the susceptibility map for mass movements published by INGEMMET (2015), based on a multivariate statistical modelling approach, shows large areas in the Rímac valley with high and very high mass movement susceptibility (cf. Figure 57).

The extreme Hazard scenario as outlined above has not been modelled in this investigation.

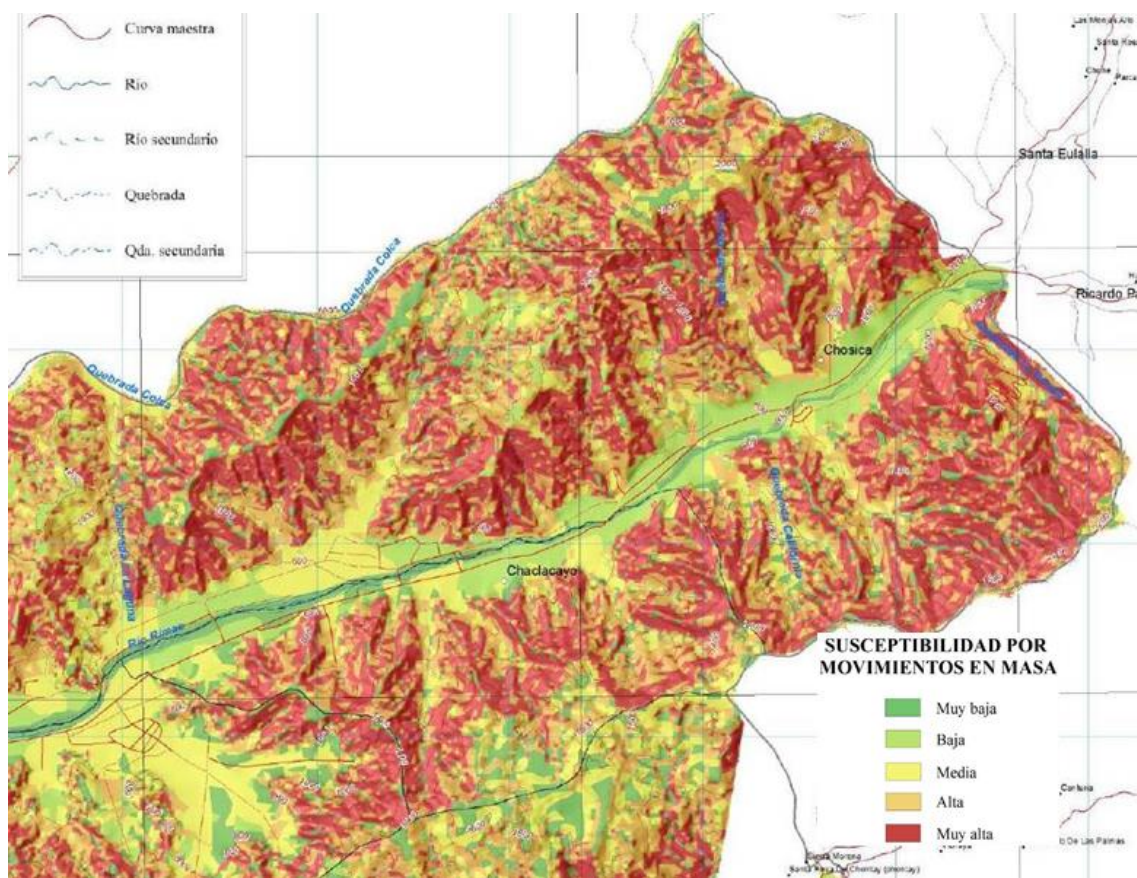


Figure 57: Susceptibility Map for Mass Movements in the Rímac Valley in eastern Lima (District of Lurigancho and Chaclacayo) (Source: INGEMMET 2015)

Flood Risk

In the 1970ies a period of rapid growth started in Lima as rural people sought opportunities for work and education. In the following decades settlements spread to the north, beyond the Rímac River, to the east, along the Central Highway and to the south. New settlements (most of them informal) evolved in the foothills of the Andean mountains spreading in the valley bottoms, on the alluvial cones of the tributaries and on parts of the steep slopes. Due to this development, Lima's infrastructure and large parts of the housing are not designed for heavy rains which every few years are caused by the El Niño phenomenon.

Generally, the authorities of Lima are well aware of the high vulnerability and risk regarding the occurrence of River and Flash Floods together with Mud and Debris Flows. Thus, there are constant efforts to develop effective prewarning and evacuation concepts for such case (cf. SIGRID database).

For many areas which are prone to floods hazard and risk maps were produced. Nevertheless, events from the past did not result in sufficient prevention and mitigation measures – as was shown in March 2017.

Flood Risk product considers both the flood hazard intensity level (susceptibility) and the exposure level related to population and assets regarding such natural event. The damage cost on the different land use categories has been estimated as exposure indicator and the risk matrix generated accordingly. For more details about the processing method, please refer to Annex 1. Nevertheless, it is important to be aware that the applied methodology involves some degree of human interpretation. Therefore, flood risk levels must be considered as relative metrics rather than absolute ones.

Examples of the Flood Risk Products are shown in the section 5.6 for all types of floods.

5.5 Accuracy Assessment

Due to the relatively low frequency of catastrophic tsunamis in the study area, no EO data exist showing the run-up of the waves and resulting damages.

Since no independent reference data are available, no state-of-the-art accuracy assessment is possible. The plausibility of the results nevertheless was evaluated on basis of available height information from the ALOS World 3D – 30m DSM as well as from scientific investigations and available reports about historical events.

The accuracy of any modelling output aiming at the delimitation of potentially flooded areas depends on the modelling approach as well as on the accuracy of the input data. Depending on the modelling approach many assumptions have to be taken which considerably affect the result. In reality, the spatial distribution of tsunami heights along the coast may be significantly modified by local topography, bathymetry, coastal irregularities, shelf resonance effects, and other topographical factors. The key factor seems to be the resonant influence of topography (Kulikov et al. 2005).

Based on three different empirical relations between earthquake magnitudes and tsunamis, Kulikov et al. (2005) estimated expected tsunami wave heights for various return periods for the whole section of the Peruvian and Northern Chile coast. The average heights were 11.2 m (50 years), 13.7 m (100 years), and 15.9 m (200 years), while the maximum height values were: 13.9, 17.3, and 20.4 m, respectively. Both the ‘averaged’ and ‘maximum’ seismological estimates of tsunami wave heights for this region are significantly smaller than the observed tsunami run-up of 24–28 m, for the major events of 1586, 1724, 1746, 1835, and 1877.

A problem with applying the Extreme Statistics theory directly for tsunami heights and with estimating tsunami risk based on these data, is that they present integral relations between earthquake magnitudes and tsunami wave heights and do not take into account local peculiarities of a given region, such as local topographic amplification of arriving tsunami waves.

Within the frame of the present investigation, the Tsunami Hazard Product based on several existing hazard maps (Dirección de Hidrografía y Naveagación (DHN), Adriano et al. 2013, Mas et al. 2014) was evaluated using the topographic information as derived from the ALOS World 3D – 30m (AW3D30) DSM.

In most areas the modelled inundation zones for the extreme scenario (generated by a seismic event of 9.0 Mw) are in good accordance with the 12 m isohypse from the ALOS DEM, and the modelled inundation zones for the most probable scenario (generated by a seismic event of 8.5 Mw) correspond with the 7 m isohypse.

It can be assumed that the accuracy of the model output would benefit considerably from the availability of LiDAR based Digital Surface Models with very high spatial resolution. Such model still is not available for the area of Metropolitan Lima.

For River and Flash Floods no independent reference data is available as well. Thus, no state-of-the-art accuracy assessment is possible. The plausibility of the results was evaluated on basis of scientific investigations and existing Hazard and Risk Maps (e.g. INGEMMET 2015). Furthermore, the plausibility of the features derived from the ALOS World 3D – 30m DSM was evaluated on basis of the patches of VHR DSMs available from the SIGRID database (cf. Chapter 4.5.2).

Accuracy assessment was however performed by SIRS for the flood extent map product generated by means of visual interpretation of WorldView-2 Images acquired on 18th and 21st of March 2017.

A single stage stratified random sampling approach was implemented for giving a reasonable balance between the relevance of the reference dataset and the effort. 300 sampling units (points) were distributed in this way:

- 200 samples were randomly selected within a first stratum corresponding to the Flood Extent.
- 100 samples were randomly selected within a 500m buffer area around the Flood Extent.

Figure 58 is showing the mapping result with the overlaid sample points.

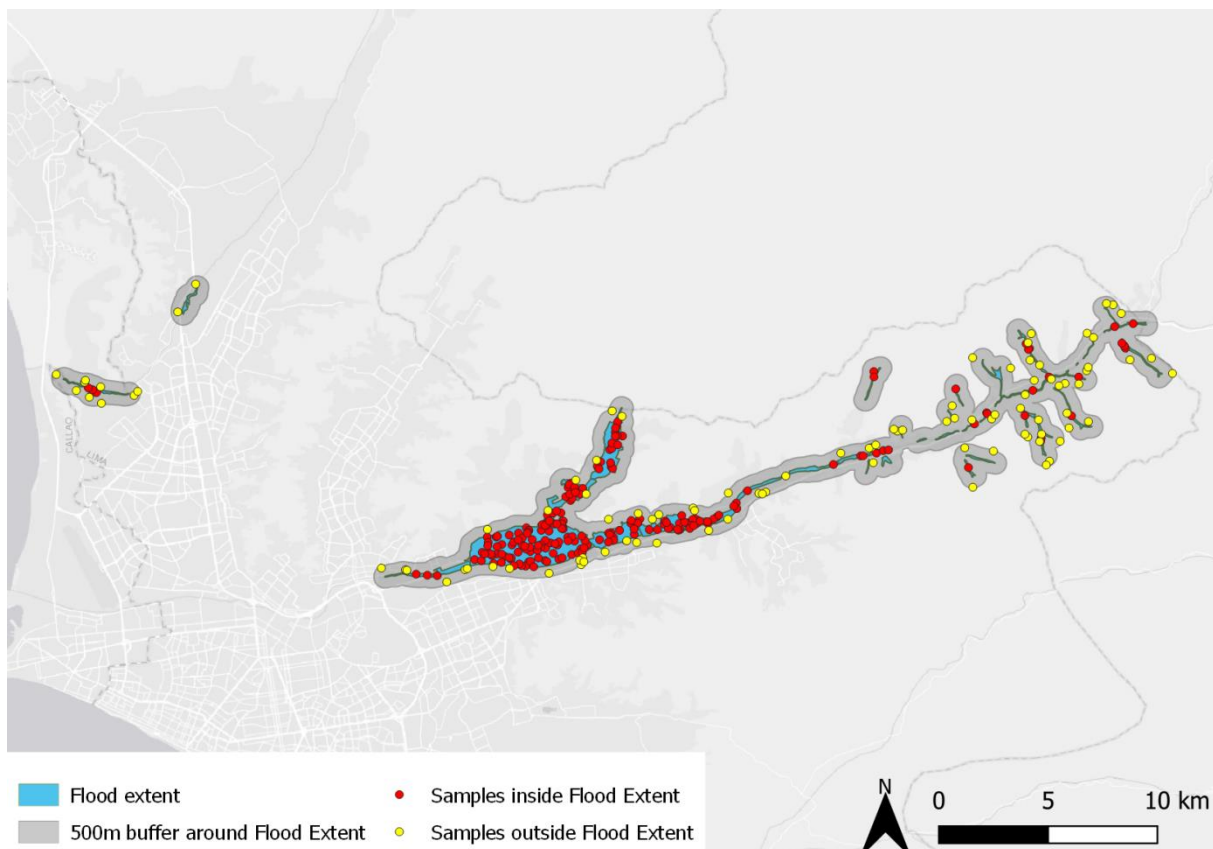


Figure 58: Mapping result of the Flood Extent of March 2017 event overlaid with randomly distributed sample points used for accuracy assessment.

In this way a reference information could be extracted for each sample point by visual interpretation of WorldView-2 images. The reference information of each sampling point was compared with the mapping results and the numbers of correctly and not-correctly classified observations were recorded. From this information the specific error matrices and statistics were computed.

The Flood Extent product related to March 2017 event and derived from VHR optical satellite imagery has an overall mapping accuracy of 97.90% with a CI ranging from 96.28% to 99.52% at a 95% CI. The detailed results of the accuracy assessment are given in Annex 2.

5.6 Analysis of Mapping Results

As described in the section 5.3 and shown in Figure 38, two different datasets regarding the urban land use were made available for this analysis:

- LULC classification (delivered by IABG through the EOWORLD project) based on 2013 imagery covering the entire AOI (approx. 1.174 km²)
- LULC product generated by SIRS through EO4SD-Urban covering only a part of the total AOI in the centre of Lima based on 2016 VHR imagery (approx. 244,56 km²)

Whereas it is possible to parallelize the two datasets for the classification of four levels of exposition and thus for the risk classification, it is not feasible to join all land use classes from the two different datasets as the nomenclature is too different – thus the detailed statistical analysis was restricted to the AOI subset in Lima centre.

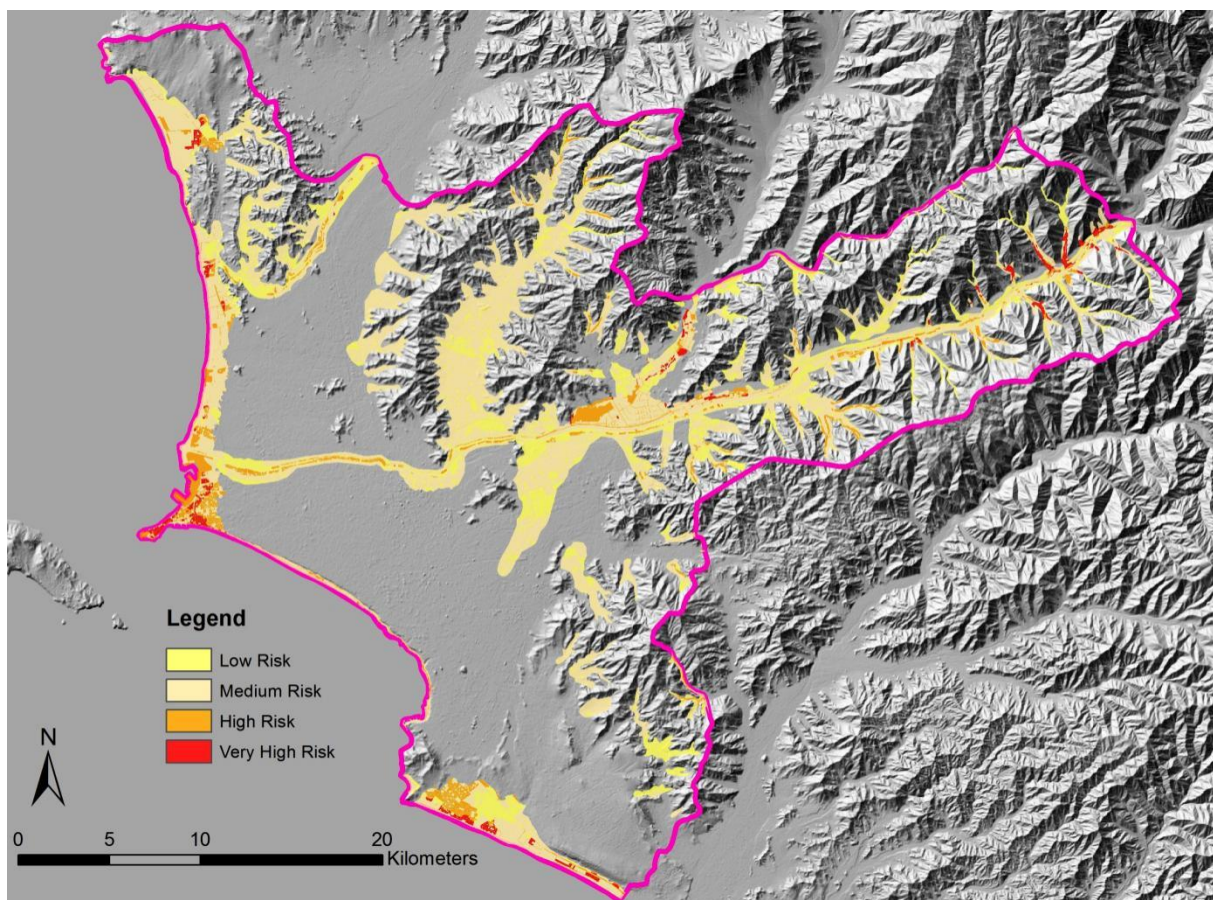


Figure 59: Flood Risk Map for Metropolitan Lima considering Tsunamis, River and Flash Floods (Background: Hillshade ALOS World 3D – 30m (AW3D30), version 2.1)

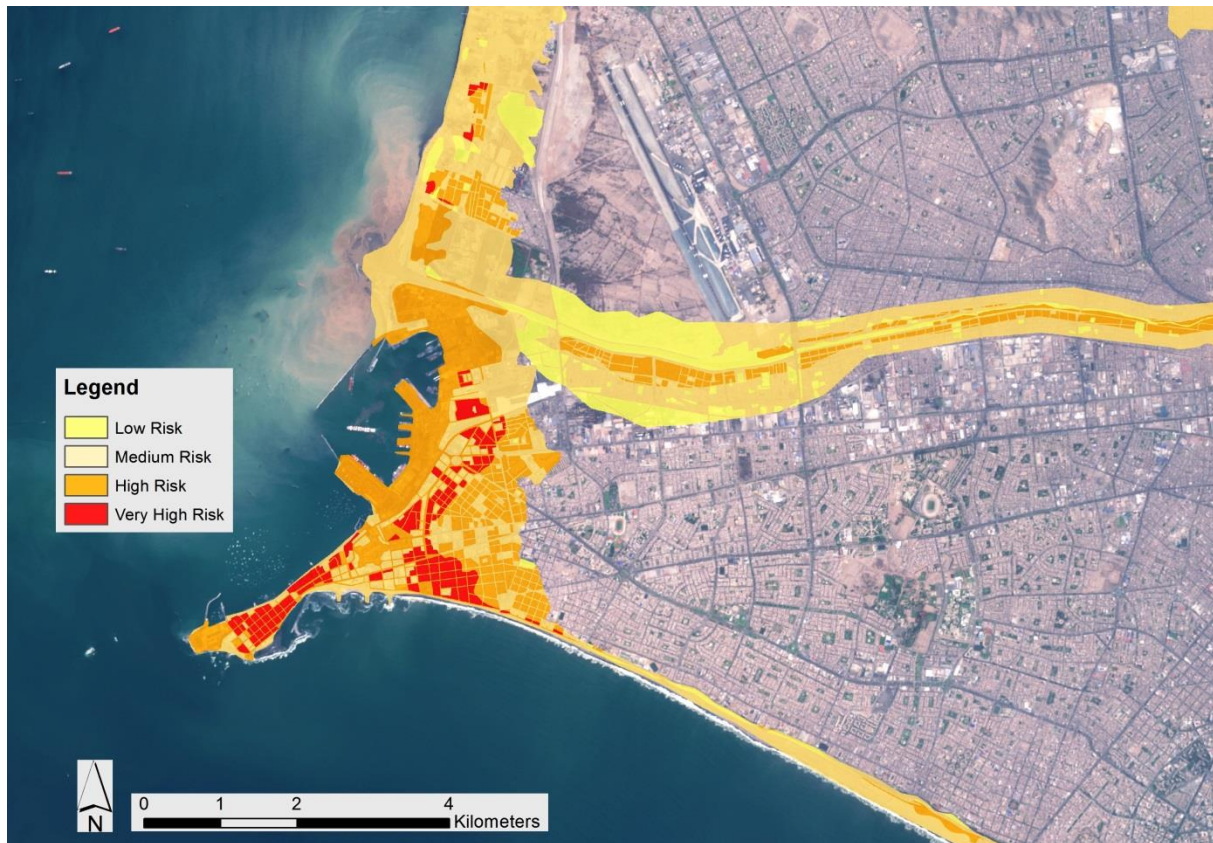


Figure 60: Subset of Flood Risk Map for Callao – La Punta and Central Lima considering Tsunamis and flooding from River Rímac (Background Image: Sentinel2A 20170220)

Residential and Public Urban Fabric (Public Buildings, Commercial Area, Business District, Education Facilities, Health Facilities, Residential Area) with high damage potential was analyzed detailed and combined with the Flood Risk Map

The statistics for Residential and Public Urban Fabric in the central area of Lima (as covered by the EO4SD-Urban LULC classification) is shown in Figure 61; a subset of the related map is given in Figure 62. Based on these statistics, approx. 19.3% of Lima Residential and Public Urban Fabric is situated in medium to very high risk zones.

Hotspots for high risk zones regarding Residential and Public Urban Fabric are in Callao – La Punta on the one hand (cf. Figure 62) – emanating from Tsunami Inundation Hazard - and in the districts of Lurigancho and Chaclacayo in the Rímac River valley in Eastern Lima, emanating from River and Flash Floods (cf. Figure 63).

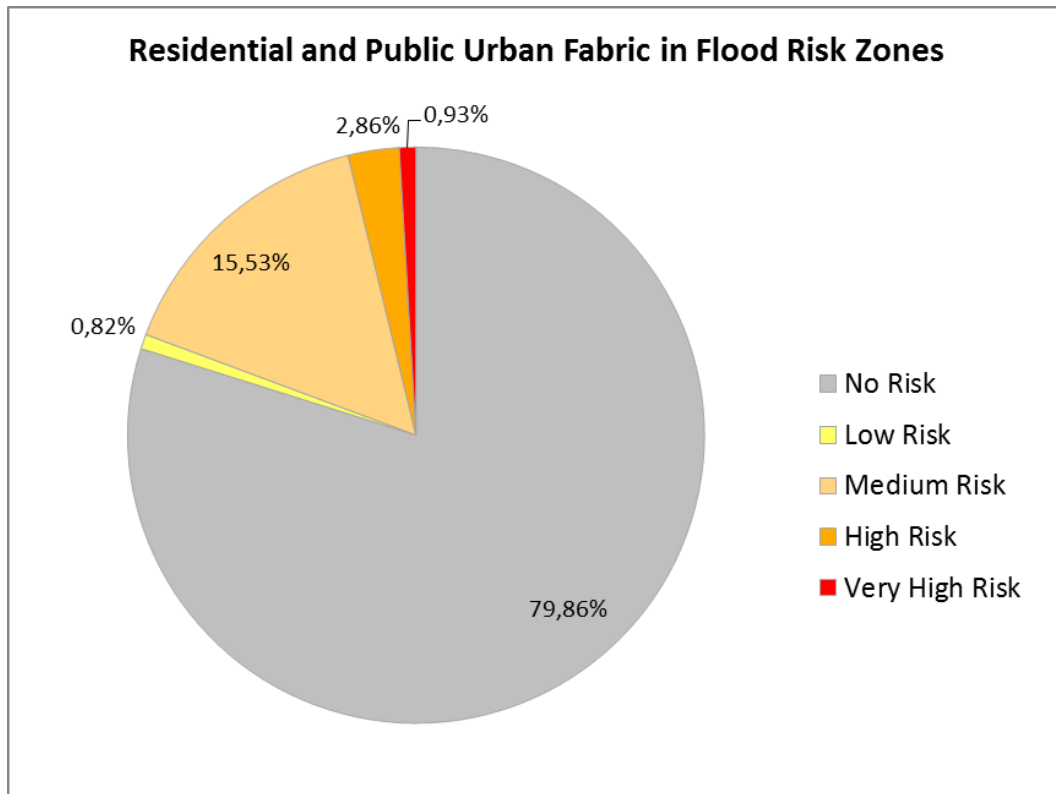


Figure 61: Proportion of Residential and Public Urban Fabric in Flood Risk Zones in Lima Central Area covered by EO4SD-Urban LULC classification (cf. Figure 38)



Figure 62: Map of Residential and Public Urban Fabric based on classification of 2016 VHR imagery combined with Flood Risk Zoning in Callao – La Punta and Central Lima (Background Image: Sentinel2A 20170220)

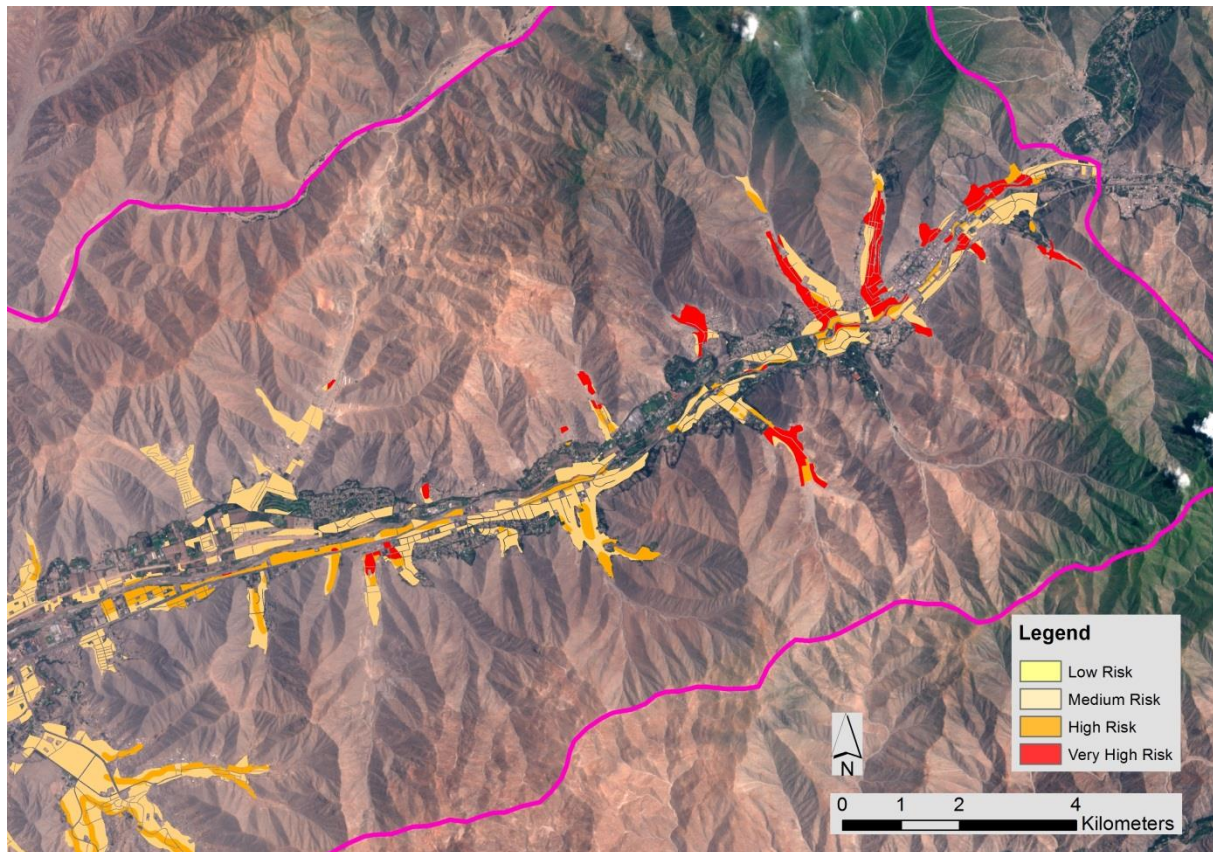


Figure 63: Map of Residential and Public Urban Fabric based on EOWORLD 2013 classification combined with Flood Risk Zoning in Eastern Lima - Districts of Lurigancho and Chaclacayo, Chosica (Background Image: Sentinel2A 20170220; Pink Line: limits of AOI)

6 References

Czaplewski, R. L. (2003). Chapter 5: Accuracy assessment of maps of forest condition: statistical design and methodological considerations, pp. 115–140. In Michael A. Wulder, & Steven E. Franklin (Eds.), *Remote sensing of forest environments: concepts and case studies*. Boston: Kluwer Academic Publishers (515 pp.).

European Union (2011). *Mapping Guide for a European Urban Atlas, Version 11.0*

Goodchild, M., Chih-Chang, L. and Leung, Y. (1994): Visualizing fuzzy maps, pp. 158-67. In Heamshaw, H.H. and Unwin, D.J. (Eds.), *Visualization in geographical information systems*. Chichester: Wiley.

Olofsson, P., Foody, G. M., Stehman, S. V., & Woodcock, C. E. (2013). Making better use of accuracy data in land change studies: Estimating accuracy and area and quantifying uncertainty using stratified estimation. *Remote Sensing of Environment*, 129, 122–131. doi:10.1016/j.rse.2012.10.031

Selkowitz, D. J., & Stehman, S. V. (2011). Thematic accuracy of the National Land Cover Database (NLCD) 2001 land cover for Alaska. *Remote Sensing of Environment*, 115(6), 1401–1407. doi:10.1016/j.rse.2011.01.020.

Flood-related products

Adriano, B., Mas, E., Koshimura, S., Fujii, Y., Yauri, S., Jimenez, C. & Yanagisawa, H.: (2013): Tsunami Inundation Mapping in Lima for Two Tsunami Source Scenarios.- *Journal of Disaster Research*, Vol.8, No.2, pp. 274-284.

Allende, T. et al (2012): Aproximación al estudio de vulnerabilidad ante desastres en Lima Metropolitana. Lima, Perú. Disponible en:
<https://ciudadesfocalesmirrima.files.wordpress.com/2012/08/una-aproximacion-al-estudio-de-vulnerabiliadl.pdf>

Capel Molina, J.J. (1999). Lima, un clima de desierto litoral. *Anales de Geografía de la Universidad Complutense Madrid: Universidad Complutense de Madrid*, 19: pp. 25–45.

Centro de Estudios y Prevención de Desastres – PREDES (2009): Diseño de escenario sobre el impacto de un sismo de gran magnitud en Lima Metropolitana y Callao, Peru.

Chira La Rosa, J.D (2016): Mejora de Red de Monitoreo para la Prevención de Peligros Hidrometeorológicos en la Cuenca del Rio Rímac.- Thesis Universidad Nacional de Ingeniería Facultad de Ingeniería Civil, Lima.

Dasgupta, S., Asif, Z., Subhendu, R., Mainul, H., Sarwar, J. & Ainun, N. (2015): *Urban Flooding of Greater Dhaka in a Changing Climate: Building Local Resilience to Disaster Risk*. Directions in Development. Washington, DC: World Bank. doi:10.1596/978-1-4648-0710-7. License: Creative Commons Attribution CC BY 3.0 IGO

DIÁLOGO (2016): Digital Military Magazine <https://dialogo-americas.com/en/articles/new-app-peruvian-navy-aims-keep-civilians-safe-during-tsunamis>: Retrieved 2019-01-014.

Dorbath, L., Cisternas, A., & Dorbath, C. (1990): Assessment of the size of large and great historical earthquakes in Peru.- *Bulletin of the Seismological Society of America*, Vol.80, No.3, pp. 551-576.

- Drenkhan, F. (2010): Balance de área y masa de glaciares tropicales en el Perú durante el período 1985 -2008 utilizando data de ASTER y Landsat. Seminario SENAMHI, 26.11.2010
- García Chaca, R.L. (2016): Alternativas para la Estabilización de la Quebrada Cantuta II con Fines de Mitigación de Huaycos.- Thesis Universidad Nacional Agraria La Molina, Lima.
- Garreaud, R. D. & Aceituno, P. (2007): Atmospheric Circulation and Climatic Variability. – In: Veblen, T. T., Young, K. R., & Orme, A. R. (2007): The Physical Geography of South America, 45-59, Oxford University Press, New York, USA.
- Indra Sistemas S.A. (2017): EMSN-038: Post-disaster situation analyses of flood and landslides in Lima, Peru. Final Report Summary.- Madrid.
- INGEMMET (2015): Peligros Geológicos en el Área de Lima Metropolitana y la Región Callao.- INGEMMET Booleetín Serie C: Geodinámica e Ingeniería Geológica, No. 59, Lima.
- INGEMMET (2017): Peligros Geológicos y Hidrogeológicos Detonados por el Evento del Niño Costero 2017 en la Región Lima y Parte de Ica.- Informe Técnico No. A6789, Lima.
- Iwahashi, J. & Pike, R.J. (2007): Automated classifications of topography from DEMs by an unsupervised nested-means algorithm and a three-part geometric signature. *Geomorphology*, Vol. 86, pp. 409–440.
- Karakouzian, M., Candia, M.A., Wyman, R.V., Watkins, M.D. & Hudyma, N. (1997): Geology of Lima, Peru.- *Environmental & Engineering Geoscience*, III, 55-88. 10.2113/gseegeosci.III.1.55.
- Kulikov, E.A., Rabinovich, A.B., & Thomson, R.E. (2005): Estimation of Tsunami Risk for the Coasts of Peru and Northern Chile.- *Natural Hazards* 35: 185–209 DOI 10.1007/s11069-004-4809-3.
- Lockridge, P. A. (1985): Tsunamis in Peru–Chile, World Data Center A for Solid Earth Geophysics.- Report SE-39, U.S. Department of Commerce, NOAA, Boulder, CO, 97 pp.

Internet

Road classification, European Commission, 2017, https://ec.europa.eu/transport/road_safety/specialist-/knowledge/road/designing_for_road_function/road_classification_en, last accessed 2017.08.17

This page is intentionally left blank!

Annex 1 – Processing Methods for EO4SD-Urban Products

This page is intentionally left blank!

Summary of Processing Methods

Urban Land Use/Land Cover and Change

The input includes Very High Spatial Resolution (VHR) imagery from different sensors acquired at different time. The data is pre-processed to ensure a high level of geometric and radiometric quality (ortho-rectification, radiometric calibration, pan-sharpening).

The complexity when dealing with VHR images comes from the internal variability of the information for a single land-use. For instance, an urban area is represented by a high number of heterogeneous pixel values hampering the use of automated pixel-based classification techniques.

For these VHR images, it is possible to identify textures (or pattern) inside an entity such as an agricultural parcel or an urban lot. In other words, whereas pixel-based techniques focus on the local information of each single pixel (including intensity / DN value), texture analysis provides global information in a group of neighbouring pixels (including distribution of a group intensity / DN values but also spatial arrangement of these values). Texture and spectral information are combined with a segmentation algorithm in an Object Based Image Analysis (OBIA) approach to reach a high degree of automation for most of the peri-urban rural classes. However, within urban land, land use information is often difficult to obtain from the imagery alone and ancillary/in situ data needs to be used. The heterogeneity and format of these data mean that another information extraction method based on Computer Aided Photo-Interpretation techniques (CAPI) need to be used to fully characterise the LULC classes in urban areas. Therefore, a mix of automated (OBIA) and CAPI are used to optimise the cost/quality ratio for the production of the LULC/LUCC product. The output format is typically in vector form which makes it easier for integration in a GIS and for subsequent analysis.

Level 4 of the nomenclature can be obtained based on additional information. These can be generated by more detailed CAPI (e.g. identification of waste sites) or by an automated approach based on derived/additional products. An example is illustration by categorising the density of the urban fabric which is related to population density and can then subsequently used for disaggregating population data.

Information on urban fabric density can be obtained through several manners with increasing level of complexity. The Imperviousness Degree (IMD) or Soil Sealing (SL) layer (see separate product) can be produced relatively easily based on the urban extent derived from the LULC product and a linear model between imperviousness areas and vegetation vigour that can be obtained from Sentinel 2 or equivalent NDVI time series. This additional layer can be used to identify continuous and discontinuous urban fabric classes. Five urban fabric classes can be extracted based on a fully automated procedure:

- Continuous very dense urban fabric (IMD > 80%)
- Discontinuous dense urban fabric: (IMD 50-80 %)
- Discontinuous medium density urban fabric (IMD: 30-50 %)
- Discontinuous low density urban fabric (IMD 10-30 %)
- Discontinuous very low density urban fabric (IMD < 10 %)

Manual enhancement is the final post-processing step of the production framework. It will aim to validate the detected classes and adjust classes' polygon geometry if necessary to ensure that the correct MMU is applied. Finally, a thorough completeness and logical consistency check is applied to ensure the topological integrity and coherence of the product.

Change detection: Four important aspects must be considered to monitor land use/land cover change effectively with remote sensing images: (1) detecting that changes have occurred, (2) identifying the nature of the change, (3) characterising the areal extent of the change and (4) assessing the spatial pattern of the change.

The change detection layer can be derived based on an image-to-image approach provided the same sensor is used. An original and efficient image processing chain is promoted to compare two dates' images and provide multi-labelled changes. The approach mainly relies on texture analysis, which has the benefits to deal easily with heterogeneous data and VHR images. The applied change mapping approach is based on spectral information of both dates' images and more accurate than a map-to-map comparison.

Summary of Processing Methods

World Settlement Extent

The rationale of the adopted methodology is that given a series of radar/optical satellite images for the investigated AOI, the temporal dynamics of human settlements are sensibly different than those of all other land-cover classes.

While addressing settlement-extent mapping for the period 2014-2015 multitemporal S1 IW GRDH and Landsat-8 data acquired at 10 and 30m spatial resolution were taken into account. Concerning radar data, each S1 scene is pre-processed by means of the SNAP software available from ESA; specifically, this task includes: orbit correction, thermal noise removal, radiometric calibration, Range-Doppler terrain correction and conversion to dB values. Scenes acquired with ascending and descending pass are processed separately due to the strong influence of the viewing angle in the backscattering of built-up areas. As a means for characterizing the behaviour over time, the backscattering temporal maximum, minimum, mean, standard deviation and mean slope are derived for each pixel. Texture information is also extracted to ease the identification of lower-density residential areas. As regards optical data, only Landsat-8 scenes with cloud cover lower than 60% are taken into consideration (indeed, further rising this threshold often results in accounting for images with non-negligible misregistration error). Data are calibrated and atmospherically corrected using the LEDAPS tool available from USGS and the CFMASK software is applied for removing pixels affected by cloud-cover and cloud-shadow. Next, a series of 6 spectral indices suitable for an effective delineation of settlements (identified through extensive experimental analysis) are extracted; these include – among others – the Normalized Difference Built-Up Index (NDBI), the Modified Normalized Difference Water Index (MNDWI) and the Normalized Difference Vegetation Index (NDVI). For all of them, the same set of 5 key temporal statistics used in the case of S1 data are generated for each pixel in the AOI. Moreover, to improve the detection of suburban areas, for each of the 6 temporal mean indices also here texture information is computed. For matching the spatial resolution of Sentinel data, the whole stack of Landsat-based features is finally resampled to 10m spatial resolution.

To identify reliable training points for the settlement and non-settlement class, a strategy has been designed which jointly exploits the temporal statistics computed for both S1 and Landsat data, along with additional ancillary information. In the case of optical data, in general the most of settlement pixels can be effectively outlined by properly jointly thresholding the corresponding NDBI, NDVI, and MNDWI temporal mean; likewise, this holds also for non-settlement pixels. Regarding radar data, it generally occurs that the temporal mean backscattering of most settlement samples is sensibly higher than that of all other non-settlement classes. Nevertheless, in complex topography regions: i) radar data show high backscattering comparable to that of urban areas; and ii) bare rocks are present, which often exhibit a behaviour similar to that of settlements in the Landsat-based temporal statistics. Accordingly, to exclude these from the analysis, all pixels are masked whose slope - computed based on SRTM 30m DEM for latitudes between -60° and $+60^{\circ}$ and the ASTER DEM elsewhere - is higher than 10 degrees.

Support Vector Machines (SVM) are used in the classification process. However, as the criteria defined above for outlining training samples might result in a high number of candidate points, for AOIs up to a size of ~10000 km² the most effective choice proved extracting 1000 samples for both the settlement and non-settlement class. Nonetheless, since results might vary depending on the specific selected training points, as a means for further improving the final performances and obtain more robust classification maps, 20 different training sets are randomly generated and given as input to an ensemble of as many SVM classifiers; then, a majority voting is applied. Afterwards, the stacks of Landsat-8-based and S1-based temporal features are classified separately as this proved more effective than performing a single classification on their merger. In both cases, a grid search with a 5-fold cross validation approach is employed to identify for each training set the optimal values for the learning. Here, those resulting in the highest cross-validation overall accuracy are then selected and used for classifying the corresponding study region.

A final post-classification phase is dedicated to properly combining the Landsat- and S1-based classification maps and automatically identifying and deleting potential false alarms. To this purpose, an advanced post-editing object-based approach has been specifically designed.

The above-described methodology has been further adapted for outlining the settlement extent in the past solely based on Landsat-5/7 imagery available since 1984; indeed, no long-term SAR data archive at comparable spatial resolution is freely accessible for the same timeframe (e.g., ESA ERS-1/2 data are available from 1991 without systematic world coverage and often proved too complicated to pre-process). In particular, for the given target period and AOI, all available Landsat imagery with cloud cover lower than 60% is pre-processed in the same fashion as described in the previous paragraphs and the same set of temporal statistics and texture features are extracted. Based on the hypothesis that settlement growth occurred over time (meaning that a pixel cannot be marked as settlement at an earlier time if it has been defined as non-settlement at a later time), all pixels categorized as non-settlement in the 2014-2015 extent map are excluded from the analysis. Then, training samples are derived by thresholding the temporal mean NDBI, MNDWI and NDVI; specifically, a dedicated strategy has been implemented for automatically determining the thresholds for the 3 indices by comparing their cumulative distribution function (CDF) for the target period with that exhibited for the period 2014-2015. Also in this case, an ensemble of 20 SVMs is used, each one trained on a different subset of 2000 samples (i.e., 1000 for the settlement and 1000 for the non-settlement class) and majority voting is then employed for generating the final map. It is worth noting that, when deriving the past settlement extent for multiple times, both the masking and threshold adaptation are performed on the basis of the results derived for the next target period.

Summary of Processing Methods

Percentage Impervious Surface

Imperviousness product is intended to represent the impervious surfaces because of urban development, layers of completely or partly impermeable artificial material (asphalt, concrete, etc.) and infrastructure construction. Therefore, the Imperviousness Degree (IMD) or Soil Sealing (SL) information can be produced relatively easily based on the Urban Extent derived from the baseline LULC information product and the linear model between impervious areas and vegetation presence that can be determined and characterized from Landsat or Sentinel-2 NDVI time series.

More precisely, the raster product is generated at 10m - 30m spatial resolution by properly exploiting Landsat-4/5/7/8 or Sentinel-2 multitemporal imagery acquired over the study area within a given time interval of interest in which no relevant changes are expected to occur (typically a time period of 1-2 years allows to get very accurate results). Each acquired EO data is pre-processed (ortho-rectification, radiometric calibration, pansharpener, cloud-masking). Then, the Normalized Difference Vegetation Index (NDVI) is extracted for each image within the urban mask (corresponding to Urban Extent product). NDVI is inversely correlated with the amount of impervious areas, i.e. the higher the NDVI is, the higher the expected presence of vegetation, hence the lower the corresponding imperviousness degree. The core idea is to compute per each pixel its temporal maximum which depicts the status at the peak of the phenological cycle. It is worth noting that for different pixels in the study area, different number of scenes might be available.

However, in the hypothesis of sufficient minimum number of acquisitions unavailable for computing consistent statistics, this does not represent an issue. Indeed, in this framework, it is also possible to get spatially consistent datasets useful for the desired analyses, even when investigating large territories. Areas associated with different levels of impervious surfaces are then extracted by visual interpretation from data sources with higher spatial resolution (e.g. VHR imagery, Google Earth imagery). OSM layers or information derived from in-situ campaigns are other auxiliary data sources which can also be used for this purpose. At the end, reference data are extracted in various parts of the study region and then rasterized and aggregated at the spatial resolution of input EO data.

A support vector regression SVR module is then used for properly correlating the resulting training information with the temporal maximum NDVI to finally derive the Percentage of Impervious Surface (PIS) or Imperviousness Degree (IMD) for the entire AOI. Specifically, 8bit integer values from the raster product range from 0 (no impervious surface in the given pixel) to 100 (completely impervious surface in the given pixel).

Summary of Processing Methods

Urban Green Areas

The location and extent of green areas are determined within the product of urban land use/ land cover at Level I. Urban green areas refer to land within and on the edges of a city that is partly or completely covered with grass, trees, shrubs, or other vegetation. This includes public parks, private gardens, cemeteries, forested areas as well as trees, river alignments, hedges etc. The product delivered within EO4SD-Urban project thus provides accurate information (1 m resolution) on the spatial location and extent of the green areas located within the Urban Extent (Level I class: 1000) derived from the baseline LULC information product.

Detecting and monitoring urban green coverage needs very high resolution optical satellite images, which explains the product generation over the Core Urban Area of AOI only. The same images have been logically used for generating the LULC information product. Consequently, the usual preliminary quality check and pre-processing tasks were already implemented.

Urban Green Areas have been detected using automated supervised classification method. More precisely, each single multispectral VHR scene has been classified by specifying the most appropriate algorithm and class number. Then, pixel units from the classes considered as representing green areas have been combined into 1 single class. From this operation results the required binary raster product. At this stage, it only remains necessary to apply some post-processing steps:

- Morphological filter is applied to fill small gaps within the green areas (caused by shadow)
- Resampling of the data to the provided spatial resolution of 1m
- Removing small pixel groups under the minimum mapping unit.
- Integrating the information provided by the LULC product (e.g. class Urban Parks, Cemeteries).
- Validation of Mapping results

Furthermore, using archive very high resolution images, current and historic extent of urban green areas are compared to identify their temporal evolution – extent growth or reduction. Quality control and accuracy assessment tasks are performed by means of visual interpretation considering also the LULC dataset.

Summary of Processing Methods

Building Footprints

Building is any structure having a roof supported by columns or walls and intended for the shelter, housing, or enclosure of any individual, animal, process, equipment, goods, or materials of any kind. Building footprint are defined as the contour of houses and other manmade buildings as they are commonly represented in cadastral systems. The product provides information on the spatial distribution, number and size of building footprints.

The spatial explicit representation of building footprints and their type is derived by visual interpretation and digitisation of Very High Resolution (VHR) optical imagery. Particular attention is given to the best possible use of the dynamic range of the datasets and to guarantee the best radiometric homogeneity, in case of multiple images to be used. Auxiliary information from Open Street Map (OSM), available cadastral information and aerial images can assist the production process regarding effort and delivery time. The product is therefore mainly based on VHR images from space borne sensors (1m resolution or better) and its results are represented as vector data.

Each digitised footprint can be further attributed with user required information to specify the type of building. Within the scope of EO4SD-Urban service, the use/function of buildings is especially derived from the LU/LC product at level IV of the ‘1000 – Artificial Surfaces’ Level I class. OSM and any ancillary data provided by users can be helpful, especially for providing also the building names when existing.

Change detection: Four important aspects must be considered to monitor building footprint changes effectively with remote sensing images: (1) detecting that changes have occurred, (2) identifying the nature of the change, (3) characterising the areal extent of the change and (4) assessing the spatial pattern of the change.

The change detection is performed by visual comparison of the images from both dates. Changes detectable from VHR optical imagery are building construction or destruction. Changes related to the type of buildings require the use of ancillary data such as OSM.

Summary of Processing Methods

Flood History and Risk

Products based on flood history monitoring or modelling provide information about spatial location and intensity of flood hazard. Thus, they represent key input into identification of exposed assets, infrastructure and population and assessment of flood-related risk. Hazard, exposure and risk levels are estimated through numeric indexes for describing the severity of phenomena. The service consists in the provision of flood-related geospatial information and is composed of three products which are all delivered in vector format:

- Product 1: Flood Extent (inventory)
- Product 2: Flood Hazard (susceptibility)
- Product 3: Flood Risk (considering exposition)

Flood events - Inventory

For the metropolitan area of Lima basically three main flood scenarios have to be considered:

- Tsunamis in coastal areas generated by major earthquakes in close proximity to the Peruvian coast
- River Floods after heavy rainstorms in the upper catchment parts of the main rivers crossing the metropolitan area (mainly December – March)
- Short-term local Flash Floods and Mud and Debris Flows in mountainous Eastern parts of Lima (mainly December – March)

The latter two scenarios may occur together.

The flood events retrieval was based on literature review and press and social media release. The major platforms used for this purpose are:

- <http://floodobservatory.colorado.edu/Archives/index.html>
- Copernicus Flood list: <http://floodlist.com/tag/peru>
- SIGRID database (Sistema de Información para la Gestión del Riesgo de Desastres, maintained by the Centro Nacional de Estimación, Prevención y Reducción del Riesgo de Desastres (Cenepred): <https://sigrid.cenepred.gob.pe/sigridv3/>

The flood inventory for significant flood events during the past 20 years is presented in Table A1. In 1998, 2009 and 2017 combined River and Flash Floods occurred while in 2000, 2008, 2010, 2012 2015 and 2018 local flash flood and debris flows in the mountainous Districts of Eastern Lima were reported. It is also relevant to mention that the worst flood in 40 years in the Metropolitan area of Lima occurred in 2017 and were used as reference for the Hazard Classification.

Data used

EO data

Available open datasets, including Landsat-5/8 and Sentinel1/2 imagery, and ALOS Digital Elevation Model (DEM) data, were selected and downloaded to evaluate their usability for the required products (cf. Tab. A2). All HR optical datasets were subjected to atmospheric correction (DOS 1 approach) and visually checked for useful information for flood detection.

However, due to the very special situation regarding flood hazard and risk in a desert town, none of the acquired satellite images could be used directly for flood extraction.

Table A1: Major flood events in Metropolitan area of Lima for last 20 years

Year	Date	Area concerned	Type
1998	Jan. to March	Chillón, Rímac, Lurin and Huaycoloro Rivers; Lurigancho - Chosica	River and Flash Floods
2000		Jicamarca/Lurigancho	Local Flash Floods
2008	Feb. to Apr.	Ñaña, Carabaylo, San Martín de Porres	Local Flash Floods
2009	Feb. and March	Lurigancho – Chosica, Chillon River (San Martín de Porres)	River and Flash Floods
2010	Feb. 1 st	Lurigancho, Comas	Local Flash Floods
2012	March, 10 th ; Apr., 4 th	Lurigancho – Chosica, Chaclacayo	Local Flash Floods
2015	Feb., 9 th ; March, 23 rd	Lurigancho – Chosica, Chaclacayo	Local Flash Floods
2017	Feb. to March	Valleys of Rímac, Chillon and Huaycoloro River, Lurigancho – Chosica, Chaclacayo, Puente Piedra, Districts of Santa Anita and Ate (Surco River)	River and Flash Floods
2018	Jan., 23 rd	Lurigancho - Chosica	Local Flash Floods

Table A2: Selected optical HR data for flood events

Year	Dataset
1998	LT05_L1TP_007068_19980215_20161225_01_T2
2000	LT05_L1GS_007068_20000205_20161215_01_T2
2008	LT05_L1TP_007068_20080126_20161102_01_T1
	LT05_L1TP_007068_20080211_20161101_01_T1
2010	LT05_L1TP_007068_20100131_20161017_01_T1
2015	LC08_L1TP_007068_20150318_20170412_01_T1
2017	LC08_L1TP_007068_20170219_20170301_01_T1
	S2A_MSIL1C_20170220T151701_N0204_R125_T18LTM
	S2A_MSIL1C_20170220T151701_N0204_R125_T18LUM
	S2A_MSIL1C_20170312T151701_N0204_R125_T18LTM
	S2A_MSIL1C_20170312T151701_N0204_R125_T18LUM
	S2A_MSIL1C_20170401T151701_N0204_R125_T18LTM
	S2A_MSIL1C_20170401T151701_N0204_R125_T18LUM
LC08_L1TP_007068_20170510_20170516_01_T1	
2018	LC08_L1TP_007068_20180121_20180206_01_T1
	LC08_L1TP_007068_20180310_20180320_01_T1
	LC08_L1TP_007068_20180411_20180417_01_T1

Ancillary Data

- ALOS Global Digital Surface Model "ALOS World 3D - 30m (AW3D30)", version 2.1 (©JAXA) was downloaded from the JAXA Global ALOS portal and used for physiographic and hydrographic analyses as well as the plausibility check of the flood hazard products.
- Very High Resolution (VHR) Optical EO Data selected and used for the generation of the baseline LULC and other derived products (current 2016 status) within two selected sub-AOIs in Central and Northern was provided by SIRS. This data gives a good impression of the rapid development and expansion of Lima but no information about flooding could be obtained.
- VHR data showing the flood extent and damages of the 2017 major flood were accessed via Google Earth (VHR data 18/03/2017, 21/03/2017 and 17/04/2017)
- The LULC product (current 2016 status) of Central Lima was used for generating the Flood Risk Product.
- For the areas which are not covered by the VHR LULC classification based on 2016 Pleiades imagery, classification results from the EOWORLD project delivered by IABG and based on 2013 satellite data were used.
- Open Street Map (OSM) data were used for complementary Waterways specification
- Tsunami inundation maps from the Dirección de Hidrografía y Navegación (DHN) together with modelling results as produced by Mas et al. (2014) were used for the definition of the Tsunami Hazard zones.
- VHR DSMs based on aerial drone survey were downloaded from the Sistema de Información para la Gestión del Riesgo de Desastres (SIGRID), maintained by the Centro Nacional de Estimación, Prevención y Reducción del Riesgo de Desastres (Cenepred) and used for the accuracy assessment of results of physiographic and hydrographic analyses

Product 1: Flood Extent

Flood extent products are derived to show the flooded area at the peak of historical event. The only event to be shown is that of March 2017: the identification of the maximum flood extent is based mainly on visual interpretation of WorldView-2 Images that cover the metropolitan area of northern Lima, acquired on 18th and 21st of March 2017 (available online via Google Earth).

Due to the relatively low frequency of catastrophic Tsunamis, no EO data exist showing the run-up of the waves and resulting damages in the Area of Interest.

Product 2: Flood Hazard

Because of the fundamental cause–effect relationships the flood hazard analysis is performed separately for the processes (1) Tsunami inundations and (2) River and Flash Floods (including Mud and Debris Flows). Regarding Tsunami inundations, hazard assessment and mapping is based on historical data and modelling results where different approaches have been applied in former studies.

For estimation of River Flood Hazard, watercourse lines of tributaries were generated from the DEM using ArcMap's hydrologic tools. Note that the results obtained do not always agree with what it is seen on the optical imagery, but this makes sense. Hydrologic features are usually redirected or channelized when crossing urban areas. Places where both datasets do not match can be explained as places where the physiography pushes the water to follow a path that humans have modified. The trajectories of the main rivers were taken from the EOWORLD LULC dataset.

For identification of Flash Flood Hazard an extensive research for reports about historical events was performed. Furthermore, for area-wide roll-out, landforms were classified according to Iwahashi & Pike (2007). The classification into 12 terrain types is based on three morphometric variables - slope gradient, local convexity, and surface texture. The resulting classes are undefined and have to be calibrated empirically by subsequent analysis. According to the event history from the SIGRID database, Class 2 (steep slope, coarse texture, high convexity) was used for the identification of flash flood hazardous areas.

For further differentiation of the Flash Flood Hazard climatological considerations were taken into account as precipitation events triggering such processes can be observed mainly in the Eastern part of Metropolitan area of Lima (valleys of Huayacoloro and Rímac River).

After classification in two classes based on Stream Order the lines were buffered with 50 m (Stream Order (Strahler) 1 and 2) and 100 m respectively (Stream Order (Strahler) 3 and 4, main rivers) to roughly estimate potential flooding zones.

Product 3: Flood Risk

Flood Risk product considers both the flood hazard intensity level (susceptibility) and the exposure level related to population and assets regarding such natural event (vulnerability). By introducing the damage cost on the different land use categories as exposure indicator, the actual impact of flood hazard on human society through different aspects is also taken into account. Consequently, Flood Risk product carries two-fold meaning in both perspectives.

Flood Hazard level

Flood Hazard intensity classification is expert-based as described before.

Exposure level - land use damage cost

Damage cost on land use indicates the exposure level of population and assets regarding flood hazard. This vulnerability indicator is assessed on 4 aspects: economic, social, physical and flood severity (the number of days the flood event lasted).

Table A3: Damage aspects

Damage aspect	Explanation
Economic costs	Income, employment, city budget/subsidy, household assets
Social damage	Population, health, social capital
Physical damage	Electricity, water, sanitation, road accessibility
Flood severity	Persistent damage after 3 days of flooding

A detailed and uniform land-use map is an important prerequisite to perform flood risk calculations, since it determines what is damaged in case of flooding.

Two different datasets regarding the urban land use were made available for this analysis:

- LULC classification (delivered by IABG through the EOWORLD project) based on 2013 imagery covering the entire AOI (approx. 1 174 km²)
- LULC product generated by SIRS through EO4SD-Urban covering only a part of the total AOI in the centre of Lima based on 2016 VHR imagery (approx. 244.56 km²)

For each LULC class, the damage cost on each aspect is estimated on a scale from 0 to 2. The damage cost level from all aspects is then summed up for further evaluation. Finally, the total damage cost values are assigned to 4 different categories of increasing exposure level: A, B, C and D. The evaluation results are provided in Table A4.

Both land-use classification results were recoded to pre-defined categories (as given in Table A4) and merged after categorization.

Table A4: Evaluation results of land use damage cost

Classes	Damage				Total	Level
	Economic Costs 0-2	Social Damage 0-2	Physical Damage 0-2	Flood Duration 0-2		
Agricultural Land	1,5	0,5	0	1	3	B
Commercial and Industrial Units	2	0,5	1	0,5	4	B
Construction Sites 2013/2016	1,5	1	1	1	4,5	C
Dump site	0	1,5	0,5	0	2	A
Forests and Shrub Lands	0,5	0	0	0	0,5	A
Formal medium and high density residential - Continuous urban fabric (Sealing level: 50%-100%)	1,5	1,5	2	1,5	6,5	D
Formal low density residential - Discontinuous urban fabric (Sealing level: 10%-50%)	1,5	1	2	1	5,5	C
Land Without Current Use	0	0	0	0	0	A
Mineral Extraction site	1	0	0,5	0,5	2	A
Military	1	0,5	1	1	3,5	B
Non-Residential Urban Fabric	1	1	0,5	1	3,5	B
Other Natural and Semi-Natural Areas including Wetlands	0	0	0	0	0	A
Roads and associated land, Railways	1,5	1	2	1,5	6	C
Port Area	2	1	0,5	1,5	5	C
Airport	2	0,5	1,5	1,5	5,5	C
Sports and leisure facilities	0,5	0,5	0	0,5	1,5	A
Other Urban / Artificial Area	1,5	1,5	1	0,5	4,5	C
Urban Greenery, Cemeteries	0,5	0,5	0,5	1	2,5	B
Village Settlements, very low density residential (Sealing level 1-10%)	1,5	1,5	0,5	1,5	5	C
Water Bodies	0	0	0	0	0	A

Flood risk matrix

The Flood risk matrix is two-dimensional, taking into account both flood hazard level and exposure level (land use damage cost). At the end, the values resulting from the combination of the ones provided by the input indicators are further grouped and classified into 4 flood risk levels: low - medium - high - very high risk. This risk level categorization, however, is relative. The flood risk matrix is provided in Table A5.

Once the values of the input indicators are well estimated and the flood risk matrix duly established, the flood hazard layer (Product 2) with level attribute information and the current LULC layer with exposure level information (damage cost) can be easily stacked together to generate the Flood Risk product. The flood risk level can then be populated for each polygon thanks to the attribute information from both input layers.

Table A5: Flood Risk Matrix

		Damage cost on land use			
		A	B	C	D
Flood Hazard	1 (low)	1A	1B	1C	1D
	2 (medium)	2A	2B	2C	2D
	3 (high)	3A	3B	3C	3D
Flood Risk classification					
Low Risk	1A 1B 2A				
Medium Risk	1C 1D 2B 2C 2D 3A 3B				
High Risk	2D 3C				
Very high Risk	3D				

This page is intentionally left blank!

Annex 2 – Filled Quality Control Sheets

Quality Control Sheets for the following products are provided in the form of independent documents:

- Urban Land Use / Land Cover
- Urban Green Area
- Building Footprints
- Flood History and Risk
 - Flood Extent
 - Flood Hazard
 - Flood Risk